

**AGH University of Science and Technology**

**Stanisław Staszic in Krakow,**

FACULTY OF ELECTRICAL TECHNOLOGY, AUTOMATION, COMPUTER SCIENCE AND ELECTRONICS

**Institute of Automation**

# **THESIS**

## **Magnetic levitation model and control.**

Supervisor Prof. Ph.D. engineer Wojciech Gega.

Author: Piotr Bania.

Rating: .....

## **Acknowledgments**

***Thank you Prof. Wojciech Grega for enabling me to complete my diploma thesis in line with my interests and for helping me during its implementation. I also submit thanks to Adam Pięt, M.A., who helped me overcome many technical difficulties, and his comments and observations allowed me to achieve my intended goals. Dr. Krzysztof Koćek and Dr. Andrzej Turnau gave me many valuable tips, for which I am grateful.***

***The work was sponsored by the TEMPUS project no. S\_JEP 11317-96, from which the magnetic levitation system was purchased.***

***Piotr Bania***

# Contents

<b>0. Markings and introductory remarks .....</b>	<b>2 1.</b>	
<b>Introduction .....</b>	<b>3 2. System</b>	
<b>description .....</b>	<b>.5 2.1. Electromagnet</b>	
and sphere position measurement system .....	6 2.2. Electronics and control panel of the	
device .....	7 2.3. Real-time system .....	9
<b>3. Mathematical model .....</b>	<b>12 3.1.</b>	
Physical mechanism of force generation in a ferromagnetic material .....	12 3.2. Model of electromagnetic	
interactions .....	13 3.3. Model	
analysis .....	19 4. Identification	
Purpose of identification .....	24 4.1.	
Identification of the position sensor characteristics .....	25 4.3. Identification of parameters $k$	
$T, uc$ .....	28 4.4. Determination of the dependence of the coil inductance	
on the position .....	31	
	,	
4.5. Identification results .....	35 4.6. Model	
verification .....	36 5. Linearized model i linear discrete	
<b>model .....</b>	<b>39 5.1. Linearization of the equations of state in the vicinity of the operating</b>	
point .....	39 5.2. Controllability and observability .....	40
5.3. Eigenvalues of the state matrix, transfer function and solution of the model equations		
linear .....	41 5.4. Linear discrete	
model .....	44 6.	
<b>Controls .....</b>	<b>47 6.1. PID</b>	
algorithm .....	47 6.2. Status	
recovery .....	54 6.2. 1. Heuristic	
method .....	54 6.2.2. Luenberger-type identity	
observer .....	55 6.3. Dynamic feedback .....	58
6.4. Regulation with pole placement .....	68 6.5. Comparison of	
algorithms .....	75 7.	
Summary .....	76	
<b>Literature .....</b>	<b>77</b>	

## Markings and introductory remarks.

$\frac{dx}{dt}$ ,  $x$  - time derivative of the function  $x(t)$

$\frac{dx^k}{dt^k}$  - kth time derivative of the function  $x(t)$

$f^{(k)}(x)$  - kth derivative of  $f$  calculated at point  $x$

$\frac{\partial f(x)}{\partial x_k}$  - partial derivative of the scalar function  $f(x)$  with respect to  $x_k$

$C$  - set of complex numbers

$\sigma(A)$  - spectrum of the

matrix  $A \operatorname{diag}(w_1, w_2, \dots, w_n)$  - diagonal matrix with elements  $w_1, w_2, \dots, w_n$  on the diagonal

$F(s)$  - Laplace transform of the function  $f(t)$

$L(f)$  - Laplace transformation

$L^{-1}(f)$  - inverse Laplace transformation  $Z(f)$

- transformation

$ZX(z)$ ,  $X(z-1)$  -  $Z$  transform of the sequence  $x(0), x(1), x(2), \dots$

$T_s$  - sampling period,  $R_r$ ,

$U=PC([0, \infty))$ , values in  $R_r$  space of functions with continuous intervals with  $U$  - control space,

$X$ - state space,  $X = R^n$

$Y$ - output space,  $Y = R^m$

### NOTE 1.

General solution of a system of linear differential equations

$$\frac{dx(t)}{dt} + Ax(t)Bu(t)x(t) = x_0 e^{At}, \quad t \geq 0,$$

has a form

$$x(t) = e^{At}x_0 + \int_0^t e^{A(t-\tau)}Bu(\tau)d\tau.$$

The method of determining the matrix  $e$  and the derivation of the above formula see. e.g. [10], [14], [21].

### NOTE 2.

Wherever this does not cause confusion, the explicit marking  $dx(t)/dt$  has been omitted

depending on time, for example Eq

$\dot{x} = f(x, u)$ , ( $x, u$ ) are written as

$$\frac{dx}{dt} = f(x, u).$$

### NOTE 3.

All solutions of nonlinear differential equations were obtained using the method *Runge – Kutta* of the fourth order, using the *SIMULINK package*. Details see e.g. [8], [28].

## 1. Introduction

Since the development of the theory of electromagnetism, people have been using electric and magnetic phenomena in many areas of life. One of the applications of the interaction of a magnetic field and matter is magnetic levitation ( *Magnetic Levitation, Magnetic suspension*, the abbreviation *MagLev* is also used ). This phenomenon is based on the well-known effect of force generation in a ferromagnetic material placed in an external magnetic field. Force, or rather the resultant of forces resulting from the action of an appropriately shaped field, counteracting the force of gravity, allows various objects to be held in space. It turns out that this simple idea now finds many practical applications. The most common use of magnetic levitation is in rail transport. Trains on a magnetic cushion are currently running in Great Britain (Birmingham), Japan (Tokyo) and Germany (Emsland, and the Berlin-Hamburg line is under construction). Magnetic bearings in which there is no friction are found

used in electrical machines and wherever there is a need for long-term continuous operation. Other applications include weight measurement in extreme conditions, thermogravimetry (in chemistry), material transport in mines, precise positioning in nanometers, vibration damping, active magnetic suspension in the automotive industry [27], [29].

Due to the great interest in this field, the Department of Automation of the AGH University of Science and Technology purchased a laboratory system enabling the study of the phenomenon of magnetic levitation from the point of view of digital control of such a process. The aim of this work is to create a mathematical model of the magnetic levitation system, analyze its properties, identify and control the system. While writing, the author also had a didactic goal in mind, because based on the results obtained, it will be possible to conduct laboratory exercises in modeling dynamic systems, identification and control theory.

The layout of the work reflects the individual stages of its creation. The second chapter is an introduction to the system and allows you to familiarize yourself with the design of the device, methods of measuring individual quantities and the real-time system used for control and data acquisition. In chapter three he stayed derived mathematical model of the object and its basic properties and limitations were analyzed. The identification procedure and model verification constitute the content chapter four, which also explains many properties of the model and is very closely related to system modeling.

The continuous and discrete-time linear model is analyzed in chapter five. Although the form of this model is a natural consequence of the equations derived in chapter three, I decided to devote a separate chapter to this issue because it forms the basis for the synthesis of regulators discussed in chapter six. Main The difficulty in controlling the magnetic levitation system is its instability and short duration (of the order of several dozen milliseconds) of dynamic states. Four different system stabilization algorithms show how to overcome these problems. In addition to the synthesis of controllers, an analysis of the impact of system nonlinearity on stability and quality was performed regulation .

All drawings, simulations and numerical calculations were made using the *MATLAB/SIMULINK package*, which is worth familiarizing yourself with before reading. *The RTW/RT-CON* real-time system compatible with *MATLAB* and the computer hardware were configured by employees of the Department of Automation at AGH, for which I would like to thank you very much.

The diskette attached at the end of the work contains object models and regulators made using *SUMULINK*, and a group of *MATLAB* m-files allowing for efficient identification and synthesis of regulators. Each file is equipped with a short description to facilitate its use.

In order to fully understand all derivations and formulas, the reader should know mathematical analysis, basic physics, theory of ordinary differential equations and control theory in the field taught in the field of automation and robotics or a related field. Detailed information and proofs of the theorems can be found in the literature, listed at the end of the work.

This study does not exhaust all the possibilities and problems related to modeling, identification and control of magnetic levitation, but the author hopes that it will constitute a starting point for further research.

*Cracow , June 1999*

## 2. System description

As already mentioned, magnetic levitation involves keeping a steel sphere in the field of an electromagnet. The laboratory system enables position measurement, control of the current flowing through the electromagnet coil, and allows cooperation with external control devices. The magnetic levitation system consists of an electromechanical part containing an electromagnet and an optical system used to measure the position of the sphere and an electronic part. The latter is responsible for controlling the current in the coil, processing the signal from the position sensor, measuring the current and cooperation of the system with the computer. Moreover, the device is equipped with an analog *PID* controller made on operational amplifiers.



Fig. 2.1. General view of the device

## 2.1. Electromagnet and sphere position measurement system

Figure 2.2 shows a diagram of the span to which the electromagnet is attached. It produces a magnetic field dependent on the current flowing through the coil. This field exerts an upward force on the sphere, and the shape of the field lines is such that it dampens the sphere's movements in the horizontal plane. The damping is effective enough to assume that the ball's movement takes place only in the vertical axis. This assumption will be important for position measurement and derivation of model equations. Figure 2.3 shows the approximate shape of the field lines.

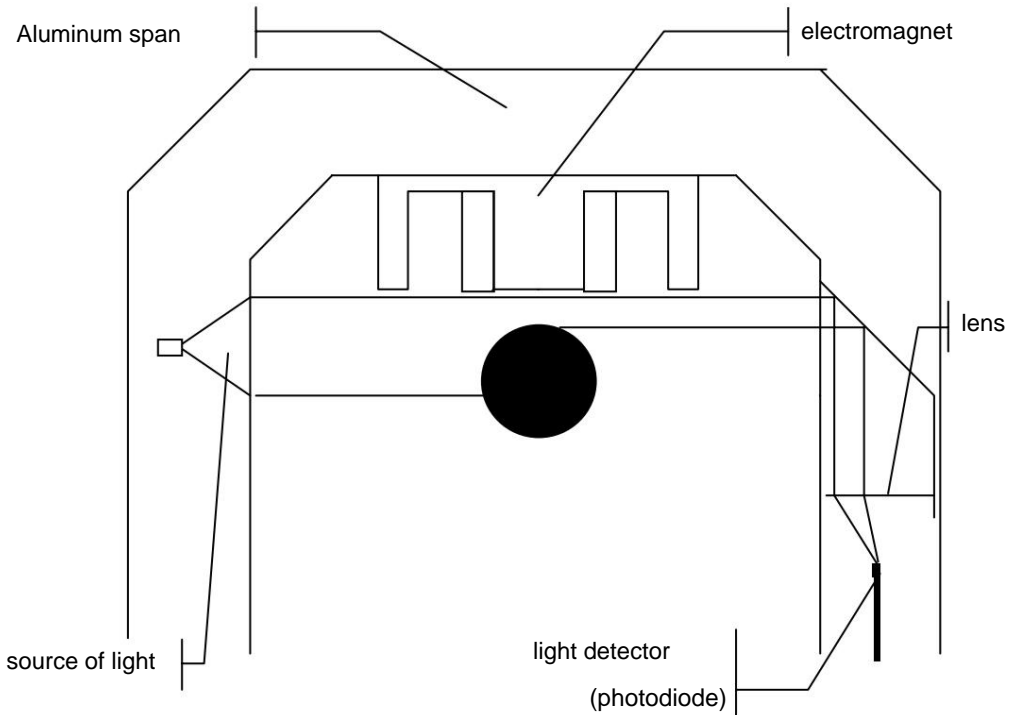


Fig. 2.2. Construction of the electromechanical part of the system and the principle of position measurement

An optical system is used to measure the position of the sphere. The reflector on the left illuminates the sphere. The light from the reflector is directed through the optical system on the right to the photodiode. The amount of light reaching the photodiode depends on the position of the sphere. The voltage on the photodiode after amplification is a measure of the position of the sphere.

The dependence of this voltage on the position of the ball is quite complicated, because the amount of light reaching the photodiode is a non-linear function of the position and the photodiode itself is a non-linear element. Determining the shape of the position sensor characteristic theoretically is practically impossible and therefore it must be determined experimentally.

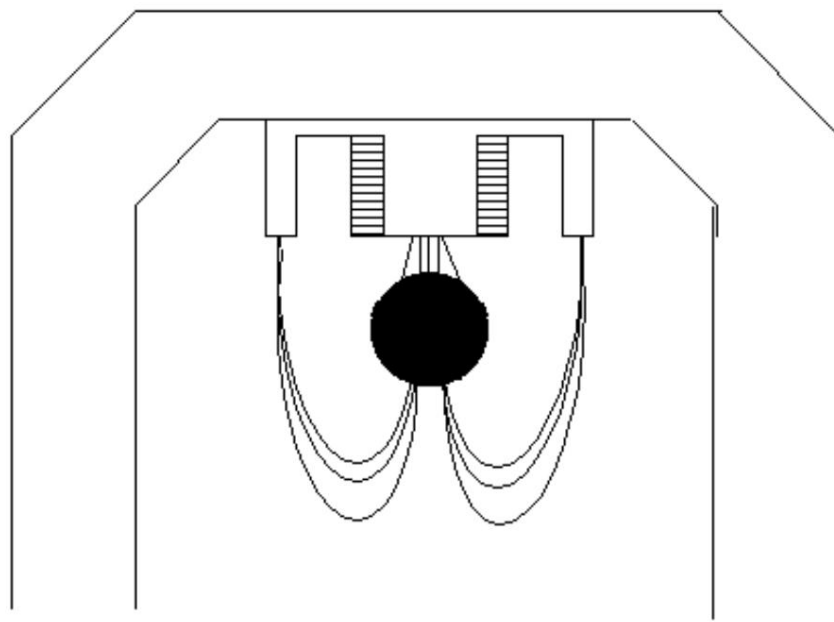


Fig. 2.3. An example of a magnetic field line

## 2.2. Electronics and control panel of the device

The electronic system of the device allows operation in internal mode using the built-in *PID controller*, and in external mode using a computer or other control device. Since the main topic of the work is digital control, we will not deal with the company's built-in *PID controller* and will limit ourselves only to providing the block diagram of the device.

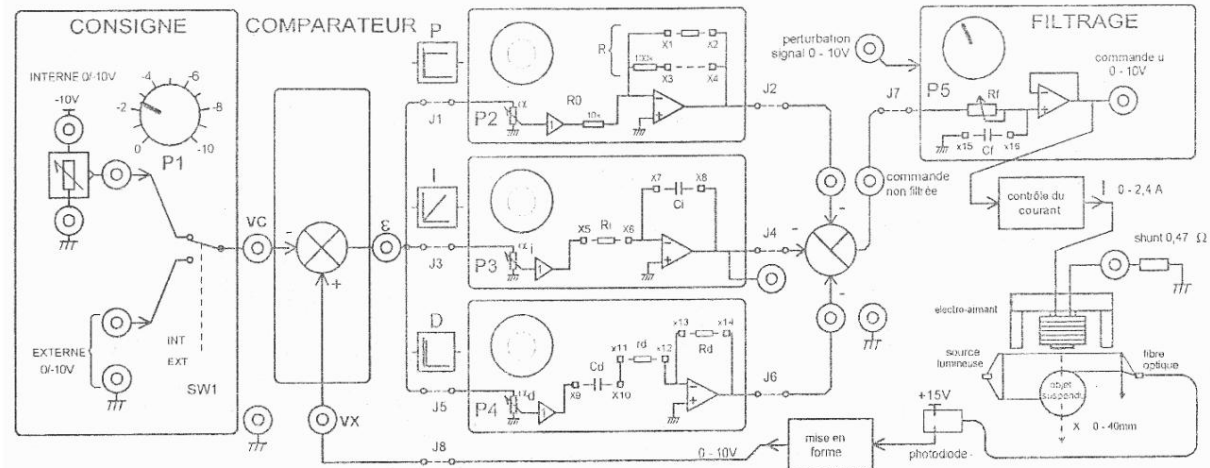


Fig. 2.4. Control and measurement panel of the device.

The switch marked *int-ext* in the diagram allows you to change the operating mode to external. The control signal is then fed directly to the current controller ( *controle du courant* block ), which ensures stabilization of the current flowing through the coil.

electromagnet . The manufacturer of the device did not provide an electronic diagram and it is difficult to say how the current control system works, only that it forces rapid changes in current by applying large voltage pulses (of the order of several dozen volts) to the coil. In other words, this system acts as a current source. The voltage drop across the resistor connected in series with the coil (*shunt 0.47*) is a measure of the current flowing through the coil.

$\ddot{y}$

The average value of this current does not exceed  $0.5 \text{ A}$ , which gives a voltage drop across the measuring resistor of  $235 \text{ mV}$  . The measuring range of the transducer is  $10\text{V}$  , which gives a quantization error of  $Uk = 2.44 \text{ mV}$  with twelve bits . The level of noise and interference from the mains estimated on the basis of measurements was approximately  $15 \text{ mV}$  in the optimistic case .

If we assume that the measuring resistor has a tolerance of  $1\%$  , we will obtain the following estimate of the current measurement error

$$\frac{\ddot{y}_{AND}}{R} = \frac{\ddot{y}_R}{R} + \frac{AT_k}{AT} + \frac{\ddot{y}_AT_p}{AT} = 0.01 + \frac{2.44}{235} = \frac{15}{235} \approx 0.075 .$$

Reducing the quantization error by amplifying the signal increases the accuracy to  $6.5\%$ . Therefore, the current measurement should be treated as indicative. The position measurement is much more precise, as it was found that if the sensor identification is performed correctly, the position of the sphere can be determined with an accuracy of  $0.3 \text{ mm}$  .

To sum up, at the output of the device we have two signals measuring the position of the sphere and the current in the electromagnet coil, and the input is the control voltage fed to the current controller. The system was coupled to a computer using an *RT-DAC* measurement card with the following parameters [34].

#### Analog inputs:

Number of channels:	16 multiplexed 12
Number of bits:	
Measurement range:	$\pm 10\text{V}$ , programmable gain ( $x1, \dots, x16$ )

#### Analog outputs:

Number of channels:	2
Number of bits:	12
Voltage range:	$0-5\text{V}, 0-10\text{V}, \pm 5\text{V}, \pm 10\text{mA}$ output amplifiers
Output current:	

#### Digital inputs/outputs:

Channels:	32
Standard:	TTL compatible

#### Interrupts:

Type:	maskable (IRQ3, ..., IRQ15) and non-maskable (NMI)
Period:	from 10 microseconds to approximately 2000 seconds, programmable

The measurement card was installed and the system was connected to the computer by Dr. Eng. Krzysztof Kołek and Adam Piętak, M.Sc. They also provided the author with appropriate drivers enabling the card to work with the *RTW system*, for which I am very grateful because this allowed me to save time and focus on issues related to modeling, identification and control.

## 2.3. Real-time system

Now we will discuss how to use the *RTW/RT-CON* package [26],[33] and the method automatic generation of algorithm code, on the example of a *PID controller*. After compiling the scheme using *SIMULINK* (Fig. 2.5), set the sampling time and base address as shown in Figures 2.6 and 2.7.

Clicking *tools/build\_rtw*

will generate a \*.dll library that can be loaded by clicking the *START button*.

The launched library already works in the background and implements the control algorithm in real time. You can now start performing experiments. For this purpose, we run simulations (*simulation/start*) with the *simulation/external option*. The system then allows you to change the controller parameters online during the experiment and record the course of any variable. To achieve this, type *MATLAB* in the window

the "rtw" instruction , which will cause a dialog box to appear where you can select the parameters or variables you are interested in. We can choose from various display options (*plot , plot parameters*) or parameter tuning (*tune*). Recorded waveforms can be saved as \*.mat files. Figure 2.8 shows an example of a screen view during real-time operation.

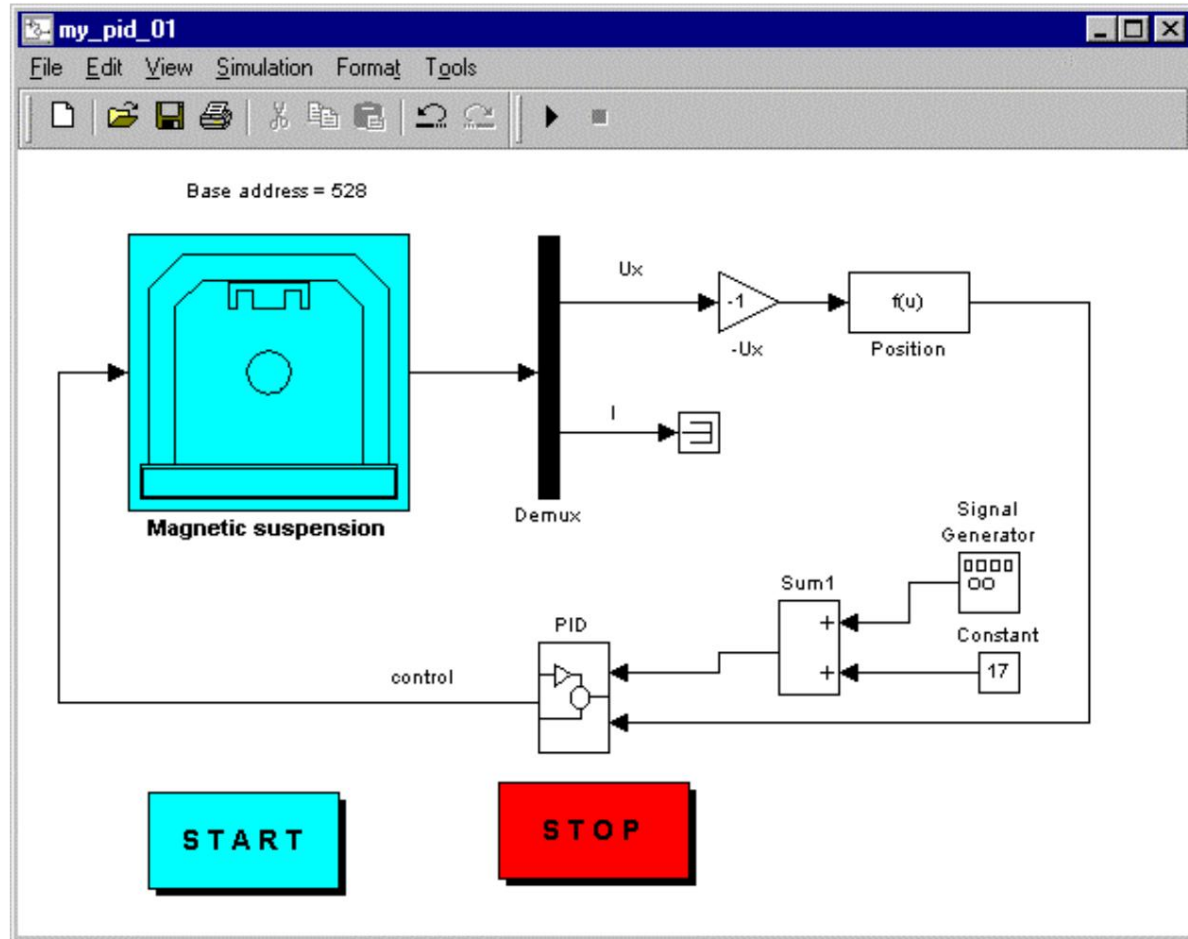


Fig. 2.5. Example implementation of a *PID controller*.

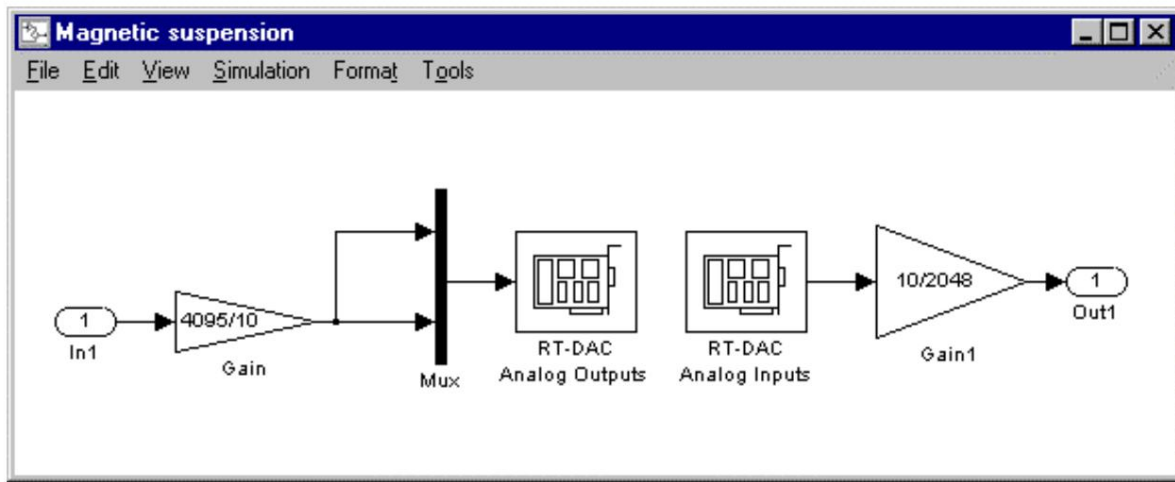


Fig. 2.6. Contents of the *Magnetic Suspension* block from Figure 2.5.

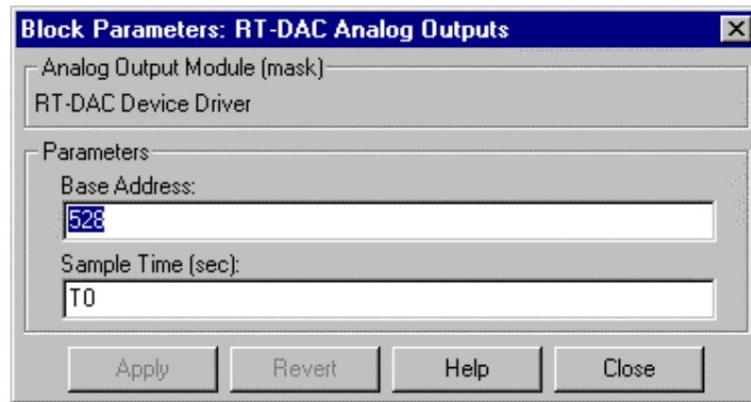


Fig. 2.7. Setting the base address and sampling time.

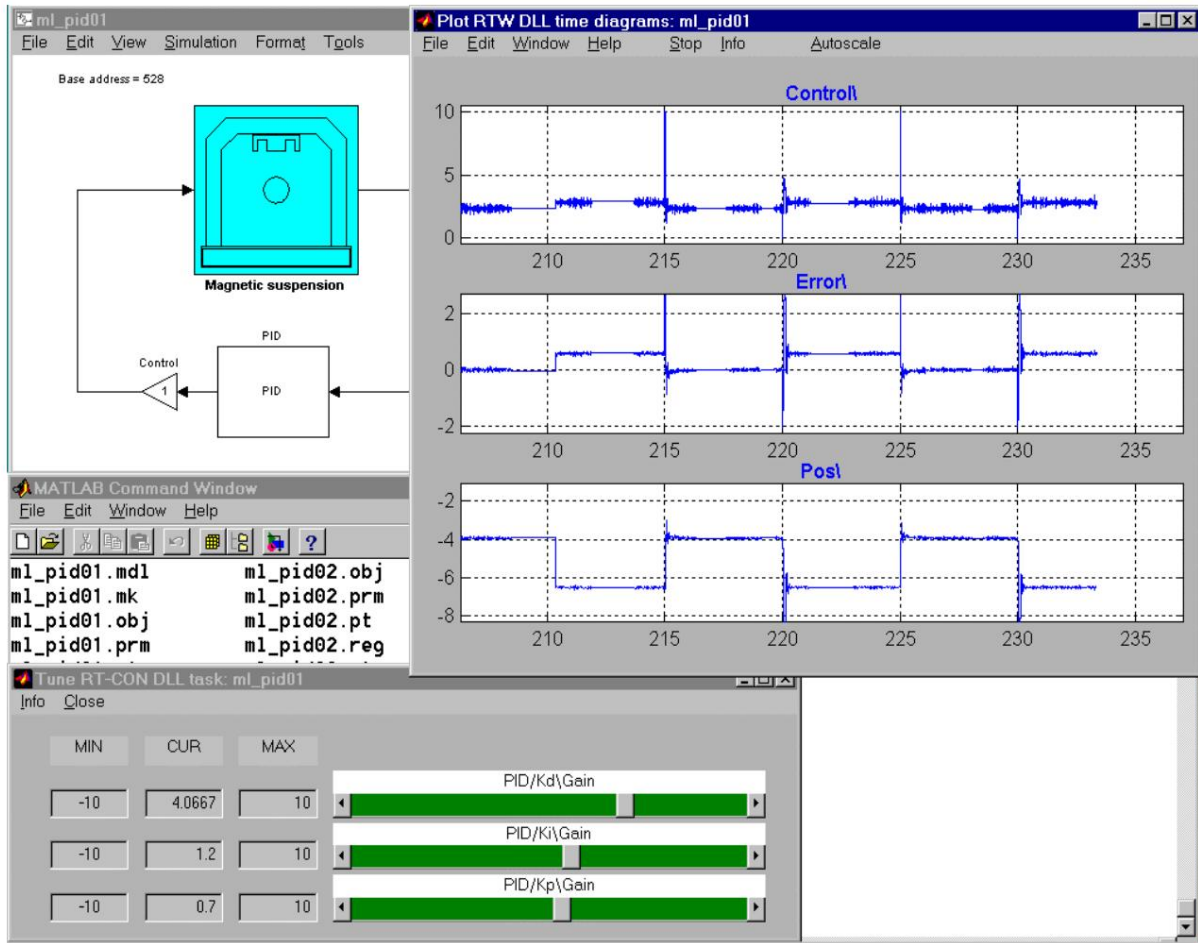


Fig. 2.8. An example of the RTW package working .

On the bottom left you can see the window for online tuning of the controller parameters, and on the top right you can see the real-time control, error and voltage from the position sensor. After completing the experiments, first stop the simulations (*simulation/stop*) and then click the *STOP button*, which will unload the previously generated \*.dll library.

This short description is intended to present the issue and does not exhaust all possibilities and problems. Detailed information about the RTW/RT-CON system can be found in [26] and [33]. Data regarding the device's structure, dimensions of individual elements, types of materials used, voltage levels, etc. can be found in the user manual [13].

After starting the regulator, when the sphere is far from the equilibrium position, the regulation error is very large and, consequently, a current close to the maximum flows through the coil. Due to the heating of the electromagnet, be careful not to let this situation last too long. The sphere should be placed in the equilibrium position by holding it from the bottom so as not to cover the light falling on the position sensor. You can also use a stand made by the author for this purpose, set the sphere in a position close to equilibrium and only then turn on the regulator.

### 3. Mathematical model

When creating mathematical models, the following assumptions should be taken into account:

- The model should ensure compliance with the experiment.
- Take into account those phenomena that have a significant impact on the behavior of the real object.
- The model equations should be able to be solved in a reasonable time.
- The model should be identifiable.

The above assumptions are generally contradictory and meeting them is practically impossible, so a compromise must be sought.

#### 3.1. The physical mechanism of force generation in a ferromagnetic material

A precise explanation of the phenomenon of ferromagnetism requires knowledge of quantum mechanics. The use of this very advanced theory is unjustified when describing macroscopic systems such as magnetic levitation. Using the classic one the theory of electromagnetism [6],[25] can estimate the dependence of the force acting on the sphere on the position and current in the coil.

For this purpose, consider a closed circuit with current flowing in a magnetic field with a non-zero gradient, as shown in Figure 3.1.

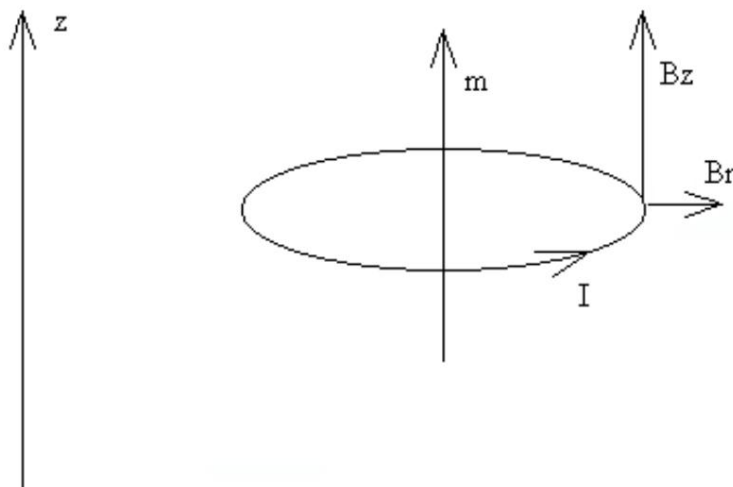


Fig. 3.1. Circuit with current in a magnetic field

A force will act on such a circumference

$$F_m = \frac{\dot{y}B}{\dot{y}_{mn}},$$

where  $m$  is the magnetic moment of the current-carrying circuit. The magnetic field interacting with such a circuit with current will "set" it so that the vector  $m$  points in the same direction side as  $B$ . Electrons have a non-zero magnetic moment and can be approximately treated as microscopic circuits with current. In ferromagnetic materials, there are a large number of electrons that can align in the direction of the field. The number of electrons for which the direction of the magnetic moment is consistent with the direction of the field is proportional to the induction  $B$ . Therefore, the resultant force will be proportional to the product of the induction, its gradient and the number of electrons

$$F_{kBz} = \frac{\dot{y}B}{\dot{y}_{mn}}.$$

Both the induction and its gradient are proportional to the current in the electromagnet coil, so we can expect the following dependence of force on current

$$F = f(x)I^2.$$

The function  $f(x)$  is decreasing because the induction and its gradient decrease with increasing distance. The above description is only an approximation of the real situation, and more detailed information on magnetic fields in solids can be found in [22].

### 3.2. Model of electromagnetic interactions

Differential equations describing the behavior of the system under consideration can be derived in many ways. One of them is a method based on Lagrange's equations. This approach is often used when describing electromechanical systems.

Basic information on this topic can be found in any textbook on functional analysis, theoretical mechanics or physics [3], [20].

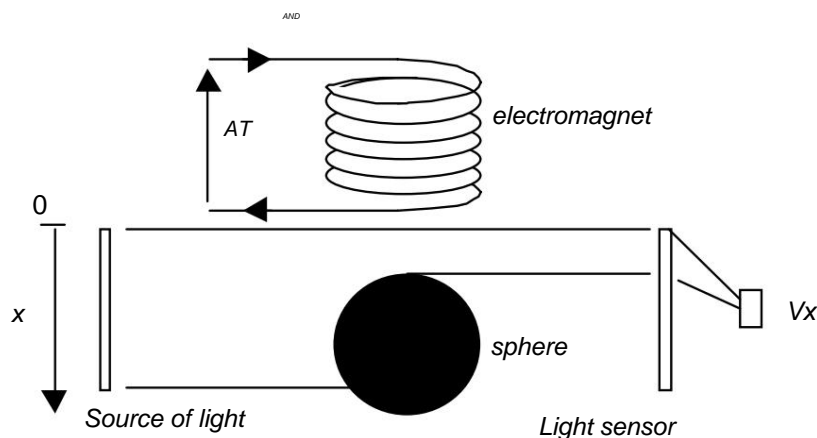


Fig. 3.2. Simplified system diagram for deriving equations of state.

Based on Figure 3.2, it can be concluded that the system has three energy storage units.

Kinetic energy is related to the motion of the sphere and the magnetic field of the coil (the movement of charge carriers justifies the name kinetic in relation to the energy of the magnetic field), and potential energy is related to the position of the sphere. When deriving the model equations, the electric component of the field was omitted, which obviously exists, but the energy associated with the existence of the electric field and energy losses resulting from the electromagnetic waves radiated by the system (changes in current in the coil) are very small and practically unmeasurable. We further assume that the electromagnet operates in a linear range and there is no core saturation. This assumption is met in practice due to the small currents flowing through the coil.

The Lagrange function, which is the difference between kinetic and potential energy, has the form:

$$T = \frac{1}{2} m \dot{x}^2 + \frac{1}{2} L(x) \dot{q}^2 + R \dot{q} \int_0^x g dx - \frac{1}{2} mgx + qu \quad (3.1)$$

Where :

$x$  - distance of the sphere from the electromagnet,  $q$  - charge flowing through the coil,  $m$  - mass of the sphere,  $R$  - resistance of the coil,  $L(x)$  - function describing changes in the inductance of the coil depending on the position of the sphere,  $I = q$  - current in the coil,  $g$  - acceleration due to gravity,  $u$  - control voltage.

The functions  $x(t)$ ,  $q(t)$  satisfy a system of differential equations

$$\begin{aligned} \frac{d}{dt} \frac{dT}{dx} &= \frac{dT}{dx} = 0, \\ \frac{d}{dt} \frac{dT}{dq} &= \frac{dT}{dq} = 0. \end{aligned} \quad (3.2)$$

From (3.1) and (3.2) we get

$$\begin{aligned} \frac{dx^2}{dt^2} &= \frac{1}{2m} \frac{dL}{dx} I^2 g dx, \\ \frac{dI}{L} &= -\left( \frac{dL}{dx} \frac{dx}{dt} I - RI u \right) dt. \end{aligned} \quad (3.3)$$

Equations (3.3) describe the dynamics of the system with the assumptions made earlier.

The first of these equations expresses Newton's second law of motion, and the second is the content of Faraday's and Kirchhoff's laws.

The desired dependence of force on position and current is expressed by the formula

$$F(x) = \frac{1}{2} \frac{dL}{dx} I^2. \quad (3.4)$$

let us note that the form (3.4) is consistent with the predictions of section 3.1 and allows us to determine force based on knowledge of the current and inductance of the coil as a function of position. Dependence The coil inductance from the sphere position is a function of the system geometry, material and number of coil turns. For an electromagnet it is always a decreasing function. Determining this relationship on the basis of theory requires solving partial field equations, which is computationally burdensome, however, in the literature [25] several forms of the function  $L(x)$  can be found

$$L(x) = L_0 + \frac{1}{ax^n + b}, \quad n > 0,$$

$$L(x) = L_0 + \frac{1}{ax^n + b}, \quad n < 0,$$

where  $L_0$  is the inductance of the coil when the sphere is very (theoretically infinitely) far away. Since  $L(x)$  is decreasing, its derivative is always negative, and equation (3.4) shows that the magnetic force always acts upwards, i.e. it attracts the sphere to the electromagnet.

We will continue with the second equation (3.3). This equation describes the current in the coil and depends on the position and speed of the sphere. However, due to the presence of an electronic system controlling the current, it requires some modifications.

The current control system is designed to force the current in the coil to follow changes in the control voltage as quickly as possible and to eliminate the influence of the sphere movement on the current. It was experimentally found (Fig. 3.3, 3.4) that the controller ensures current stabilization regardless of the movement of the sphere and its position.

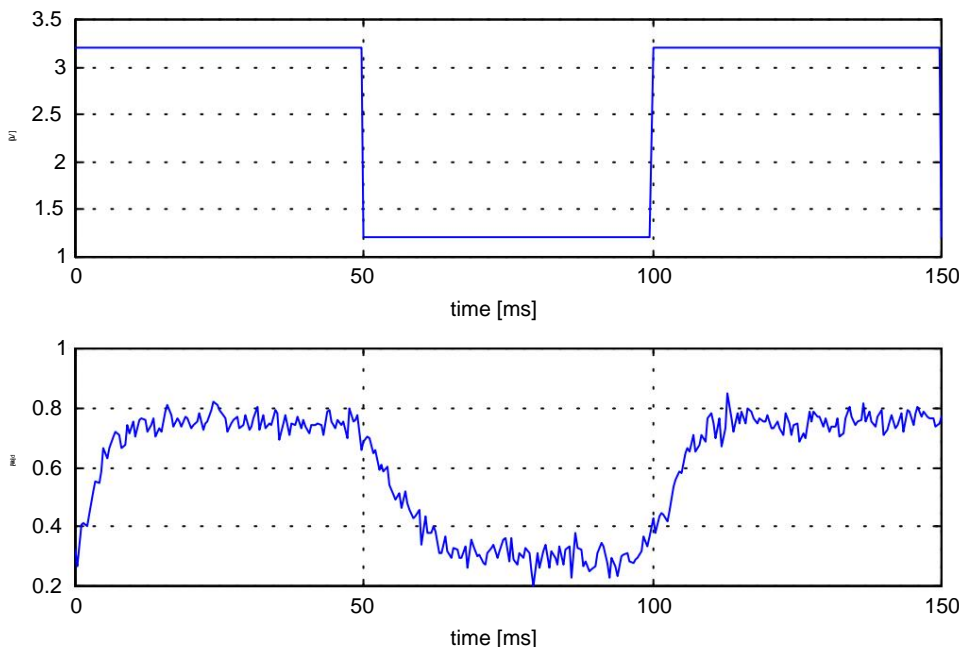


Fig. 3.3. Control and current waveform in the coil with a stationary sphere.

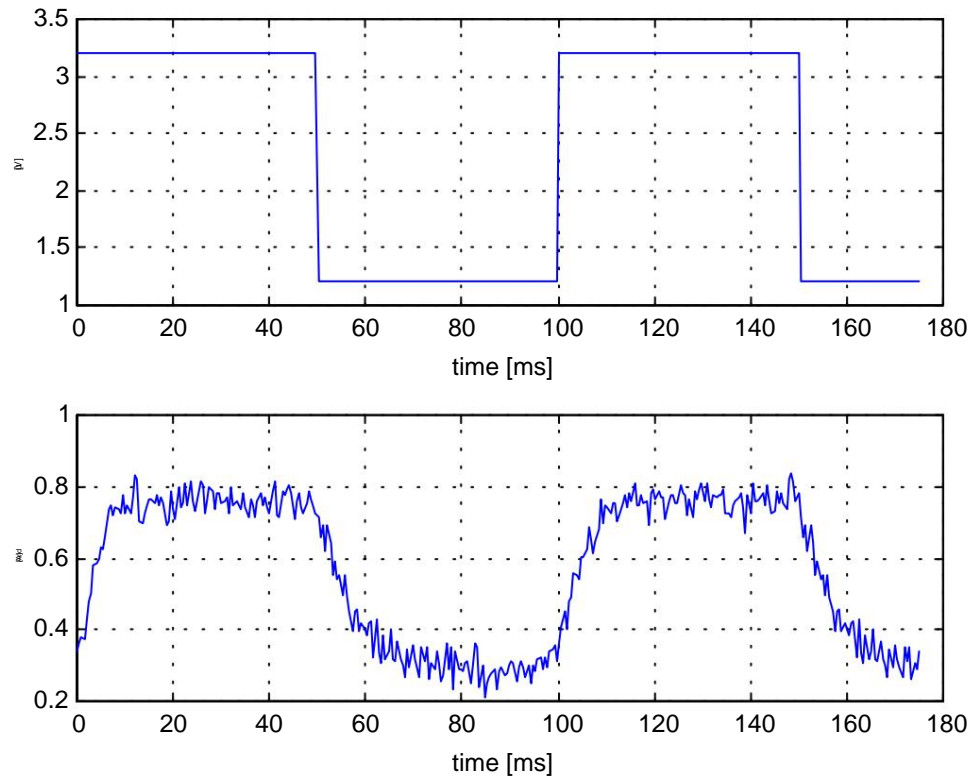


Fig. 3.4. The course of control and current in the coil with a moving sphere.

It can be seen that the current pattern is similar to the response of a first-order inertial system. However, increasing the current takes place with a different time constant than decreasing it. This phenomenon is probably the result of the nonlinearity of the electronic components used. Due to the difficulties in modeling this type of waveforms and the lack of technical details regarding the electronic part of the device, it was decided to adopt a linear equation in the form instead of the second equation (3.3).

$$\frac{dl}{dt} = \frac{1}{T} (u - u_c) \quad (3.5)$$

Where :

$T$  – time constant,  
 $k$  – gain factor,  $u$  – control voltage,  
 $u_c$  – small constant voltage on the coil.

The model equations will now take the form

$$\begin{aligned}\frac{dx^2}{dt^2} &= \frac{1}{2m} \frac{dL}{dx} I g dx , \\ \frac{dI}{dt} &= \ddot{y} + \frac{1}{T} \text{ AND } \frac{k}{T} (u u - u_c ).\end{aligned}\quad (3.6)$$

Note that the second equation no longer depends on the position and velocity of the sphere. This is the effect of the current controller. From the control point of view, this phenomenon is beneficial because: allows you to control the current in the coil independently of other state variables.

Since in the laboratory system the position of the sphere is measured in millimeters and the duration of transients is of the order of several dozen milliseconds, it is convenient to rescale the time and position.

Taking the position of the sphere, its velocity and the current in the coil as state variables, we can write the equations of state

$$\frac{dx_1}{dt} = x_2 , \quad (3.7)$$

$$\frac{dx_2}{dt} = \frac{1}{2} \frac{dL(x_1)}{dx_1} 10 + 3 g z t - 1 ( ) , \quad (3.8)$$

$$\frac{dx_3}{dt} = \frac{1}{T} x_2 - \frac{k}{T} (u u + u_c + u_2 ( ) ) , \quad (3.9)$$

where:

$x_1$  – position of the sphere

[mm],  $x_2$  – speed of the

sphere [m/s],  $x_3$  – current

in the coil [A],  $u$  – control

voltage [V],  $u_c$  – positive

constant [V],

$m$  – mass [g],  $dL(x_1)/$

$dx_1$  - [H/m],  $g =$

9.81 [m/s<sup>2</sup>],  $z_1(t)$ ,  $z_2(t)$  –

interference,  $t$  – time in [ms].

The system output is the voltage measured by the position sensor

$$y = g x_1 \cdot \quad (3.10)$$

The design of the device discussed in chapter two shows that the state variables i control must meet the following conditions

$$x_1 \in [0, x_{max}] , \quad (3.11)$$

$$(t) \in R( ) , \quad (3.12)$$

$$x_3( ) \in [k_c, k_u] u_{max} , \quad (3.13)$$

$$u \in [0, u_{max}] . \quad (3.14)$$

Additionally, the disturbances affecting the system were taken into account in the model. The disturbance  $z1(t)$  represents the forces acting on the sphere. Such forces result from ground vibrations, air movements, etc. The disturbance  $z2(t)$  represents the voltages induced in the coil, which cause undesirable current changes. These voltages are induced by other external devices, the power supply network, etc.

Equations (3.7), (3.8), (3.9), (3.10) describe the dynamics of the system under the constraints (3.11), (3.12), (3.13), (3.14). Using the MATLAB/SIMULINK package [19],[28], a simulation model presented in Figure 3.5 was created based on equations (3.7) - (3.14).

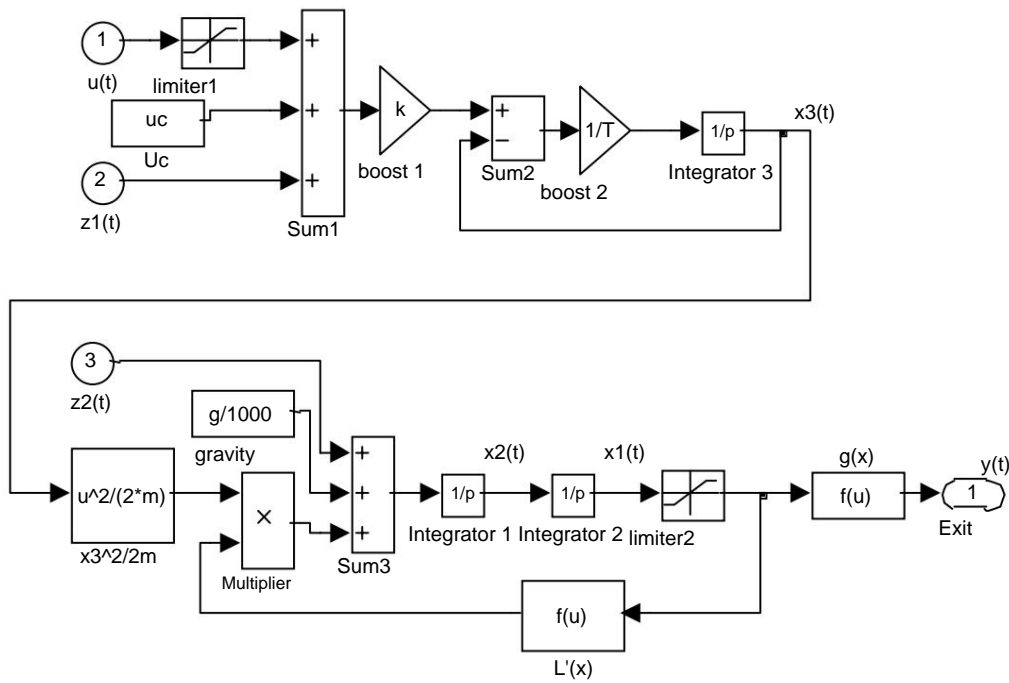


Fig. 3.5. Simulation model made using the MATLAB\SIMULINK package.

### 3.3. Model analysis

Equations (3.7) – (3.9) are non-linear and it is difficult to indicate methods for their analytical solution. However, the basic properties of the system can be determined without solving the equations. We can write model (3.7) – (3.9) in the compact form  $dx$

$$\frac{d}{dt} = (0x((),()),() , fxtu\ddot{x}t R ut R x, \ddot{y})^3 - \dot{y} \propto R^3, t \ddot{y}, \\ fRRR^3 \times \dot{y}^1 = \dot{y}^3. \quad (3.15)$$

If the function  $L(x)$  is of class  $Ck$ , then  $f(x,u)$  is of class  $Ck-1$  with respect to the first argument and class  $C$  with respect to  $u$ . Equating the right side of (3.15) to zero, taking into account the constraints (3.11)-(3.14) we will get a set of model equilibrium points.

$$0 \approx [\dot{y}x]_{\max}, \\ x_{20} = 0, \\ x_{30} = \sqrt{\frac{2mg}{|Lx(10)|}}, \\ at_0 = \frac{1210mg}{k\sqrt{|Lx(-10)|}} \cdot at_c. \quad (3.16)$$

There are infinitely many equilibrium points and each of them is unstable [15]. Indeed, any deviation from the equilibrium point will result in a consequent change in the position of the sphere. If the sphere moves up, the magnetic force will overcome the gravitational force and the sphere will be attracted to the electromagnet, but if it moves down, the gravitational force will prevail and the sphere will fall.

Equations (3.8) and (3.9) show that the magnetic force is always directed upwards and its minimum value is

$$F_{\min} = \left| \frac{1}{2} \frac{dL}{dx_1} \right|_{\text{min}}^2$$

while the maximum value of the magnetic force is equal to

$$F_{\max} = \left| \frac{1}{2} \frac{dL}{dx_1} \right|_{\text{max}}^2 >> mg$$

(See also the comment on the function  $L(x)$  in sections 3.1 and 3.2)

Therefore, the force with which the sphere can be pulled down is no greater than  $mg$ , while the force moving the sphere upwards can be several to several dozen times greater, as long as we allow for sufficiently high current values. In the laboratory system  $F_{\max} 4.4mg$ .

This asymmetry allows you to move the sphere up in a short time, but doing it the other way takes much more time. This reasoning explains the observed differences in the behavior of the system when moving up and down. In order to

To better illustrate this phenomenon, sets of states available at moments  $T = 8 \text{ ms}$  and  $T = 12 \text{ ms}$  were determined, from the equilibrium point  $x_0 = [15 \ 0 \ 0.5225]T$ . The set of achievable states is closely related to the time-optimal problem and Pontryagin's maximum principle, which we will quote here from [10].

The minimum-time problem consists in moving the system (3.15) from state  $x_0$ , with initial  $x_0$  to the given final state  $x_k$  in the shortest time  $t^*$  limit (3.14) on the control amplitude.

Let constraints be imposed on the initial and final states

$$\begin{aligned} & (x_0, u_0) = \\ & h R^{2n} \quad R \in CR^{-1}(\mathbb{R}^{2n}). \end{aligned}$$

An expression is called a Hamilton function

$$H(\dot{x}, x, u, t) = \dot{x}^T f(x, u) + u^T R \dot{x}$$

*The maximum principle for a minimum time problem*

If  $u^*$ ,  $x^*$ ,  $t^*$ , are a solution to the time-optimal problem, then there is a non-zero vector  $Rk$  such that the maximum condition of the function occurs almost everywhere in the time interval  $[0, t^*]$ . Hamilton

$$H(\dot{x}, u, t) = \dot{x}^T f(x, u) + u^T R \dot{x} \quad (x, u, t) \in [0, t_{\max}],$$

and the conjugate function  $\lambda$  satisfies the adjoint equation

$$\begin{aligned} \frac{d\lambda}{dt} &= -\frac{\partial H}{\partial x} = -\frac{\partial f(x, u)}{\partial x} \lambda^T, \\ \lambda(0) &= \frac{\partial H}{\partial x}(0), \\ \lambda(k) &= \frac{\partial H}{\partial x}(k). \end{aligned} \tag{3.17}$$

If the final and initial states are predetermined, the last two conditions do not matter no information about the conjugate function.

Let us write equation (3.15) in an equivalent form

$$\frac{dx}{dt} = f(x_0 + x, u_0 + u), \quad x(0) = 0 \tag{3.18}$$

where  $x_0, u_0$  are given by (3.16).

The condition for maximizing the Hamiltonian is satisfied when

$$\begin{aligned} \dot{y}^{at}_{\max} & , \text{ When } \ddot{y}_3 > 0 \\ at = \dot{y} & , 0 \text{ when } \ddot{y}_3 < 0 \\ \dot{y}^{at_0} & , \text{ When } \ddot{y}_3 = 0. \end{aligned} \quad (3.19)$$

By inserting (3.19) into the state equation (3.18), we obtain a system of differential equations (3.17), (3.18) for the state and the conjugate variable. If we now reverse the direction of time in the coupled equation and solve this system of equations with the initial condition  $x(0) = x_0$  in the direction from the point  $x_0$ , then after time  $T$  we will reach a certain point  $x(T)$ . While the control defined by (3.19) is optimal, this point lies on the edge of the set reachable from point  $x_0$  at time  $T$ . This does not have to be the case because the maximum principle is a necessary condition for optimality. By choosing many different initial conditions for the adjoint function, we will obtain an approximation of the edge of the set of achievable states. Figure 3.6 shows the projection of the set of achievable states onto the  $x_1, x_2$  plane.

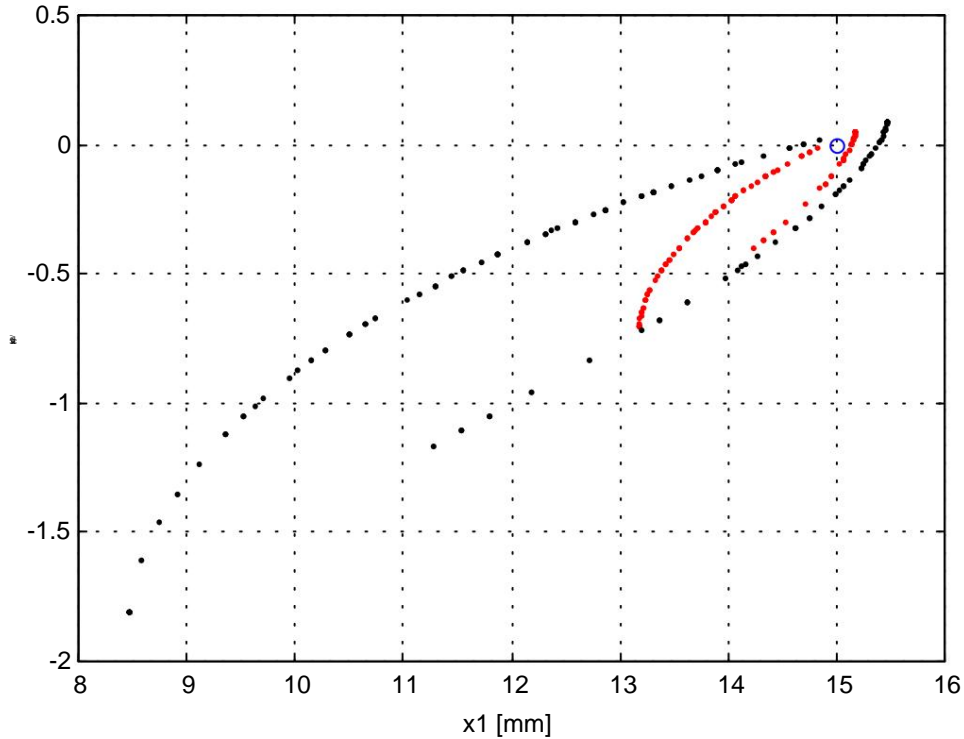


Fig. 3.6. Projection of the set of states achievable from the equilibrium point  $x_0 = [15, 0, 0.5225]$  onto the plane  $x_1, x_2$  at times  $T = 8 \text{ ms}$  and  $T = 12 \text{ ms}$ .

We see that the set of achievable states is very asymmetric with respect to the starting point  $x_0$ . The sphere accelerates very quickly and moves towards the electromagnet, while the movement in the opposite direction is much slower. This behavior is consistent with the previous considerations regarding the magnetic force and is caused primarily by the nonlinear dependence of the force on the current in the coil.

This asymmetric behavior of the system will have a significant impact on the synthesis and operation of regulators. Most controller synthesis methods are based on a model linearized around the operating point [14]. This model describes the behavior of an object in a certain way

very small surroundings of the operating point, and the synthesis of the controller stabilizing the system involves shifting the eigenvalues of the closed system state matrix so as to obtain stability and desired dynamic properties, such as noise suppression, tracking, etc.

Suppose we demand from the controller that the duration of the transient state when transitioning from a certain initial state to the steady state be shorter than the set one. If the longest time constant of a closed system is  $T$ , after  $3T$  we practically reach a steady state. Let us further assume that the sphere is to move down and that at the initial moment it is distant from the operating point by  $x$ . This will be achieved fastest if the sphere falls freely under the influence of gravity. Newton's second law leads to the conclusion that the time it takes for a sphere to travel . This gives an approximate estimate of what the time constant of a closed system should meet.

$$\ddot{y} \text{ is } t = \sqrt{\frac{2\ddot{y} x}{g}}$$

$$3T \ddot{y} \sqrt{\frac{2\ddot{y} x}{g}} = \dots \quad (3.20)$$

In the discrete case, the equivalent of the time constant is a parameter

$$\ddot{y} = \exp^{\ddot{y}} \cdot \frac{T_s \ddot{y}}{T} \ddot{y},$$

where  $T_s$  is the sampling period, hence from (3.20) we have an estimate

$$\ddot{y} \ddot{y} \exp^{\ddot{y}} \frac{3T_s}{\sqrt{\frac{2\ddot{y} x}{g}}} \ddot{y} \quad (3.21)$$

Inequalities (3.20) and (3.21) impose constraints on the eigenvalues of the state matrix of a closed system. For example, for  $x = 5mm$ ,  $T_s = 2ms$  we have  $\ddot{y} T 10ms$  and 0.83. This means that the controller should be designed so that the duration of the transient state at the output is greater than  $3T$ . If the state matrix of a closed system has real single eigenvalues, the output will be a linear combination of exponential functions  $\exp()$

$$yt(\zeta) = 1 \exp(\ddot{y} - tc + 12) \ddot{y}_2 t + \dots + n \exp(\ddot{y} - nv).$$

Conditions (3.20), (3.21) require that all eigenvalues satisfy the inequality  $-0.1 \ddot{y} k < 1$  in the discrete case. If the eigenvalues are complex and increasing (3.20) should be carried out for the natural frequencies of the system. As the sphere moves upwards, the estimates (3.20), (3.21) also remain correct, but due to the large value of the magnetic force, they do not impose such stringent constraints on the controller. If the above limitations are not met, even in a very small environment of the operating point, the linear theory will not give predictions consistent with experience. We will then observe

different waveforms when moving down and up, even though the linear model of the system does not provide for such a phenomenon. Inequalities (3.20) and (3.21) give only a rough estimate, however

they show that the system under consideration cannot be accelerated arbitrarily and this limitation should be taken into account during the synthesis of controllers. Figure 3.7 shows the experimental results for the case when condition (3.21) is met, while Figure 3.8 shows the experiment result when condition (3.21) is not met.

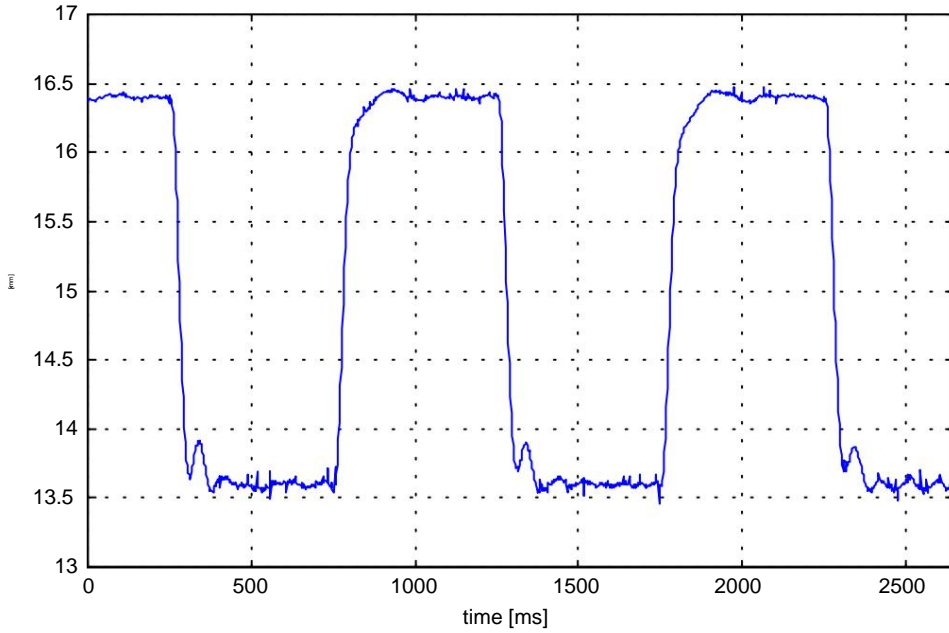


Fig. 3.7. The result of the experiment when condition (3.21) is met.

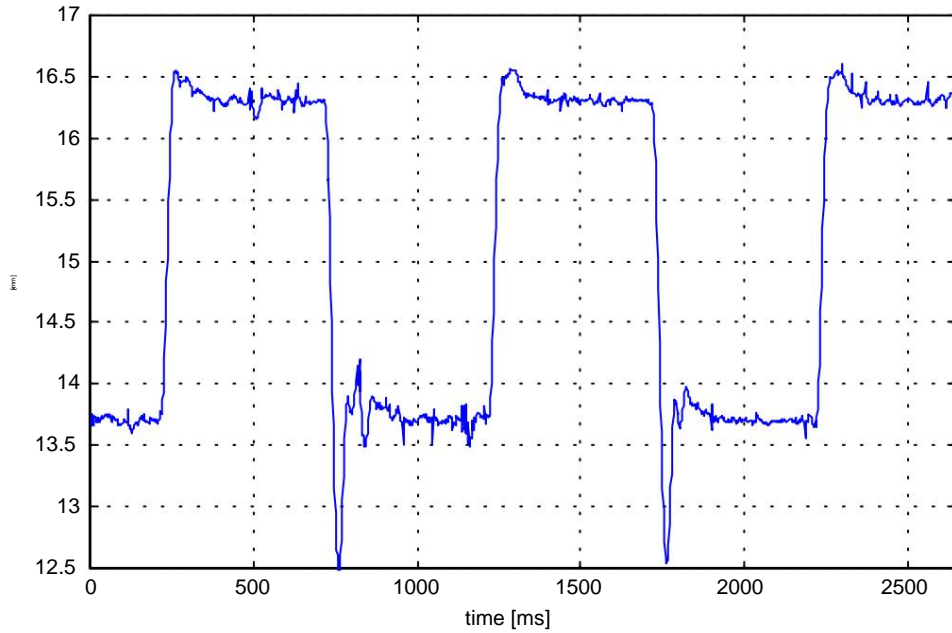


Fig. 3.8. The result of the experiment when condition (3.21) does not apply.

## 4. Identification

The identification of nonlinear models is a source of serious theoretical and practical problems. While for linear models the task of identification is possible most often solved by the least squares method with relatively weak assumptions, in the non-linear case the least squares method generally gives biased parameter estimation [4], and the solution to the task may be ambiguous. The computational complexity of the task is usually very high, because calculating the identification error, i.e. the difference in the response of the model and the object, requires the numerical solution of nonlinear differential or difference equations. If the identified object is unstable, and this is what we are dealing with, it must be stabilized first, but the stabilization task requires knowledge of the model. Identifying a nonlinear model can be greatly simplified by decomposing the problem into simpler subproblems so that each of them has a clear and easy-to-find solution. Analysis of the structure of the object and model and skillful decomposition often allow the identification task to be reduced to several dozen measurements and simple transformations.

algebraic.

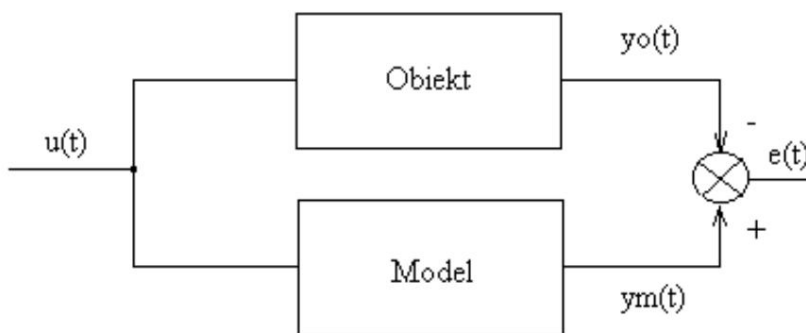
### 4.1. Purpose of identification

The purpose of identification is to determine the parameters  $L(x)$  of the function  $L(x)$  or its derivative, and the characteristics of the position sensor  $g(x)$ . The functions and parameters sought should minimize the quality index

$$JL(x, g(x), \mu, \dots, c) = \int_0^T \|\hat{y} - y(t)\|^2 dt, \quad 0 \leq t \leq T \quad (4.1)$$

$\hat{y}$  is the estimated output,  $y(t)$  is the measured output.

Instead of (4.1), any norm in the output space  $\mathbf{Y}$  can be used. The number of outputs depends on what variables are being observed. In a laboratory setup, position and current can be measured, but the speed of the sphere is not measured.



For the discrete model, we replace the integral (4.1) with the appropriate sum, e.g.

$$\int_{\mu}^{\mu} g(x) dx \approx \sum_{i=1}^{N-1} \bar{y}_i \Delta x_i \quad \text{and } \Delta x_i = T$$

$$y_i = (u_m(t_i), \dots, u_c(t_i))$$
(4.2)

The identification task now takes the form

$$\min_{L(gk, Tu, \dots, uc)} L(gk, Tu, \dots, uc)$$

however, solving it may be very difficult and for the reasons given above, identification will be made using other methods.

## 4.2. Identification of the characteristics of the position sensor

The structure and principle of operation of the position sensor are described in the second chapter. Let us recall that the measure of the distance of the sphere from the electromagnet is the  $ux$  voltage measured by the A/D converter. This voltage is a certain non-linear function of the position  $ux = g(x)$  and it is difficult to give an analytical form of this function. To determine the relationship  $g(x)$  we need to know the position of the sphere. For this purpose, a special base was made on which the sphere is placed. The thread pitch of the adjustment screw is 1.25 mm, so knowing the number of revolutions of the screw can determine the position of the sphere with sufficient accuracy.

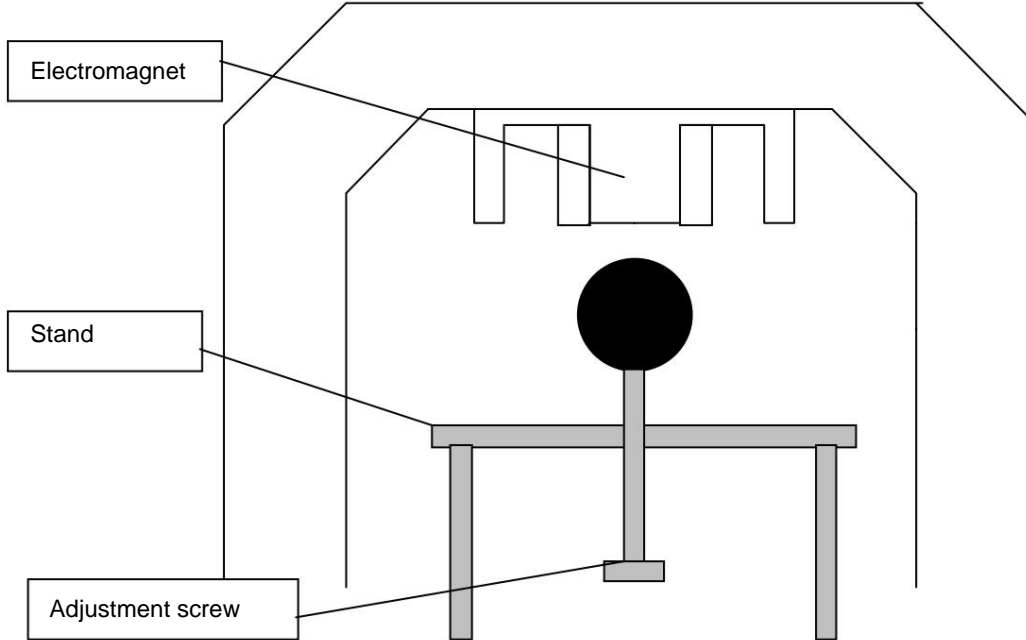


Fig. 4.1. Method of measuring the position of the sphere when identifying the sensor.

Due to the presence of noise, the  $ux$  voltage measurement should be performed over an appropriately long period of time (e.g. 2-3s), and then the measured waveform should be averaged. If the noise is Gaussian, averaging gives good results. You can also use it to eliminate interference an appropriately selected digital low-pass filter [16]. The measurement method is as follows:

1. Attach the sphere to the adjustment screw.
2. Position the sphere so that it is in contact with the electromagnet and is on its axis symmetry.
3. Measure the  $ux$  voltage and save its course.
4. Turn the adjusting screw and note the number of revolutions.
5. Repeat points 3 and 4 until the entire measurement range is covered.

Figure 4.2 shows the sensor characteristics measured in this way and its approximation with a fifth-order polynomial.

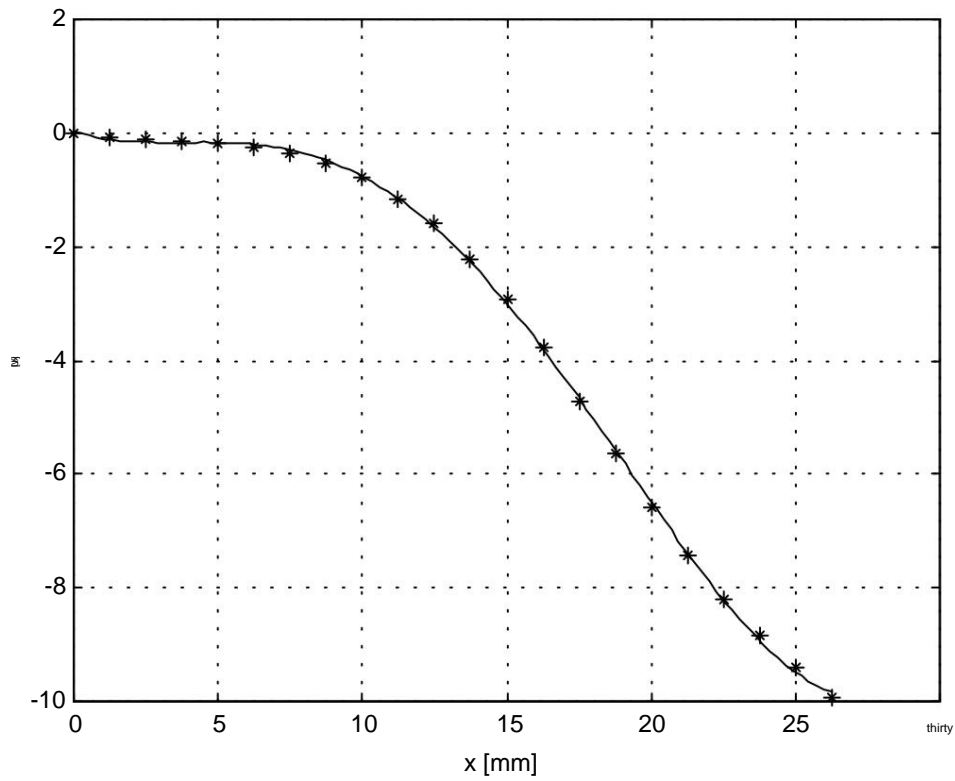


Fig. 4.2. Characteristics of the position sensor,  $\ddot{y}$  - measurement, - approximation

In the range of 0–8 mm, the  $ux$  voltage practically does not change, which in the presence of noise prevents good position measurement in this area. This is a disadvantage of this type of measurement system.

The relationship shown in Figure 4.2 decreases uniformly, so it can be determined the inverse function  $x = g^{-1}(ux)$ , or  $x = h(-ux)$ . Knowing this function we will have directly with the position of the sphere, which will eliminate the function  $g(x)$  from further considerations and simplify the synthesis of regulators. It turns out that the inverse characteristic cannot be well approximated by polynomials, even with high degrees of these polynomials. Therefore, an approximating function was selected by trial and error

$$x = \frac{y}{u} = \frac{at}{1 + ae^{2t}} = \frac{3u}{1 + ae^{3u}} = \frac{2at}{1 + ae^{4t}} = \frac{at}{1 + ae^{5t}} + \frac{a^3 u^3}{6} - \frac{a^5 u^5}{120} + \frac{a^7 u^7}{5040} - \frac{a^9 u^9}{45360} \quad (4.3)$$

Figure 4.3 shows the relationship  $x = h(-ux)$  and its least squares approximation with the function (4.3).

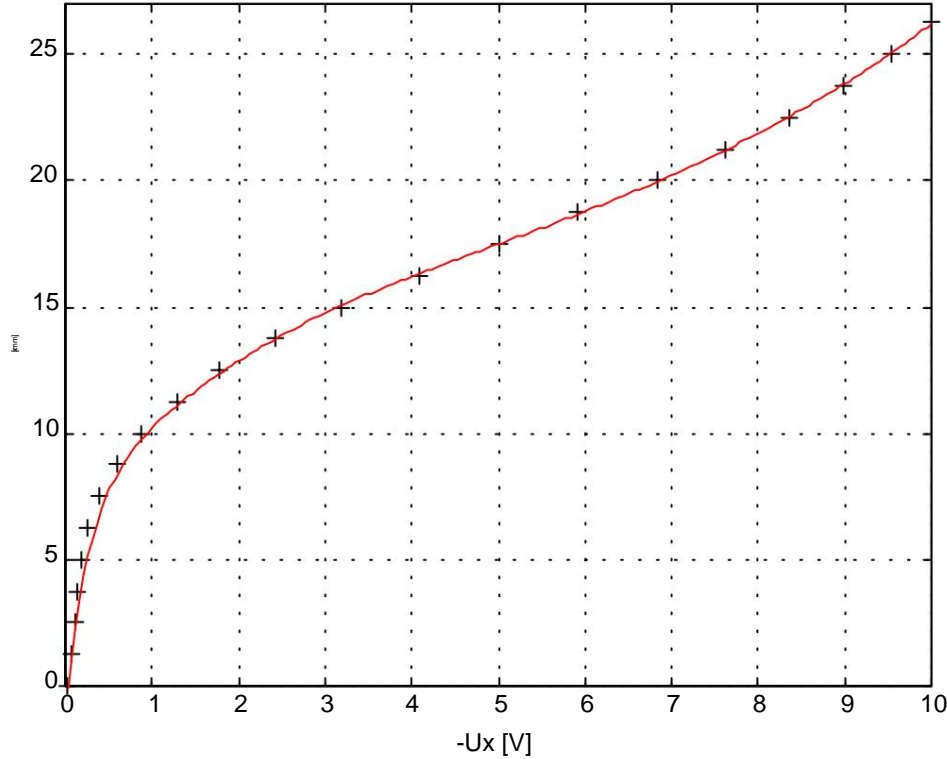


Fig. 4.3. Inverse characteristic of the position sensor.

The files id\_czuj.mdl and inv\_czuj.m are located on the diskette attached at the end of the work.

The first one allows for position measurement and averaging, and the second one is used to determine the coefficients of the function (4.3).

### 4.3. Identification of parameters, $k$ , $u_c$

Equation (3.9) in the steady state predicts a linear dependence of the current on the control voltage.

$$I = ku_c + u_c \quad (4.4)$$

By measuring the current in the coil in the steady state for various control values, we will obtain a sequence of points  $(u, I)$ . Then, using the least squares method, we find the parameters  $k$  and  $u_c$ . In the second chapter it was found that the current measurement has a large error and therefore a digital oscilloscope was used for identification by measuring the voltage drop across the measuring resistor (this resistor is marked with the *shunt* symbol in Fig. 2.4, page 7). Measurement with an oscilloscope ensures greater accuracy and suppression of network interference. Similarly to the identification of a position sensor, a sufficiently large number of samples should be remembered and averaged. Figure 4.4 shows the dependence of the current on the control voltage.

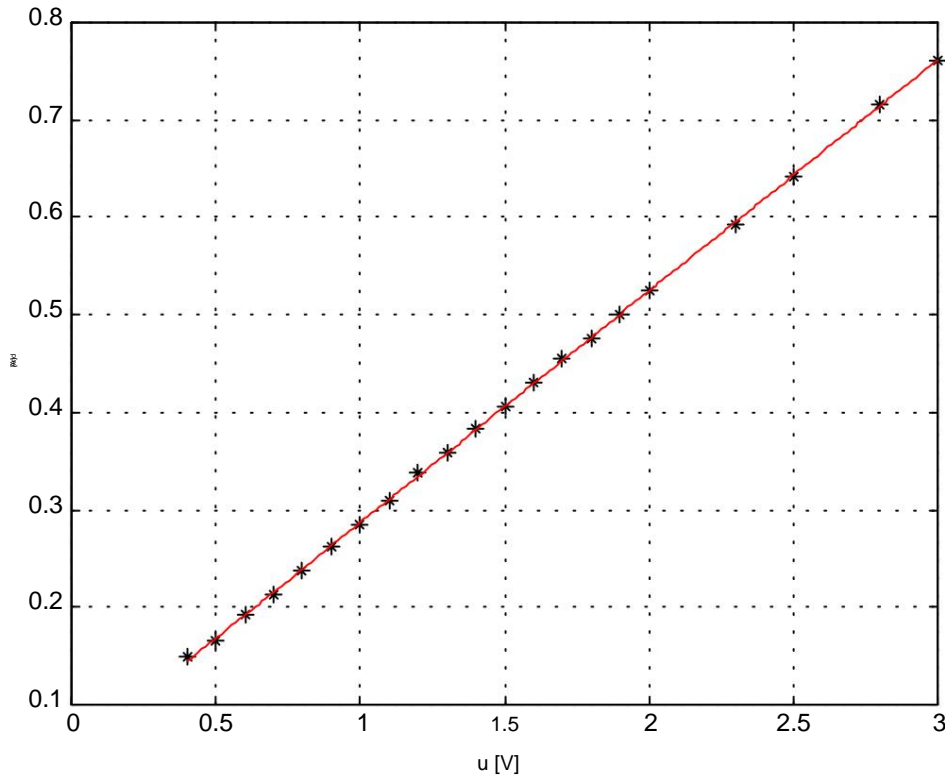


Fig. 4.4. Dependence of the current in the coil on the control voltage, \* - measurement, - approximation.

It can be seen that the characteristic is an almost perfect straight line and replacing the second equation (3.3) with a linear equation (3.5) was justified.

We will determine the time constant  $T$  from the measurement of the step response. Figures 3.3 and 3.4 show the current response to a step change in control. They show that the increase in current in the coil corresponds to a shorter time constant, and its decrease takes place with a longer time constant. This is the result of the non-linearity of the electronic components used.

The  $T$  parameter should be selected to obtain a compromise between a rapid increase in current and a slower decrease in current. Equation (3.9) can be discretized [14],[21].

$$x_i \in \{0, 1, 2, \dots\} \quad (4.5)$$

$$and \quad d = \exp \frac{\bar{y}}{\bar{y}} - \frac{T}{T - \frac{\bar{y}}{\bar{y}}} \quad (4.6)$$

$$bk_d = \frac{\bar{y} \bar{y} \bar{y}}{\bar{y}} \exp \left( -\frac{T_p \bar{y} \bar{y}}{T \bar{y} \bar{y}} \right) \quad (4.7)$$

We select the  $ad$  and  $bd$  parameters to obtain a minimum quality index.

$$J_{ab} = \frac{1}{2} \sum_{i=1}^N (\lambda_i(x))^{2^a} (\lambda_i(x))^{2^b} \quad (4.8)$$

where  $I(i)$  is the value of the current measured at the moment  $iTs$ , and  $x3(i)$  is the solution of equation (4.5). The minimum of the indicator (4.8) is achieved if  $ad$ ,  $bd$  meet the so-called system of Gaussian normal equations [4], [8], [17], [23].

Knowing the parameters  $ad$ ,  $bd$ , the value of the time constant  $T$  is determined from equality (4.6) or (4.7).

Of course, the identification of the parameters of equation (3.9) or (4.5) can be carried out using many other methods, e.g. the instrumental variable method or error prediction [4], [17], and the graphical method also gives good results.

Figure 4.5 shows the response of the object and model with a square drive waveform with a frequency of 20 Hz.

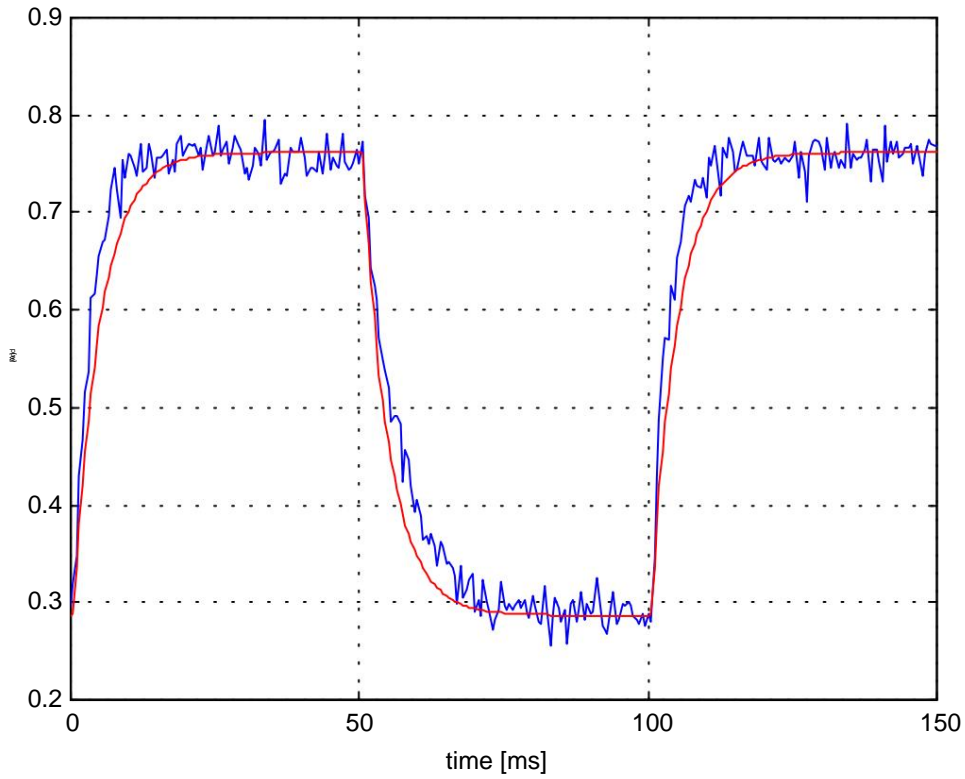


Fig. 4.5. Comparison of the model response in the form of equation (3.9) with the actual current waveform in the coil.

We see that the model behaves well in the steady state, but errors occur in the transient state. Many non-linear first-order equations can be given that better approximate the course in Fig. 4.5, but this involves introducing certain non-physical and difficult-to-interpret parameters into the model, the identification of which may be difficult.

## 4.4. Determination of the dependence of coil inductance on position

According to what was said in sections 3.1 and 3.2, the inductance of the coil is a decreasing function of position. Knowledge of this function or its derivative allows us to determine the magnetic force acting on the sphere. The derivative of the inductance can be calculated from equations (3.16), which describe the steady state of the system. However, achieving a steady state requires the use of a controller to stabilize the system. You can try to determine the controller parameters by trial and error, but in the case of an unstable system, this is a burdensome task. Therefore, the  $L(x)$  relationship was initially determined using the open system method, while the steady state method can be used to determine the magnetic force once we are able to stabilize the system.

Let us assume the following form of the function  $L(x)$  (see chapter 3)

$$L(x) = + \frac{2 \cdot 10 \cdot mg}{ax^3 + b} = -L_0 \quad \frac{2 \cdot 10 \cdot mg}{ax^3 + ab} = -L_0 \quad \frac{2 \cdot 10 \cdot mg}{y \cdot x + y} , ab, y, y, L_0 > \quad (4.10)$$

where  $L_0$  is the inductance of the coil when the sphere is very far from the electromagnet.

The parameters can be found using the least squares method. For this purpose, we transform (4.10) into the form

$$y \cdot x + y = \frac{2 \cdot 10 \cdot mg}{L \cdot x + L_0} \quad (4.11)$$

and we match the straight line to the measurement points. Knowing from patterns

$y$ ,  $y$  we calculate  $a$  and  $b$

$$a = \sqrt{y} \quad (4.12)$$

$$b = \frac{y}{\sqrt{y}} .$$

We will now discuss the method of measuring inductance in an open system. This method involves supplying an electromagnet with alternating voltage and measuring the voltage drop across the coil and the current flowing through it, as shown in Figure 4.6. Using Ohm's law for alternating current, the formula for the coil inductance can be derived [5]

$$L = \frac{1}{y} \sqrt{\frac{AT^2}{R^2}} \quad (4.13)$$

where:

$\omega = 314 \text{ rad/s}$  – frequency of the supply  
 $U$  – effective voltage measured on the coil  
 $I$  – current flowing through the coil in [A],  $R$  – coil resistance.

In order to perform the measurement, the electromagnet was disconnected from the electronic system, which is absolutely necessary, otherwise the electronic part may be damaged.  
devices.

Before measuring the inductance, measure the coil resistance, e.g. with an ohmmeter (during identification,  $R=3.2$  was obtained). Inductance is measured using a non-magnetic base made for this purpose. Note that if it was made of a magnetic material, e.g. steel, we would get incorrect results. The method of using the stand is discussed in section 4.2, and measurements can be performed according to the diagram

1. Attach the sphere to the adjustment screw.
6. Position the sphere so that it is in contact with the electromagnet and is on its axis symmetry.
7. Measure the voltage and current.
8. Turn the adjusting screw and note the number of turns.
9. Repeat points 3 and 4 until the entire measurement range is covered.

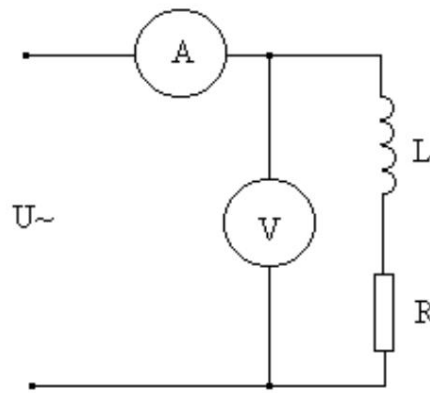


Fig. 4.6. Inductance measurement.

After performing the measurements, we determine the function  $L(x)$  using the equations (4.10), (4.11), (4.12), (4.13) . Figure 4.7 shows the identification result of this method.

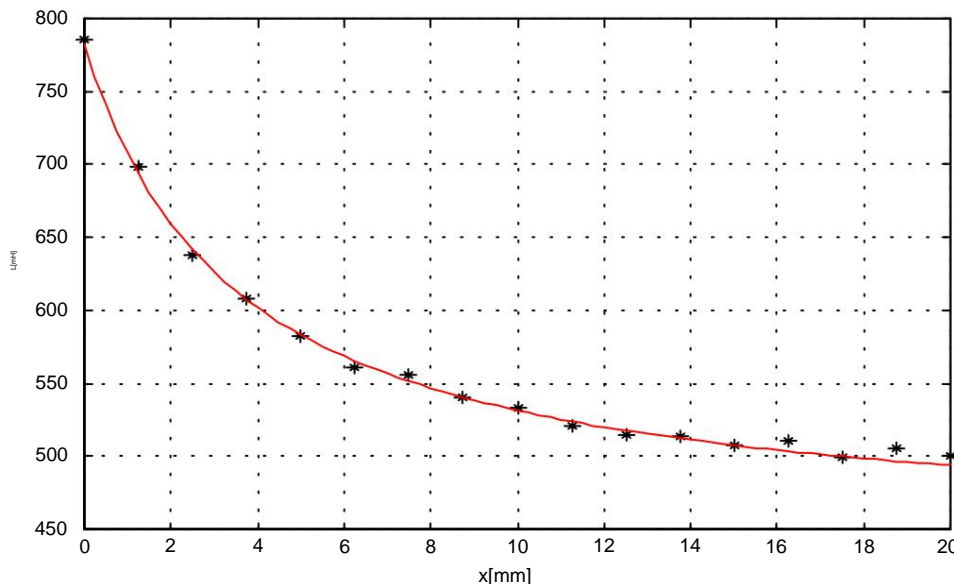


Fig. 4.7. Dependence of coil inductance on position obtained by open system experiment, - measurement, - approximation.

Having a controller stabilizing the system at your disposal, you can use the equations (3.16) to determine the magnetic force. The derivative of the function  $L(x)$  calculated from formula (4.10) is

$$Lx( ) = \frac{2 \cdot 10 \cdot mg^3}{(ax + b)^2} \quad (4.14)$$

hence, from the steady state equation ( 3.16) we have

$$\frac{2 \cdot 10 \cdot g^3}{(ax + b)^2} = \frac{2 \cdot 10 \cdot g^3}{A \cdot \dot{q} \cdot x}$$

by comparing the denominators and taking into account the fact that the current is always positive, we obtain a linear equation

$$b = Ix = ku + c \quad (4.15)$$

The above formula predicts a linear dependence of the steady-state current on the position, and Figure 4.8 proves that this is actually the case.

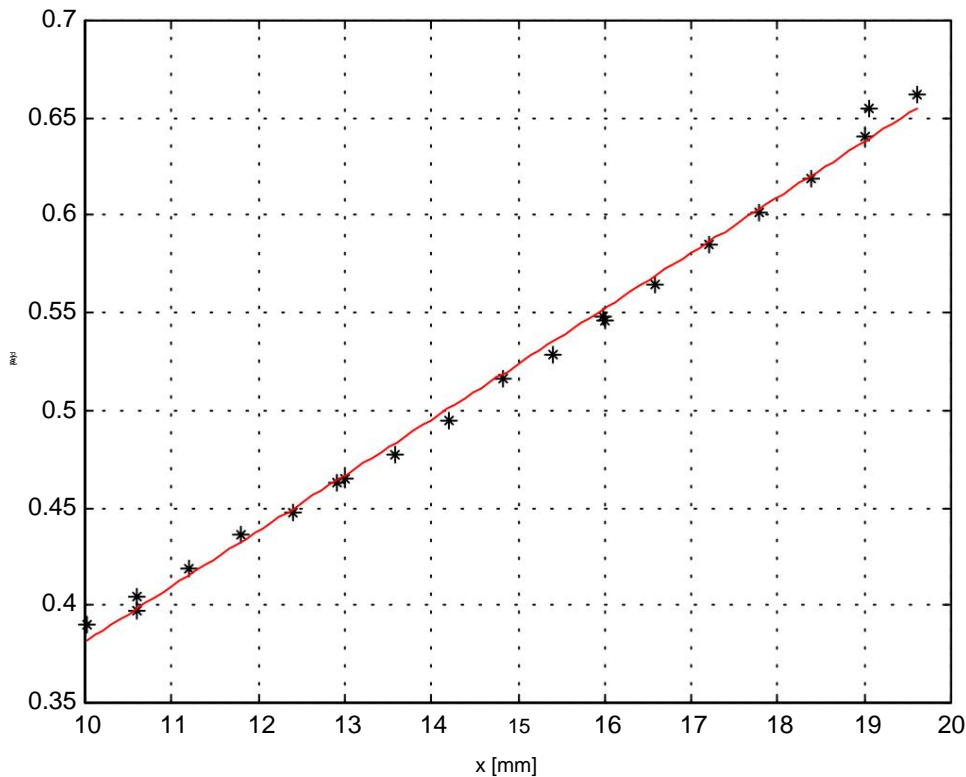


Fig. 4.8. Dependence of current on position in steady state, \* measurement result, - approximation.

We find the coefficients  $a$  and  $b$  using the least squares method. Figure 4.9 compares the results obtained with both methods.

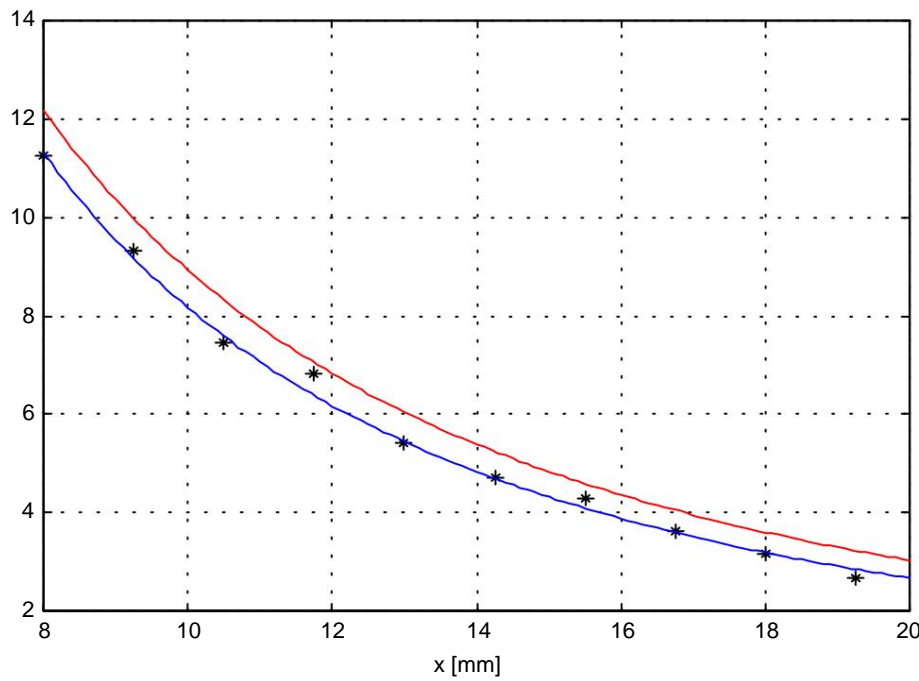


Fig. 4.9. The course of the function  $L'(x)$  obtained by both identification methods. The relationship obtained from the measurement of inductance using the open circuit method is marked in red,  
- measurement using the closed system method, blue – approximation.

Knowledge of the  $L'(x)$  function allows us to determine the course of the magnetic force acting on the sphere depending on the position and current in the coil, which is shown in Figure 4.10. The current in the coil was assumed to be 0.52 A, which approximately corresponds to the steady state  $x_0 = 15 \text{ mm}$ .

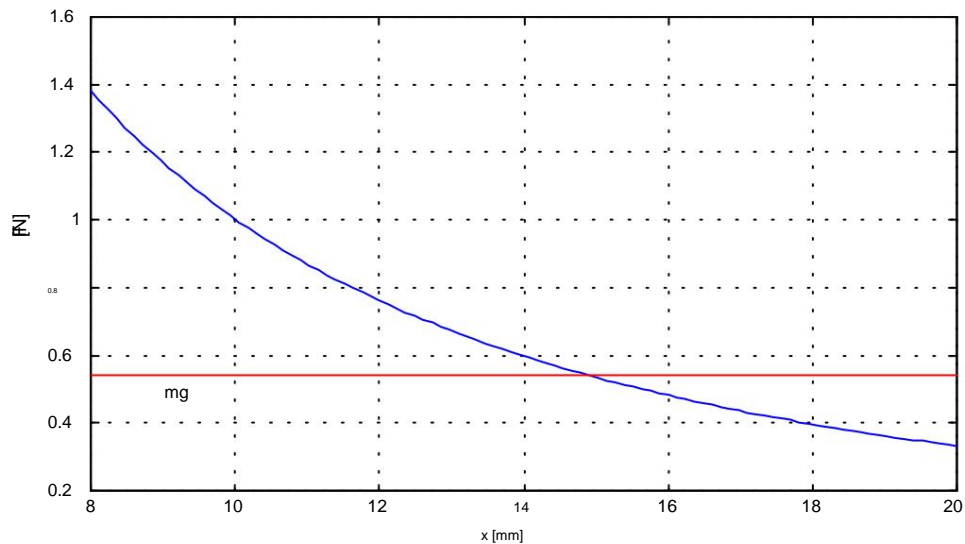


Fig. 4.10. Dependence of force on position calculated based on the model assuming that the current in the coil is 0.52 A  
- The weight of the sphere is marked in red.

Even though the identification relationship  $L'(x)$  carried out using two different methods, gave similar results, each of these methods has its advantages and disadvantages. The method of measuring inductance in an open system requires disassembling the device, assembling the measuring system and is time-consuming. However, it allows the identification of the model at all permissible positions of the sphere and gives a better estimate of the error than the steady-state method. In turn, the method based on the measurement of static characteristics allows you to easily determine the  $L(x)$  function and does not require disassembling the device, but its main disadvantage is the need to stabilize the system first, which is not easy if we do not have a model.

## 4.5. Identification results

Table 4.1. Identification results.

Parameter Value		Comments
$k$	0.2375 [ $\ddot{y}$ -1]	Amplification factor time constant
$T$	6.83 [ms]	ball mass
$M$	55 [g]	constant
$U_c$	0.2077 [V]	voltage prevailing on coil
Function		
$ux = g(x_1)$	$ux \approx -0.0236 + 0.1461x_1 - 0.0419x_1^2 + 0.0045x_1^3 - 0.0001x_1^4$ $c_0 = -0.0236$ $c_1 = 0.1461$ $c_2 = -0.0419$ $c_3 = 0.0045$ $c_4 = -0.0001$	Characteristics of the position sensor
$x_1 = h(-ux)$	$x_1 \approx -7.7518 + 11.3053x_1 - 17.5637x_1^2 + 10.6277x_1^3 - 0.012548x_1^4 - 0.1444x_1^5 + 1.6984x_1^6 + 11.1093x_1^7$ $a_1 = -7.7518$ $a_2 = 11.3053$ $a_3 = 17.5637$ $a_4 = -10.6277$ $a_5 = 0.012548$ $a_6 = -0.1444$ $a_7 = 1.6984$ $a_8 = 11.1093$	Inverse characteristic of the position sensor
$L(x_1)$	$L(x_1) = \frac{39.56}{0.0273x_1 + 0.0908} + 460.2[\text{mH}]$	Dependence of the coil inductance on the ball position
$L'(x_1)$	$L'(x_1) = \frac{1.08}{(0.0273x_1 + 0.0908)^2} [\text{H/m}]$	Derivative of inductance

## 4.6. Model verification

It would be naive to believe that the control stabilizing the model (3.7) - (3.9) will ensure similar, stable behavior of the object and, conversely, the control stabilizing the object will not stabilize the model. Object and model instability, model errors and disturbances will immediately cause stability loss. Therefore, the model can only be verified in a closed system, i.e. by comparing the response of the model with the controller and the response of the object controlled by the same controller. Based on the model, the *PID* controller settings were selected and used to control the facility, and then a model simulation was performed with the same controller. The results are shown in Figures 4.11 and 4.12.

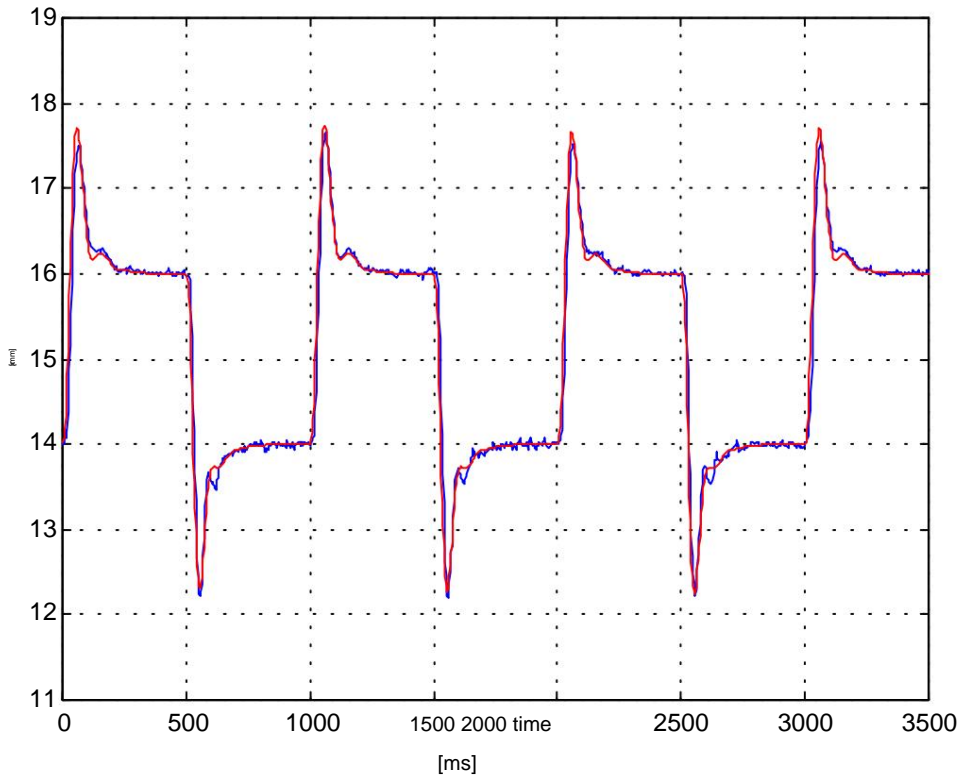


Fig. 4.11. Comparison of model and object responses. The model's response is marked in red. The set value was a square signal with a frequency of 1 Hz.

We see that the model behaves similarly to the object, but not in the same way. The most probable reasons for these differences are:

- Approximation of the nonlinear electronic system with a coil with a simple model linear .
- The impact of disturbances affecting the object, which are reproduced during the simulation impossible.
- Identification errors.
- The assumption of no saturation in the core of the electromagnet, which means , that stream magnetic is exactly proportional to current, which never happens in reality.
- Omission of certain components of the object's dynamics, e.g. vibrations of the ball in the horizontal direction.

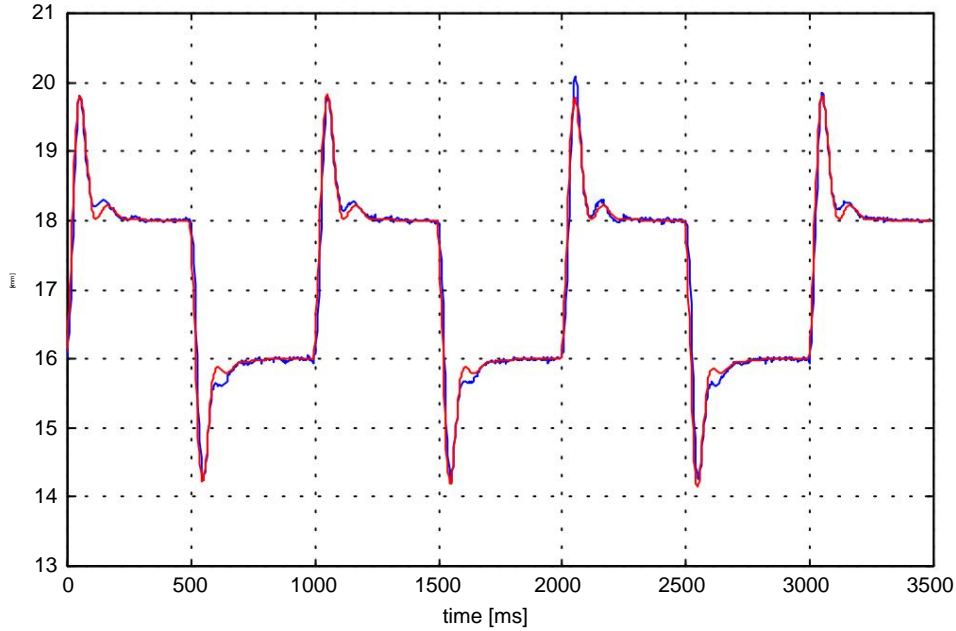


Fig. 4.12. Comparison of model and object responses. The model's response is marked in red. The set value was a square signal with a frequency of 1 Hz.

Since the value of the time constant  $T = 6.83\text{ms}$  is small compared to the duration of the transients, the third equation of the model could be omitted. Such an attempt was made, but as it turned out (Fig. 4.13 and 4.14), the model simplified in this way did not provide good agreement with the experiment.

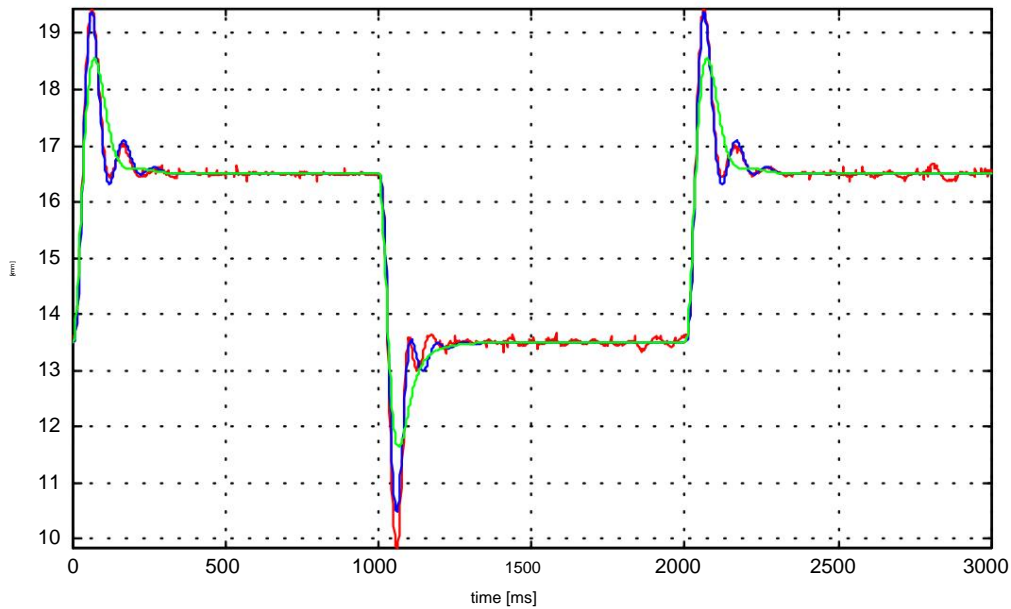


Fig. 4.13. Comparison of model and object responses. Red indicates the answer object, and blue is the model's response. The answer is marked in green model with equation (3.9) omitted. The set value was a square wave signal with a frequency of 0.5Hz.

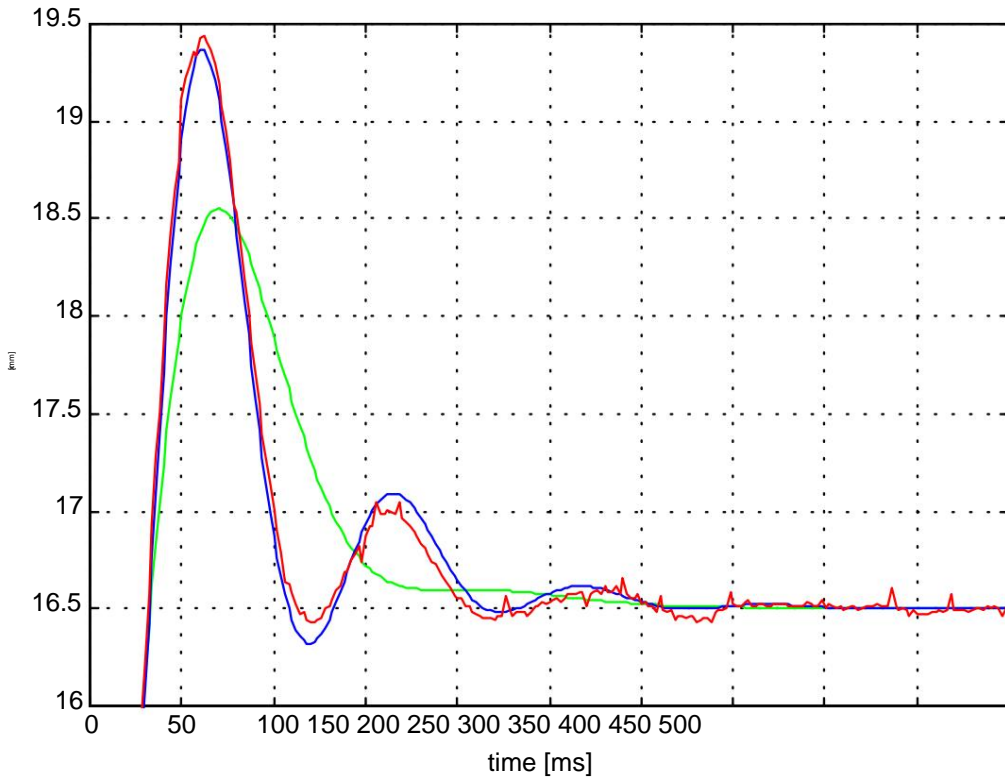


Fig. 4.14. The initial fragment of the waveforms from Figure 4.13.

The value of the quality index (4.2) calculated for the course marked in blue in Figure 4.13 was  $J1 = 1.2754$ , while if the third equation of state was omitted,  $J2 = 32.4992$  was obtained. It follows that the model cannot be simplified by removing the third equation of state.

The question is whether taking into account the above-mentioned factors would increase compliance model with experience remains open. However, it is certain that further expansion of the model will make its identification much more difficult or even impossible, and will also complicate the theoretical analysis of the model's properties and the synthesis of controllers. The sixth chapter on control is an indirect confirmation of the adequacy of the model, because all controllers selected on its basis operated in accordance with the theory's predictions.

# 5. Linearized model and linear discrete model

Most regulator synthesis methods are based on linear models. General stabilization methods are known for this class of systems, and the synthesis of the controller is most often reduced to: to solve algebraic equations. The linear model provides information about the local behavior of an object in a certain environment of a selected operating point [14], [21], [23], [24]. In this chapter, we will derive a linear model and analyze its basic properties.

## 5.1. Linearization of the equations of state in the vicinity of the operating point.

Let  $x_0(t) = [x_{10}(t), x_{20}(t), x_{30}(t)]^T$  denote a certain solution of the equations of state (3.7)-(3.9) such that the constraints (3.11) - (3.14) are satisfied, and let  $u_0(t)$  be the control corresponding to this solution. In particular,  $x_0(t), u_0(t)$  can mean steady state determined from equality (3.16). Based on formula (4.10) and the considerations contained in section 3.3, page 19, we can conclude that the right side of the state equations is of class C with respect to both arguments, so it can be expanded into an infinite power series with respect to trajectory and control deviations from the  $x_0(t)$  solution, and control  $u_0(t)$ .

This expansion has the form

$$\begin{aligned} \frac{d}{dt} \begin{pmatrix} \ddot{x}_1 \\ x_2 \\ \ddot{x}_3 \end{pmatrix} &= \begin{pmatrix} \ddot{y}_1 \\ \ddot{y}_2 \\ \ddot{y}_3 \end{pmatrix} + \begin{pmatrix} 0 & 0 & 0 \\ 0 & 0 & b \\ 0 & b & 0 \end{pmatrix} \begin{pmatrix} \dot{x}_1 \\ \dot{x}_2 \\ \dot{x}_3 \end{pmatrix} + \begin{pmatrix} 0 \\ 0 \\ 0 \end{pmatrix} \quad (5.1) \\ \ddot{y}_1 &= \frac{1}{2m} L \dot{x}_1^2 > 0 \\ \ddot{y}_2 &= \frac{1}{m} L \dot{x}_2^2 > 0 \\ \ddot{y}_3 &\stackrel{1}{\Rightarrow} 0 \\ b &= \frac{k}{T} \quad 0 \end{aligned}$$

where  $x_1, x_2, x_3$ , contains  $u$  now denote deviations from the point  $x_0(t), u_0(t)$ , and the function  $d(x_1, x_3)$  only terms of order higher than the first one and can be presented in the following form

$$d(x_1, x_3) = \frac{x_{30}^2}{2mk_{k=2}} - \frac{1}{k!} (L \dot{x}_1^2)_{10}^{k+1} + \frac{x_{30}}{mk_{k=1}} \ddot{y}_3 - \frac{1}{k!} (L \dot{x}_1^2)_{10}^k + \frac{1}{2mk_{k=0}} \ddot{y}_3 - \frac{1}{k!} (L \dot{x}_1^2)_{10}^k. \quad (5.2)$$

It's easy to show that

$$\frac{\|dx_1, x_3\|_3}{\|x\|} \rightarrow 0$$

from which it follows that for small deviations from the point  $x_0, u_0$ , the dominant component in (5.1) is the linear part and it will determine the local behavior of the solution of the equations

state. Let us also note that if  $x_0, u_0$  is determined from equality (3.16), the parameters are constant. In the general case, when  $x_0$  and  $u_0$  depend on time (this will be the case, for example, they will be certain functions of solving the keeping-up task), coefficients entail non-stationarity in time, which of the linear model.

Omitting the nonlinear terms in (5.1) and assuming that  $x_0$ ,  $u_0$  do not depend on time we can write a stationary linear model

$$\begin{aligned}
 \frac{dx(t)}{dt} &= Ax(t)Bu(t) \\
 x(\bar{y}) &= \begin{pmatrix} 0 & 0 & 0 \\ 0 & 0 & 0 \\ 0 & 0 & 0 \end{pmatrix} \begin{pmatrix} 1 \\ 0 \\ 0 \end{pmatrix} \begin{pmatrix} 0 & 0 & 0 \\ 0 & 0 & 0 \\ 0 & 0 & 0 \end{pmatrix} \begin{pmatrix} 0 \\ 0 \\ 0 \end{pmatrix} = 0 \\
 \text{AND} &= \begin{pmatrix} 1 & 0 & 0 \\ 0 & 1 & 0 \\ 0 & 0 & 1 \end{pmatrix} \\
 &= \begin{pmatrix} 0 & 0 & 0 \\ 0 & 0 & 0 \\ 0 & 0 & 0 \end{pmatrix} \\
 B &= \begin{pmatrix} 0 & 0 & 0 \\ 0 & 0 & 0 \\ 0 & 0 & 0 \end{pmatrix} \\
 &= \begin{pmatrix} 0 & 0 & 0 \\ 0 & 0 & 0 \\ 0 & 0 & 0 \end{pmatrix} \\
 C &= \begin{pmatrix} 0 & 0 & 0 \\ 0 & 0 & 0 \\ 0 & 0 & 0 \end{pmatrix} \\
 D &= 0
 \end{aligned} \tag{5.3}$$

The coefficients  $b$  are given by the equalities (5.1). The form of the C matrix may change depending on the observed variables, but knowledge of the inverse characteristics of the position sensor allows us to assume that the observed variable is directly the position of the sphere.

## 5.2. Controllability and observability

The controllability matrix [14],[21] of system (5.3) has the form

$$Q\bar{B}A|B AB \quad , \quad ]^2 = \begin{matrix} \bar{y}^0 & 0 \\ 0 & \bar{y}^b b \bar{y} \\ \bar{y}^b & \bar{y}^b \end{matrix}, \quad (5.4)$$

and the controllability condition,  $\text{Order}(Q)=3$ , is met when

$$\det(\mathbf{A})Q = \vec{y}^T b \quad \vec{y}^T \vec{y} > 0 \quad (5.5)$$

Observability matrix

$$S = \begin{vmatrix} \ddot{y} & C^T & \ddot{y} & \ddot{y} & 1 & 0 & 0 \\ & CA & & & 0 & 1 & 0 \\ & CA^2 & & & 0 & \ddot{y} & \ddot{y} \end{vmatrix}, \quad (5.6)$$

has full row when

$$\det(S) = \ddot{y} \quad \ddot{y} \quad \ddot{y} \quad 0. \quad (5.7)$$

It is therefore clear that the system (5.3) is controllable and observable. Controllability and observability ensure the existence and uniqueness of the solution to the linear-quadratic problem and enable setting eigenvalues and restoring the state [14],[18],[21],[24].

### 5.3. Eigenvalues of the state matrix, transfer function and solution of the equations of the linear model.

We will now determine the eigenvalues of the state matrix, the fundamental matrix  $e^{At}$ , and system transmittance. The eigenvalues of matrix  $A$  satisfy the characteristic equation

$$\det(sI - A) = 0$$

$$(sI - A) = \begin{vmatrix} s & p & 1 & 0 & \ddot{y} \\ & \ddot{y} & p & \ddot{y} & \\ & & & & \\ & & 0 & 0 & p + \ddot{y} \end{vmatrix},$$

by calculating the determinant we get

$$\det(sI - A) = s^2 - \ddot{y}(s + \ddot{y})(s + \sqrt{\ddot{y}})(s + \sqrt{-\ddot{y}}), \quad (5.8)$$

from where we can see that matrix  $A$  is unstable (see e.g. [21]) and has real eigenvalues. Equality (5.1) shows that two of these values  $s_1 = -\ddot{y}$  and  $s_2 = \sqrt{-\ddot{y}}$  depend on the choice of the equilibrium point (operating point), while the third one  $s_3 = 0$  is constant. This dependency

is illustrated in Figure 5.1, which shows the values of the time constant  $T = 1/s_1$  as a function of position. We see that as we move away from the electromagnet, the value of the time constant increases and at a distance of 25 mm it is almost three times greater than near zero. This means that close to the coil the system is almost three times faster than at the maximum distance from the sphere. Consequently, it is more difficult to achieve stabilization for operating points close to zero. Figure 5.2 shows how the eigenvalues change when the operating point changes. Due to large changes in the parameters of the linear model depending on the selected linearization point, this model will be adequate only in a small environment of the operating point. As a consequence, regulators whose synthesis will be based on a linear model may

stabilize the system in a very small area around the linearization point.

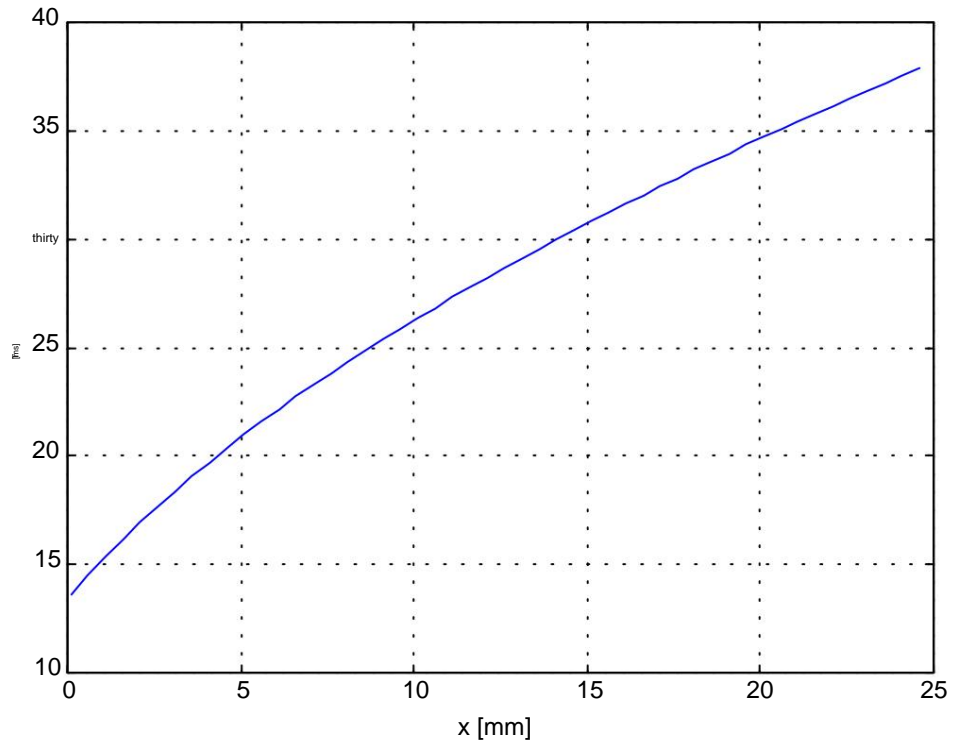


Fig. 5.1. Dependence of the time constant on the choice of the linearization (work) point.

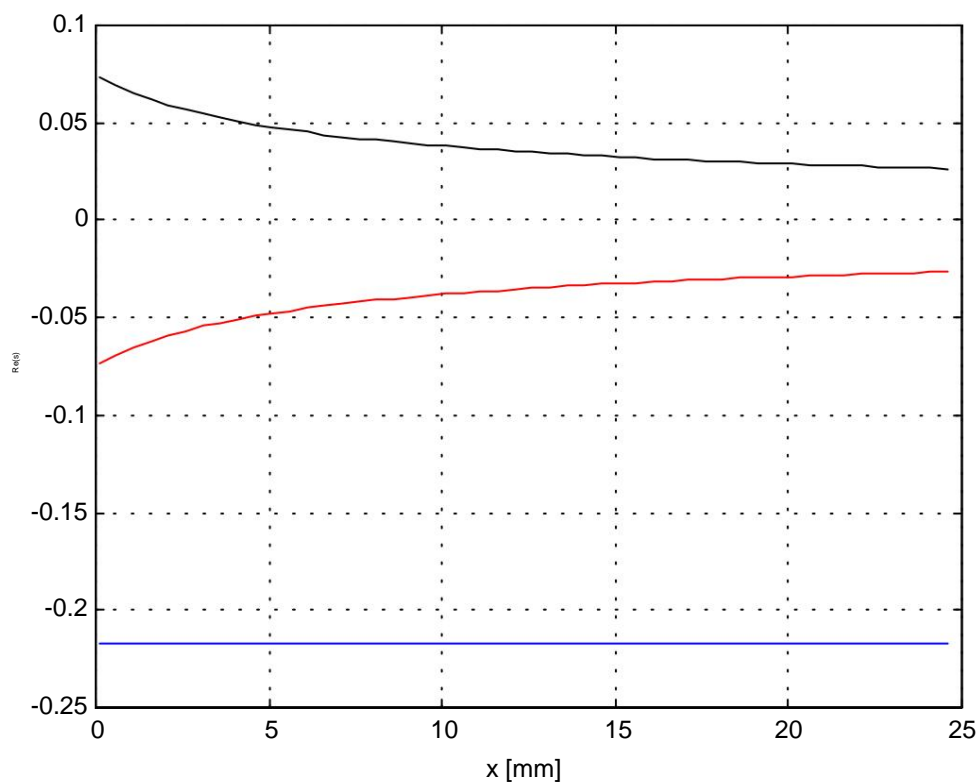


Fig. 5.2. Location of eigenvalues depending on the choice of linearization point. Red color s1, black color s2, blue color s3.

Fundamental matrix  $e^{At}$  we calculate using the Laplace transformation method [14],[21],[24] using the formula

$$= L^{-1}\{sI - \tilde{A}^{-1}\} \{(\quad \quad \quad )^{\tilde{y}^1} e^{\tilde{y}} ,$$

where  $L^{-1}\{sI - A\}^{-1}$  means the inverse Laplace transform of the function

$$\begin{pmatrix} \tilde{y} & p & 1 & \tilde{y} & \tilde{y} \\ & \frac{p}{\tilde{y}} & \frac{1}{\tilde{y}} & (\tilde{y}^2 + p^2) & \tilde{y} \\ & \tilde{y} & \tilde{y} & \tilde{y}^2 & \tilde{y} \\ (sI - \tilde{A})^{-1} & \frac{\tilde{y}}{\tilde{y}^2 + p^2} & \frac{p}{\tilde{y}^2 + p^2} & \frac{\tilde{y}^2}{(\tilde{y}^2 + p^2)(1 + \tilde{y}/p)} & \tilde{y} \\ 0 & 0 & \frac{1}{\tilde{y}^2 + p^2} & \frac{1}{(1 + \tilde{y}/p)^2} & \tilde{y} \\ \tilde{y} & & & & \tilde{y} \end{pmatrix}.$$

By calculating the inverse transform, we get:

$$e^{At} = \begin{pmatrix} \tilde{y} & \cosh \sqrt{\tilde{y}} & \frac{\sinh(\sqrt{\tilde{y}})}{\sqrt{\tilde{y}}} & \frac{\tilde{y}}{\tilde{y}^2 + p^2} \cosh \sqrt{\tilde{y}} & \frac{\tilde{y}}{\sqrt{\tilde{y}}} \sinh(\sqrt{\tilde{y}}) & \tilde{y} \\ & & & \tilde{y} & & \tilde{y} \\ & & & \tilde{y} & & \tilde{y} \\ & & & \tilde{y} & & \tilde{y} \\ & & 0 & 0 & e^{\tilde{y}} & \tilde{y} \\ \tilde{y} & & & & & \tilde{y} \end{pmatrix}. \quad (5.9)$$

Knowing the fundamental matrix, we can write the general solution of equations (5.3)

$$x(t) = e^{At} \int_0^t \tilde{y} e^{A(t-\tau)} B u d\tau. \quad (5.10)$$

Applying the Laplace transformation to equations (5.3) with zero initial conditions, we obtain the transfer function of the system

$$G(p) = \frac{Y(s)}{At(s)} = C \tilde{A}^{-1} B = \frac{b\tilde{y}}{(p^2 + \tilde{y})(p + \tilde{y})}. \quad (5.11)$$

The negative sign in (5.11) means that the effect of positive control is to bring the sphere closer to the electromagnet.

Note: If shows that  $\tilde{y} = \tilde{y}^2$ , then this case should be considered separately. However, Figure 5.2 this is not the case.

## 5.4. Linear discrete model

Assuming that the control is constant intervals and the A/D and D/A converters are working synchronously with the  $T_s$  period, we can discretize [21] equations (5.3)

$$\begin{aligned}
 1) \quad & x(t) = Ax(t) + Bu(t) \quad (5.12) \\
 & y(t) = Cx(t) + Du(t) \\
 & x(0) = R \quad x_i \in \mathbb{R}^3, \quad i = 1, 2, 3, \dots
 \end{aligned}$$

where  $x(i)$  denotes the solution of equation (5.3) at time  $t = iT_s$ .

We determine the  $AD$ ,  $BD$ ,  $CD$ ,  $DD$  matrices using the formulas

$$\begin{aligned}
 A_D &= e^{AT_p} \\
 B_D &= \int_0^{T_p} e^{At} B dt \\
 C_D &= \\
 D_D &= 0
 \end{aligned} \tag{5.13}$$

Performing the appropriate calculations leads to

$$\begin{aligned}
 A_D &= \frac{\sinh(\sqrt{y} T_p)}{\sqrt{y}} \quad \frac{\cosh(\sqrt{y} T_p)}{\sqrt{y}} \quad \frac{\sinh(\sqrt{y} T_p)}{\sqrt{y}} \quad \frac{\cosh(\sqrt{y} T_p)}{\sqrt{y}} \quad \frac{\sinh(\sqrt{y} T_p)}{\sqrt{y}} \quad \frac{\cosh(\sqrt{y} T_p)}{\sqrt{y}} \\
 &= \frac{\sinh(\sqrt{y} T_p)}{\sqrt{y}} \cosh(\sqrt{y} T_p) \quad \frac{\cosh(\sqrt{y} T_p)}{\sqrt{y}} \quad \frac{\sinh(\sqrt{y} T_p)}{\sqrt{y}} \quad \frac{\cosh(\sqrt{y} T_p)}{\sqrt{y}} \quad \frac{\sinh(\sqrt{y} T_p)}{\sqrt{y}} \quad \frac{\cosh(\sqrt{y} T_p)}{\sqrt{y}} \\
 &= 0 \quad 0 \quad e^{-\sqrt{y} T_p} \\
 B_D &= \frac{b}{y^2} \frac{1}{\sqrt{y}} \sinh(\sqrt{y} T_p) \quad \frac{y}{y^2} \cosh(\sqrt{y} T_p) + \frac{1}{y} e^{-\sqrt{y} T_p} \quad \frac{1}{y} \frac{y}{y} \\
 &= \frac{b}{y^2} \frac{1}{\sqrt{y}} \sinh(\sqrt{y} T_p) \quad \frac{y}{y^2} \cosh(\sqrt{y} T_p) + \frac{1}{y} e^{-\sqrt{y} T_p} \quad \frac{b}{y} (1 - e^{-\sqrt{y} T_p})
 \end{aligned}$$

Let  $\lambda_i$  denote the eigenvalue of the  $AD$  matrix, if  $Ts/m(2j)=0, k=0,2,\dots$  then the controllability of the pair  $(A,B)$  implies the controllability of the pair  $(AD,BD)$ , and 1, the observability of the pair  $(C,A)$  entails the observability of the pair  $(CD,AD)$  [21]. It is easy to see that for  $\lambda_i$ , the above condition is not met in the  $AD$  and  $BD$  matrices

$$\sqrt{\lambda_i} = \lambda_i$$

infinities appear. However, it turns out (see Fig. 5.2) that in the system under consideration, the state matrix  $A$  always has single eigenvalues and the discrete system is controllable and observable.

Let  $AD = f(A)$ , where  $A$  and  $B$  are square matrices, and let  $f()$  be an analytical function. Then we can write

$$AD = \sum_{k=0}^{\infty} c_k A^k$$

If  $\lambda_i$  is the eigenvalue of the matrix  $A$ ,  $v_i$  is the eigenvector corresponding to the eigenvalue

and this

$$Ad_i v = \lambda_i v = \sum_{k=0}^{\infty} c_k \lambda_i^k v = c_0 \lambda_i^0 v + \sum_{k=1}^{\infty} c_k \lambda_i^k v = c_0 v + \sum_{k=1}^{\infty} c_k \lambda_i^k v$$

from which it follows that the  $\lambda_i$  are the eigenvalues of the  $AD$  matrix. In the considered number  $f()$  is the case

$$A_D e^{-ATs}$$

therefore, the  $AD$  matrix has the following eigenvalues

$$\text{from } \overline{1} \quad \sqrt{\lambda_1} Ts, \text{ from } \overline{2} \quad \sqrt{\lambda_2} Ts, \text{ from } \overline{3} \quad \sqrt{\lambda_3} Ts$$

The discrete system (5.12) has similar properties to the continuous system (5.3).

The eigenvalues of the  $AD$  matrix are real positive and single, two eigenvalues  $z_1, z_2$  depend on the choice of the linearization point and lie symmetrically relative to the point (1,0), while the third one  $z_3$  remains constant. As you move away from the electromagnet, the system becomes slower. Figure 5.3 shows the dependence of the eigenvalues on the selection of the operating point, calculated on the basis of the model, with a sampling period of 2 ms. As you can see, the further from the electromagnet, the closer the eigenvalues are to unity, which means that the system is slower than for positions close to zero. The  $AD$  matrix is unstable because one of the eigenvalues always lies outside the unit circle.

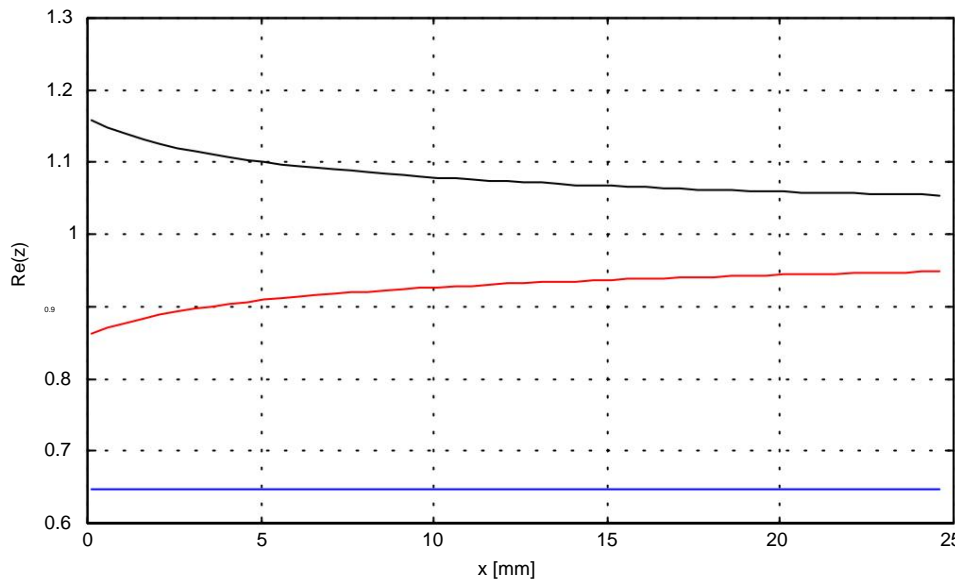


Fig. 5.3. Dependence of the eigenvalues of the  $AD$  matrix on the choice of the linearization point. Black color  $z_1$ , red color  $z_2$ , blue color  $z_3$ .

A complex function defined by equality

$$X(z) = \sum_{n=0}^{\infty} x(n) z^{-n} \quad (5.14)$$

we call  $Z$  – the sequence transform

$$x(0), x(1), x(2), \dots$$

and it is defined for those *with* the  $\Re - C$ , for which the series (5.14) converges. Properties  $Z$  transformation , see [14],[21],[24].

The  $Z$  transformation applied to equations (5.12) with zero initial conditions determines the discrete transfer function of the system

$$G(z) = \frac{Y(z)}{U(z)} = C \cdot \frac{z^3 + a_2 z^2 + a_1 z + a_0}{z^3 + b_2 z^2 + b_1 z + b_0} \quad (5.15)$$

Multiplying the transform by  $z^{-1}$  is equivalent to shifting the signal by one sample backwards, i.e.  $z^{-1}X(z) = x(i-1)$ . It is convenient to write the expression (5.15) in the form (see e.g. [23])

$$y(i) = \frac{B(z^{-1})}{U(z^{-1})}(u(i)) = \frac{b_0 z^{-1} + b_1 z^{-2}}{1 + a_2 z^{-1} + a_1 z^{-2} + a_0 z^{-3}} u(i), \quad (5.16)$$

which is equivalent to the difference equation

$$+ b_1 y(i-1) + b_0 y(i-2) + a_2 y(i-2) + a_1 y(i-1) + a_0 y(i) = b_0 u(i) \quad (1) \quad (2) \quad .$$

Such an equation is known in the literature [4], [23] as the ARMA model ( Auto Regressive Moving Average ). This model defines the output at time  $i$  as a linear function of previous outputs and controls.

## 6. Controls

In the previous chapters, a mathematical model of the magnetic levitation phenomenon was formulated and the constraints imposed on the control and the state vector were discussed. Since the object is unstable, we will mainly focus on its stabilization using various methods, and then compare the controllers that stabilize the system. As criteria characterizing the quality of the control algorithm, we will assume the area of attraction of the balance point, the ability to shape dynamic properties and computational complexity

algorithm.

### 6.1. PID algorithm

*PID* control is one of the simplest methods of control, however it turns out that in the case under consideration it does not allow to obtain the desired properties of a closed system.

Let us consider the system described by equations (5.3), with additional considerations disturbances  $z1(t)$ ,  $z2(t)$  occurring in equations (3.7) – (3.9)

$$\begin{aligned} \frac{d}{dt} \begin{pmatrix} \ddot{x}_1 \\ x_2 \\ x_3 \end{pmatrix} &= \begin{pmatrix} \ddot{y}_1 \\ \ddot{y}_2 \\ \ddot{y}_3 \end{pmatrix} = \begin{pmatrix} \ddot{y}_1 \\ \ddot{y}_2 \\ \ddot{y}_3 \end{pmatrix} + \begin{pmatrix} 0 \\ 0 \\ 0 \end{pmatrix} \\ yx &= \begin{pmatrix} 1 \\ 1 \\ 1 \end{pmatrix} \end{aligned} \quad (6.1)$$

The disturbance  $z1(t)$  represents the external forces acting on the sphere resulting from vibrations ground of air movements, etc., while  $z2(t)$  expresses the fact that certain voltages are induced in the coil, which are not the result of control. These voltages are generated by other external devices, the power supply network, etc. The regulation algorithm has the form

$$u = k_x w - k_x \ddot{x} + \sum_{i=1}^n \dot{y}_i \quad (6.2)$$

where  $w$  is the set value.

Since we assume that the set value can be a continuous function with intervals, differentiating the control error would give theoretically infinite, but practically very large control values. Then the control does not fit within the constraints and the system cannot be analyzed using linear methods. Therefore, formula (6.2) deviates from the classic *PID algorithm*, which differentiates the control error.

Assuming a new state

$$\frac{dx}{dt} = \begin{pmatrix} 0 \\ 0 \\ 0 \end{pmatrix} + \begin{pmatrix} 10th century \\ 1 \\ 1 \end{pmatrix} \quad (6.3)$$

and using (6.1), (6.2) we will obtain the equations of a closed system

$$\begin{aligned} \frac{d}{dt} \begin{pmatrix} \ddot{x}_1 \\ x_2 \\ x_3 \\ \ddot{x}_4 \end{pmatrix} &= \begin{pmatrix} 0 & 1 & 0 & 0 \\ 0 & 0 & 1 & 0 \\ b_k k_{Mr} & d & 0 & 0 \\ 0 & 0 & 0 & 0 \end{pmatrix} \begin{pmatrix} \ddot{x}_1 \\ x_2 \\ x_3 \\ \ddot{x}_4 \end{pmatrix} + \begin{pmatrix} 0 \\ 0 \\ b_k k_{Mr} \\ 0 \end{pmatrix} \ln \dot{y} \\ &\quad + \begin{pmatrix} 0 \\ 0 \\ 0 \\ 0 \end{pmatrix} \begin{pmatrix} \ddot{y} \\ \ddot{y} \\ \ddot{y} \\ \ddot{y} \end{pmatrix} \end{aligned} \quad (6.4)$$

and the bills take into account that

$$\frac{dx_1}{dt} = x_2.$$

Applying the Laplace transformation to this equation, we will obtain a transfer function description

$$G_p_{yw}(\omega) = \frac{b_k k_{Mr}}{\omega^4 - (b_k k_{Mr})^2 s^2 - (b_k k_{Mr}) s b_k k_{Mr}} \quad (6.5)$$

$$G_p_{y'1}(\omega) = \frac{\omega^4 + \omega^2}{\omega^4 - (b_k k_{Mr})^2 (\omega^2 + \omega^2) - (b_k k_{Mr}) s b_k k_{Mr}} \quad (6.6)$$

$$G_p_{y'2}(\omega) = \frac{b_k k_{Mr}}{\omega^4 - (b_k k_{Mr})^2 (\omega^2 + \omega^2) - (b_k k_{Mr}) s b_k k_{Mr}} \quad (6.7)$$

From (6.5) it follows that system stabilization can be achieved using a *PID* controller and cannot be done using the *P*, *PI* or *PD* algorithm. Indeed, if any of the coefficients  $k_p$ ,  $k_i$ ,  $k_d$  was equal to zero, the assumptions of the Hurwitz stability criterion [14] are not met. Additionally, at  $k_i = 0$  the transfer function degenerates (the common factor  $s$  in the numerator and denominator is shortened) and observability is lost. Let's assume that we know the coefficients  $k_p$ ,  $k_i$ ,  $k_d$  that ensure stable operation of the system. If the set value changes abruptly  $w = w_0(t)$ , the controller reduces the error to zero

$$\lim_{\omega \rightarrow \infty} (w \omega^{-1}) \lim_{\omega \rightarrow 0} G_p_{yw}(\omega) = 0 \quad (6.8)$$

In a similar way, using (6.6), (6.7) it can be shown that the controller compensates for constant disturbances  $z_1$  and  $z_2$ .

We will now analyze the stability of equation (6.4) or what comes to the same (6.5). The  $k_p$ ,  $k_i$ ,  $k_d$  parameters can be used to determine the stability region in the parameter space Hurwitz criterion. A necessary condition requires that all coefficients of the characteristic polynomial

$$M(s) = s^4 + s^3 + (b_k k_{Mr})^2 s^2 + (b_k k_{Mr}) s + b_k k_{Mr} \quad (6.9)$$

were of the same sign, where we got them from

$$\begin{aligned} b\dot{k}_d \ddot{y} &> 0 \\ b\dot{k}_{Mr} \ddot{y} &> \ddot{y}\ddot{y} \quad 0, \\ k_d &> 0 \end{aligned} \quad (6.10)$$

and the sufficient condition says that the leading minors of the matrix

$$H = \begin{vmatrix} \ddot{y}\ddot{y} & b\dot{k}_d & b\dot{k}_{Mr} & \ddot{y}\ddot{y} & 0 & 0 & \ddot{y} \\ b\dot{k}_d & \ddot{y} & & & b\dot{k}_d & 0 & \\ b\dot{k}_{Mr} & & \ddot{y} & & & & \\ \ddot{y}\ddot{y} & & & \ddot{y}\ddot{y} & 0 & & \\ 0 & 1 & & b\dot{k}_d & \ddot{y} & b\dot{k}_{Mr} & \ddot{y} \end{vmatrix}$$

are supposed to be positive. Calculating the appropriate determinants gives

$$\begin{aligned} D_1 &= \ddot{y} > 0 \\ D_2 &= \ddot{y} (\ddot{y} - b\dot{k}_d) (b\dot{k}_d \ddot{y} - b\dot{k}_{Mr} \ddot{y}\ddot{y}) = (b\dot{k}_d \ddot{y} - b\dot{k}_{Mr} \ddot{y}) > 0 \\ D_3 &= \ddot{y} (\ddot{y} - b\dot{k}_d) (b\dot{k}_{Mr} \ddot{y}\ddot{y}) - \ddot{y}^2 b\dot{k}_d b\dot{k}_{Mr} (\ddot{y} - b\dot{k}_{Mr} \ddot{y}\ddot{y})^2 > 0 \\ D_4 &= D_3 > 0 \end{aligned} \quad (6.11)$$

After simple transformations from (6.10) and (6.11), we obtain five inequalities defining the stability region

$$\begin{aligned} b\dot{k}_d \ddot{y} &> 0 \\ b\dot{k}_{Mr} \ddot{y} &> \ddot{y}\ddot{y} \quad 0 \\ k_d &> 0 \\ \ddot{y}^{penal\,code}_{Mr} &< 0 \\ (b\dot{k}_{Mr} \ddot{y}\ddot{y}) \cdot \ddot{y}^2 k_d &> 0 \end{aligned} \quad (6.12)$$

For a fixed  $k_d > 0$ , we can proceed as follows to determine the stability region.

After transforming the fifth inequality (6.12) into the form

$$k_d > \frac{k}{b\dot{y}} + \frac{k_{Mr}}{\ddot{y}}, \quad (6.13)$$

we draw a curve on the plane  $(kp, kd)$  (Fig. 6.1),

$$k_d = \frac{k}{b\dot{y}} + \frac{k_{Mr}}{\ddot{y}}, \quad k_{Mr} > \frac{\ddot{y}\ddot{y}}{b\dot{y}}, \quad (6.14)$$

and its asymptotes

$$k_{_M} = \frac{\ddot{y}}{b\dot{y}} \quad (6.15a)$$

$$k_d = \frac{k_{_M}}{\dot{y}} \quad (6.15b)$$

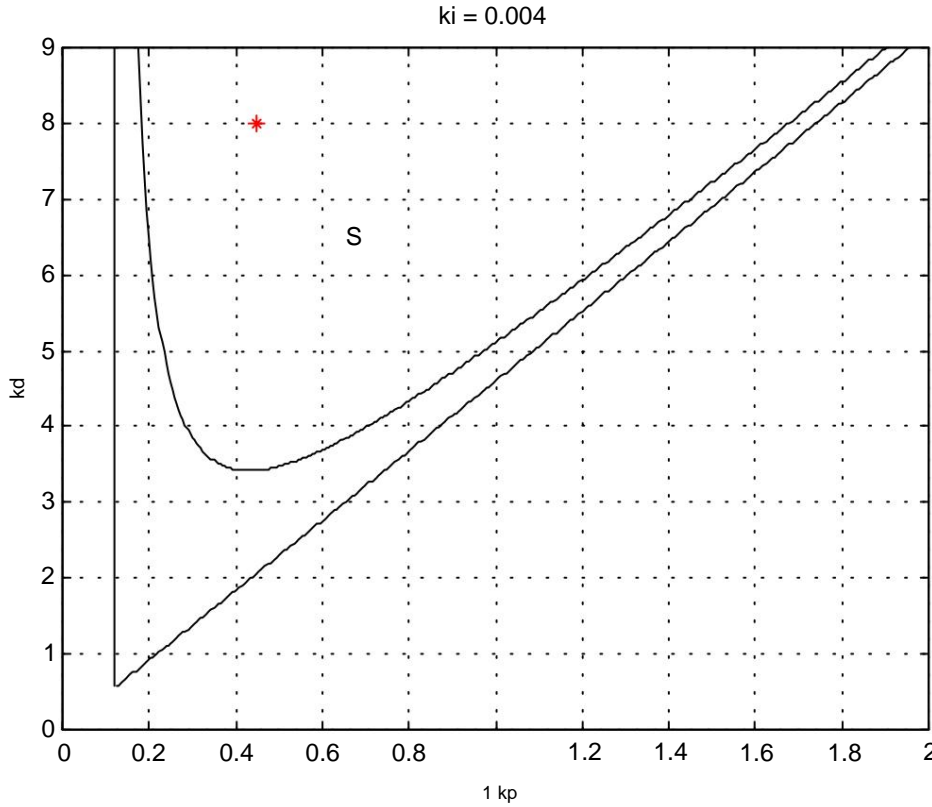


Fig. 6.1. The stability area  $S$  on the  $(kp, kd)$  plane determined for the operating point  $x_0 = 15 \text{ mm}$ .

The area  $S$  lying above the curve (6.14) is the stability area for a fixed  $ki > 0$ . When  $ki \rightarrow 0$ , the curve (6.14) becomes increasingly closer to the lines (6.15a) and (6.15b). If  $ki$  increases, the curve moves up. It is easy to see that the stability region is defined by three conditions

$$k_{\_} > 0$$

$$k_{_M} > \frac{\ddot{y}}{b\dot{y}} \quad (6.16)$$

$$k_d > \frac{k_{\_}}{\frac{b\dot{y}}{\ddot{y}} k_{_M} - \dot{y}} + \frac{k_{_M}}{\dot{y}}$$

the fulfillment of which is equivalent to the inequalities (6.12).

Conditions (6.16) define the set of parameters  $[kp, ki, kd]$  that stabilize the system (6.4). The question of how to select controller settings in the stability area can be answered in many ways. One method may be to minimize the quality index

$$J_{pid} = \int_0^T \left( \ddot{y}^2 + \dot{y} \frac{\dot{y}}{dt} \right)^2 dt \quad (6.17)$$

$\ddot{y}(t) \neq 0, \ddot{y}_1 > 0$

For the linear system (6.4), the quality index (6.17) can be determined analytically, and the appropriate calculation formulas can be found in the works [10], [14].

It turns out, however, that the settings determined by this method give strongly oscillatory waveforms with a long decay time, and although the linear model (6.4) is stable, the controller does not stabilize the object. The loss of stability is the result of large control values calculated by the controller that exceed the limits. If we impose constraints on the amplitude in (6.17). control, the transients are much milder, but solving the problem is difficult in this case because calculating the control amplitude requires numerical integration of the model equations. The introduction of constraints on the control approximately corresponds to the fulfillment of conditions (3.20) or (3.21). Therefore, the controller settings were selected experimentally, taking into account the shape of the transient waveform in Figure 6.1 and the location of the eigenvalues of the closed system (6.4), taking into account the inequality (3.20).

The computer implementation of algorithm (6.2) requires approximation of the integral with an appropriate sum and the derivative with a difference and the selection of the sampling time. After discretization, the algorithm (6.2) in the incremental version takes the form:

$$\ddot{y} = u_k \quad \text{and} \quad \ddot{y} \text{ and } (1) \quad \text{is} \quad \ddot{y}(t) = \frac{k}{T_p} \left( \ddot{y}(t) + k \frac{d}{dt} \ddot{y}(t) + k_i \ddot{y}(t) + k_d \ddot{y}(t) \right) \quad (6.18)$$

$$\ddot{y}(t+T_p) = \ddot{y}(t) + (1) \quad (6.19)$$

Note: In the model, time is counted in milliseconds and in the real-time system in seconds, therefore, during implementation, the  $ki$  factor should be multiplied by 1000 and  $kd$  divided by 1000.

The sampling period  $T_s$  can be selected using Shannon's theorem, which assumes that the sampled signal does not contain frequencies higher than  $b$ . In practice, this signal, due to the presence of interference, contains frequencies higher than  $b$ . This means that the sampling rate should be higher than required by Shannon's theorems. Let  $H(j)$  denote the transmittance of a continuous closed system. The bandwidth of such an object is defined as

$\ddot{y}$

$$|H(j)| = |H(0)| \sqrt{\frac{1}{2}}$$

It is assumed [2] that the sampling period should be

$$T_p = \frac{\ddot{y}}{b}, \quad \text{and} \quad \ddot{y} = b$$

where  $a = 10$  if the system is subject to random interference with a bandwidth exceeding 5, in the absence of such interference. After selecting the settings  $b = 5$ ,  $a = 2.5$  of the controller, the frequency response was determined based on closed system (Fig. 6.2).

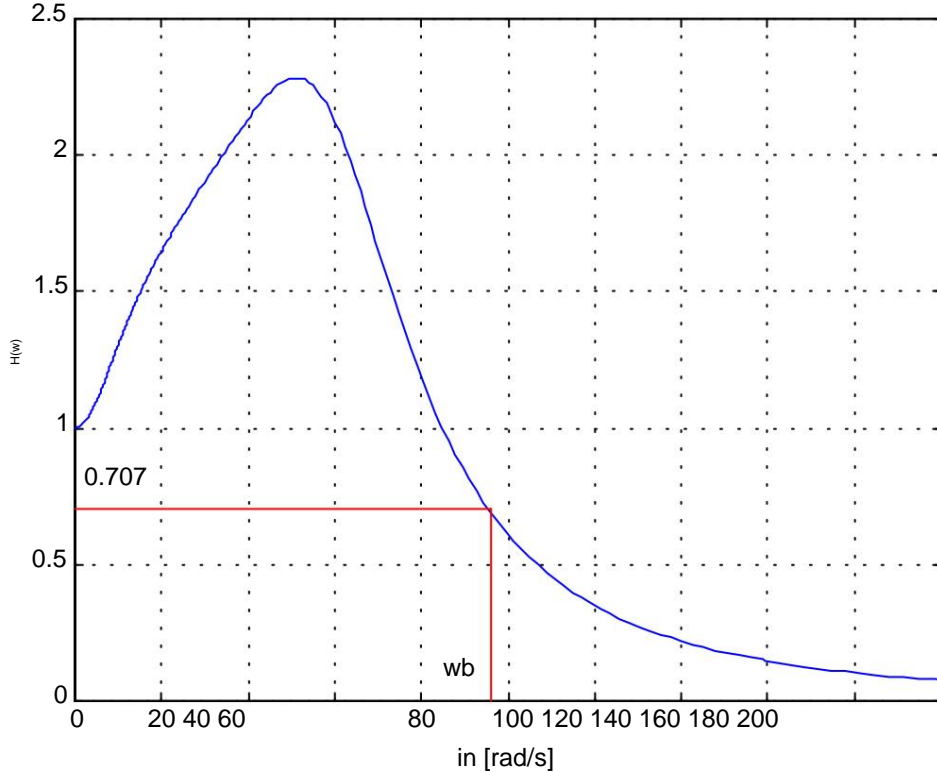


Fig. 6.2. Frequency characteristics of a continuous closed system with a *PID* controller determined on the basis of a linear model at the equilibrium point  $x_0 = 15 \text{ mm}$ . The method of determining the bandwidth band is marked in red.

Assuming  $a = 10$ ,  $b = 95 \text{ rad/s}$ , we have  $T_s = 3.3 \text{ ms}$ .

Figure 6.3 shows the experimental results with a rectangular set value waveform, and Figure 6.4 shows the control waveform when the set value was a sine wave with a frequency of 1 Hz. The sampling time was 2ms. Linearization was performed at the point  $x_0 = [15 \ 0 \ 0.5]T$ ,  $u_0 = 1.9$ . The closed system had the following eigenvalues

$$\begin{aligned} 1 &= -0.1461 \\ 2 &= -0.0271 + 0.0487i = -0.0271 \\ 3 &- 0.0487i = -0.01714 \end{aligned}$$

yyy

and the controller settings were  $kp = 0.45$ ,  $ki = 4$ ,  $kd = 0.008$ .

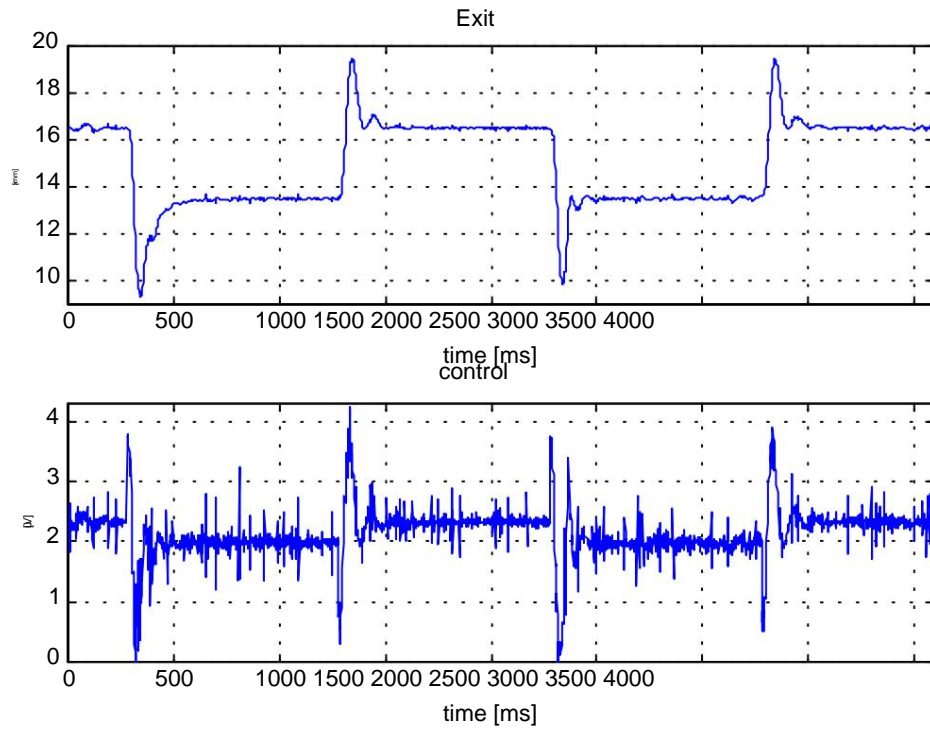


Fig. 6.3. Experiment result ( PID controller). Following a square wave signal with an average value of 15 mm, an amplitude of 1.5 mm and a frequency of 0.5 Hz.

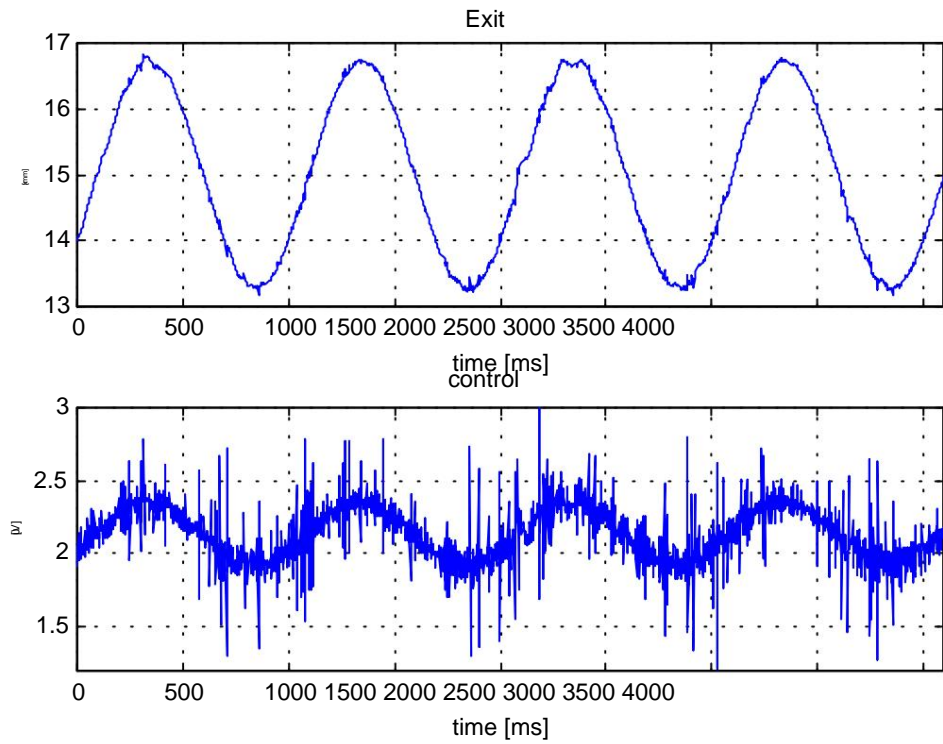


Fig. 6.4. Experiment result ( PID controller). Following a sinusoidal signal with an average value of 15mm, an amplitude of 1.5mm and a frequency of 1Hz.

In equality (6.9) three coefficients can be varied. It follows that using With a *PID* controller , it is impossible to obtain any distribution of the eigenvalues of the closed system state matrix. This is a serious drawback of this regulation system, because it cannot achieve the desired dynamic properties, in particular it cannot get rid of oscillations in the transient. Theoretically, the settings can be selected so that the characteristic equation (6.9) has real roots, but it was found that the control amplitude is then very large, the system enters saturation and, consequently, the controller does not stabilize the object.

Analogous considerations can be carried out for the discrete case described by the equalities (5.12), but they do not bring anything new and will not be presented here. The described algorithm, despite its simplicity, does not provide the required quality of regulation and the area of attraction of the balance point is small because a loss of stability was observed when the operating point changed by only 1.5 mm. This behavior of the system is a consequence the non-linear dependence of the magnetic force on the current and the position of the sphere (see formulas 3.4 and 4.15), and the limitations (3.13, 3.14) imposed on the current and control.

The files pid\_01.m and pid\_reg.mdl are located on the diskette attached at the end of the work. The first one draws Figure 6.1 for a given operating point and calculates the eigenvalues and transmittance of the closed system, while the second one is the implementation of the controller.

## 6.2. State recovery

Knowledge of the entire state vector allows you to construct effective control algorithms. In particular, it is then possible to solve the linear-quadratic problem and set eigenvalues. Both the continuous (5.3) and discrete (5.12) systems are controllable and observable. Observability means that the system state  $x(t)$  can be clearly determined from the control measurement  $u$  and the output  $y$ , over a certain time interval  $[t - q, t]$ ,  $q > 0$ . A precise formulation of this concept can be found in [21]. Accurate state recovery is difficult to achieve. It is much easier to construct a device that reproduces the state asymptotically. In other words, if the observation time increases, the state estimate tends to its exact value.

### 6.2.1. Heuristic method

In our system, the variable  $x1(t)$  is known exactly, while the other two components of the state  $x2$  and  $x3$  need to be estimated. Note that equation (3.7)  $x! = x$  allows us to determine the variable  $x2(t)$ , and integrating equation (3.9) gives the value  $x3(t)$ . The implementation of an ideal differentiation system is, of course, impossible, but the derivative in (3.7) can be numerically approximated by an appropriate difference. The operation of the state observer was checked by performing a simulation. The results of reproducing the second and third state components with noise at the input and output are shown in Figure 6.5. It can be seen that the two state components  $x1$  and  $x3$  can be determined precisely, while the  $x2$  component can be approximated by the difference quotient ( $\hat{x}_2 = \frac{x_2(t+T_p) - x_2(t)}{T_p}$ ).

$$\hat{x}_2(t) = \frac{x_2(t+T_p) - x_2(t)}{T_p}.$$

If the noise level at the system output is not too high and the sampling frequency is higher than the maximum frequency occurring in the  $x1(t)$  signal, this approximation gives good results.

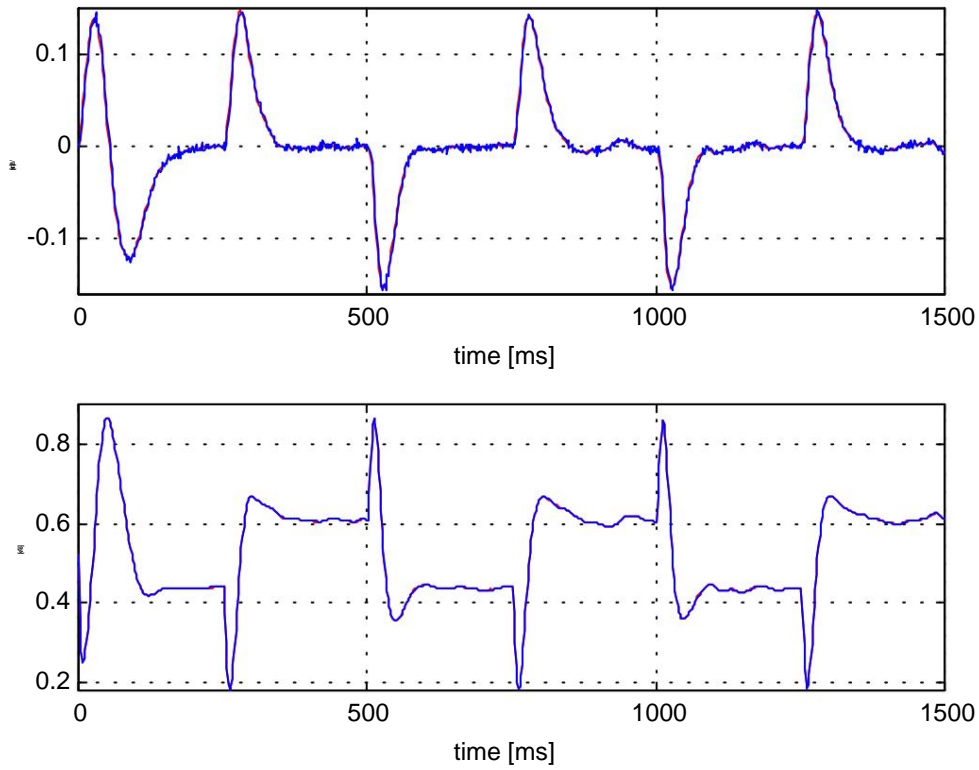


Fig. 6.5. Reproducing the second and third state components (Simulation). The exact value of the state is marked in red and its estimate in blue, which is not visible because both waveforms are very similar.

### 6.2.2. Luenberger-type identity observer

We now turn to asymptotic state recovery [14],[18],[21],[24]. For this purpose, let us consider a linear system described by equations

$$\begin{aligned} \frac{dx}{dt} &= Ax + Bu \\ y &= Cx \end{aligned} \tag{6.20}$$

$x(t), \dot{x}(t), \ddot{x}(t)$  the following form  
observer form

$$\begin{aligned} \frac{dw}{dt} &= Fw + Gy + Hu + My + Nw \\ w &= R^T \dot{x} + R^P \hat{x} + R^N \hat{y} \end{aligned} \tag{6.21}$$

$F, G, H, M, N$  are constant real matrices.

We will call the expression estimation error

$$e(t) = w(t) - Px(t) \quad (6.22)$$

$e(t) \in R^s$ ,  $P$  is a constant real matrix.

If we accept

$$\begin{aligned} \begin{bmatrix} C \\ P \end{bmatrix} &= PA, MN \quad C^T = IH, PB = \\ &= \begin{bmatrix} C^T \\ P \end{bmatrix} \end{aligned} \quad (6.23)$$

then after simple transformations it will turn out that

$$\frac{de}{dt} = Fe, x^*(t) x(t) Ne(t) \quad (6.24)$$

If the matrix  $F$  is exponentially stable, the observer reproduces the state asymptotically. To obtain a full-order observer we assume  $s=n$ ,  $P=I$ ,  $M=0$ , and from (6.23) we have

$$F = A - GC, \quad H = B, \quad N = I.$$

We can now write the observer's equation in the form

$$\hat{\frac{dx}{dt}} = (A - GC)x + GyBu + tR x, \quad \hat{x}(0) = x_0, \quad (6.25)$$

where the matrices  $A$ ,  $B$ ,  $C$  are defined by (5.3), and  $G$  is a constant real matrix and has 1. If the estimation  $x$  matrix  $(A-GCT)$  has eigenvalues with negative dimensions of 3 real parts, then the error  $e(t) = x^*(t) - x(t)$  tends asymptotically to zero. When calculating the derivative of the error, we obtain

$$\frac{de}{dt} = \hat{\frac{dx}{dt}} - \frac{dx}{dt} = (A - GC)x + GyBu - Ax - GCe \quad (6.26)$$

Since the system (5.3) is observable, there exists a matrix  $G$  such that  $(A-GCT)$  has eigenvalues in the left half-plane. In particular, the matrix  $G$  can be obtained by solving the algebraic Riccati equation

$$\begin{aligned} AD - DA - DCR - CDW^{-1} - T &+ = 0 \\ RR &=> 0 \\ WW &= 0 \\ G - BCR &= 0 \end{aligned} \quad (6.27)$$

whereby the matrix  $W$  is selected so that the pair  $(W, AT)$  is detectable (or observable).

In the case under consideration, the matrix  $W$  has dimensions  $3 \times 3$ , the matrix  $D$  with dimensions  $3 \times 3$  is the only symmetric and positive definite solution of equation (6.27), and  $R$  is the number positive.

In the discrete case described by the equalities (5.12), the reasoning is analogous, and the observer's equation has the form

$$E(D) \hat{x}(i+1) = A\hat{x}(i) + G y(i) + \dots \quad (6.28)$$

If the  $AD$ -GCD matrix  $A^T D^{-1} A$  has eigenvalues in the unit circle, the estimation error  $e(i) = \hat{x}(i) - x(i)$  tends asymptotically to zero. Indeed, by calculating the error at time  $i+1$  we will receive

$$\begin{aligned} e(i+1) &= (\hat{x}(i) - x(i)) + (A^T D^{-1} A \hat{x}(i) + A^T D^{-1} B u(i) - x(i)) \\ &= (A^T D^{-1} G C \hat{x}(i)) \end{aligned}$$

Since the system (5.12) is observable, there is a matrix  $G$  such that  $A^T D^{-1} G C$  has eigenvalues in the unit circle. In particular, the matrix  $G$  can be determined by solving the discrete equivalent of the algebraic Riccati equation

$$\begin{aligned} D A^T D C R Q D A W_D &= \begin{pmatrix} 1 & & \\ & D & \\ & & 1 \end{pmatrix} \begin{pmatrix} 1 & & \\ & D & \\ & & 1 \end{pmatrix} + \\ R \bar{R} &= > 0 \\ W \bar{W} &= 0 \\ G^T D C R Q D A &= \begin{pmatrix} 1 & & \\ & D & \\ & & 1 \end{pmatrix} \begin{pmatrix} 1 & & \\ & D & \\ & & 1 \end{pmatrix} \end{aligned} \quad (6.29)$$

whereby the matrix  $W$  is selected so that the pair  $(W, A^T D)$  is detectable (or observable). As before, the  $W$  matrix has dimension  $3 \times 3$ , the  $3 \times 3$   $D$  matrix is the only symmetric and positive definite solution of equation (6.29), and  $R$  is the number positive.

Algorithms for solving equations (6.27) and (6.29) can be found in [14],[21]. MATLAB numerical procedures included in the *Control System Toolbox* [11] can also be used to determine the  $G$  matrix. The *lqr* and *dlsqr* functions from this toolbox solve equations (6.27) and (6.29).

The algorithm described above is called Luenberger's identity observer. The observer's performance was checked using simulation. Figure 6.6 compares the state and its estimate obtained using equation (6.28). More detailed information on state recovery can be found in [21], on which the content is based this point.

The Luenberger observer has some disadvantages compared to the heuristic method described in point 6.2.1. For large deviations from the operating point, the state estimate obtained from equations (6.21) or (6.24) is incorrect because the nonlinearity of the system begins to play a role. The heuristic method is free from this drawback and allows you to recreate the state for any positions spheres. On the other hand, by appropriate selection of the  $G$  matrix, optimal noise suppression can be achieved [24], which speaks in favor of the Luenberger observer.

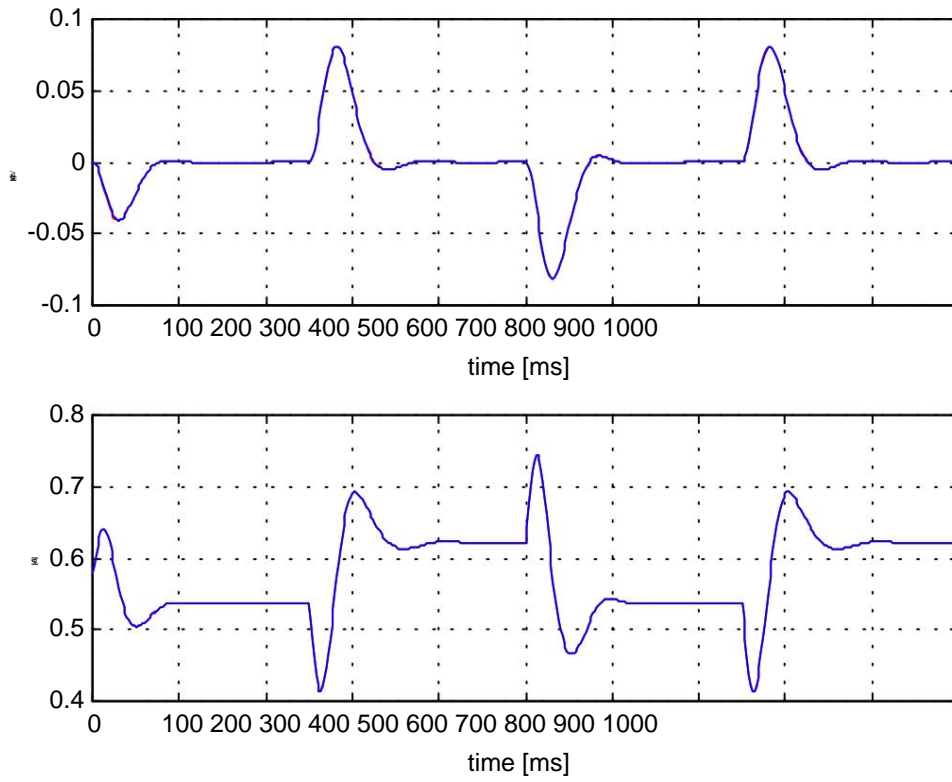


Fig. 6.6. Reproducing the second and third state components using the Luenberger observer (Simulation). The exact value of the state is marked in red, and its estimate in blue, which is not visible here because both waveforms are very similar.

### 6.3. Dynamic feedback

Let us consider the linear system (5.3),

$$\frac{dx}{dt} = Ax + Bu \quad (0) \quad \dot{x}(t) \in \mathbb{R}^3, \quad \dot{x}(0) = x_0 \quad (6.30)$$

$y = Cx^T$

and state observer (6.25)

$$\frac{dx}{dt} = (A - GCT)x + Gy \quad (0) \quad \dot{x}(t) \in \mathbb{R}^3, \quad \dot{x}(0) = x_0 \quad (6.31)$$

where the matrix  $G$  is such that the matrix  $(A - GCT)$  is stable and can be determined from equality (6.27). The estimation error is

$$e(t) = \hat{x}(t) - x(t) \quad (6.32)$$

and satisfies the differential equation

$$\frac{de}{dt} = (A - GCT)e^T. \quad (6.33)$$

If we introduce control in the system (6.30).

$$u = \ddot{y}Kx^* \quad (6.34)$$

and the matrix  $K$  is constant and real with dimensions 1 3, then by (6.30) – (6.34) we will obtain the following closed system

$$\frac{d\dot{y}}{dt} = A\dot{y} + BK\dot{x} \quad (6.35)$$

Where

$$D = \begin{bmatrix} A & BK \\ 0 & I_3 \end{bmatrix} \quad \text{And the } GC^T = \begin{bmatrix} 0 \\ I_3 \end{bmatrix}. \quad (6.36)$$

The pair  $(A,B)$  is controllable, so there exists a matrix  $K$  such that the matrix  $(A-BK)$  has eigenvalues with negative real parts. The form of the matrix  $D$  allows you to set the eigenvalues of the matrix  $(A-BK)$  and  $(A-GCT)$  independently , and its spectrum satisfies the equality

$$\ddot{y}(D) = \ddot{y}(A - BK) = \ddot{y}(A - GC^T)$$

Proofs of the above theorems can be found in [14], [24]. A system consisting of a proportional controller cooperating with a state observer is called a dynamic compensator or dynamic feedback [14],[21],[24].

Reference [21] provides algorithms for setting the eigenvalues of the matrix  $(A-BK)$  and  $(A-GCT)$ . In particular, the  $K$  matrix can be determined using the solution of the Riccati equation

$$\begin{aligned} AD + DA^T + DBRBDW^{-1}C^T &= 0 \\ WW^T &= 0 \\ RR^T &= 0 \\ KRBDW^{-1}C^T &= 0 \end{aligned} \quad (6.37)$$

We choose the matrix  $W$  so that the pair  $(W,A)$  is detectable (or observable). In the case under consideration, the matrix  $W$  has dimensions 3 3, the matrix  $D$  with dimensions 33 is the only symmetric and positive definite solution of equation (6.37), and  $R$  is the number positive. It can be shown [7],[9],[10] that the control  $u = -Kx$ , with the  $K$  matrix determined from (6.37) minimizes the quality index

$$J(x,u) = \int_0^t (x^T W x + u^T R u) dt$$

where  $x$  is the solution of equation (6.30) and the spectrum of the matrix  $(A-BK)$  satisfies the condition

$$\max\{\operatorname{Re}(s) : s \in \sigma(A - BK)\} < 0$$

To numerically determine the  $K$  matrix, the *lqr* function from the *MATLAB Control System Toolbox* library [11] can be used .

In the discrete case described by equations (5.12) and (6.28), the reasoning is analogous. The pair  $(AD, BD)$  is controllable, which guarantees the existence of a matrix  $K$  such that the matrix  $(AD - BDK)$  has eigenvalues in the unit circle. As before, the discrete equivalent of the Riccati equation can be used to determine the  $K$  matrix

$$\begin{aligned} & D A \tilde{D} I B \tilde{B} D A W = \begin{pmatrix} 1 & T \\ D & D \end{pmatrix}^{-1} \begin{pmatrix} 1 & T \\ D & D \end{pmatrix} + \\ & R \tilde{R} = > 0 \\ & W \tilde{W} = \ddot{y} = 0 \\ & K R \tilde{B} D I B \tilde{B} D A = \begin{pmatrix} 1 & T \\ D & D \end{pmatrix}^{-1} \begin{pmatrix} 1 & T \\ D & D \end{pmatrix} \end{aligned} \quad (6.38)$$

whereby the matrix  $W$  of dimensions 33 is selected so that the pair  $(W, AD)$  is detectable (or observable). The matrix  $D$  of dimensions 33 is the only symmetric and positive definite solution of equation (6.38), and  $R$  is a positive number. It can be shown[7],[9],[10] that the control  $u(i) = -Kx(i)$ , with the  $K$  matrix determined from (6.38) minimizes the quality index

$$J(x, u) = \sum_{i=0}^{\infty} W^T x(i) R x(i) + \frac{1}{2} \dot{x}(i)^T \dot{x}(i)$$

where  $x$  is the solution of equation (5.12) and the matrix spectrum  $(AD - BDK)$  satisfies the condition

$$\max\{|z| \mid z \in (A - BK)\} < 1$$

To numerically determine the  $K$  matrix, the *dlsqr* function from the *MATLAB Control System Toolbox* library [11] can be used .

If the sampling rate is many times (more than 10 times) greater than the highest frequency contained in the signal  $x(t)$ , then it can be used to synthesize the controller continuous model. In the case of larger sampling periods, a controller based on a discrete model will provide better results.

It follows that the linear system (5.3) and, consequently, the nonlinear system (3.7)-(3.9) can be stabilized by dynamic feedback defined by the equalities (6.31) and (6.34). When stabilizing a nonlinear system, we also need to add constant control  $u_0$  corresponding to the selected operating point to the control calculated by the controller (6.34) . Figure 6.7 shows a scheme for stabilizing an object using dynamic feedback.

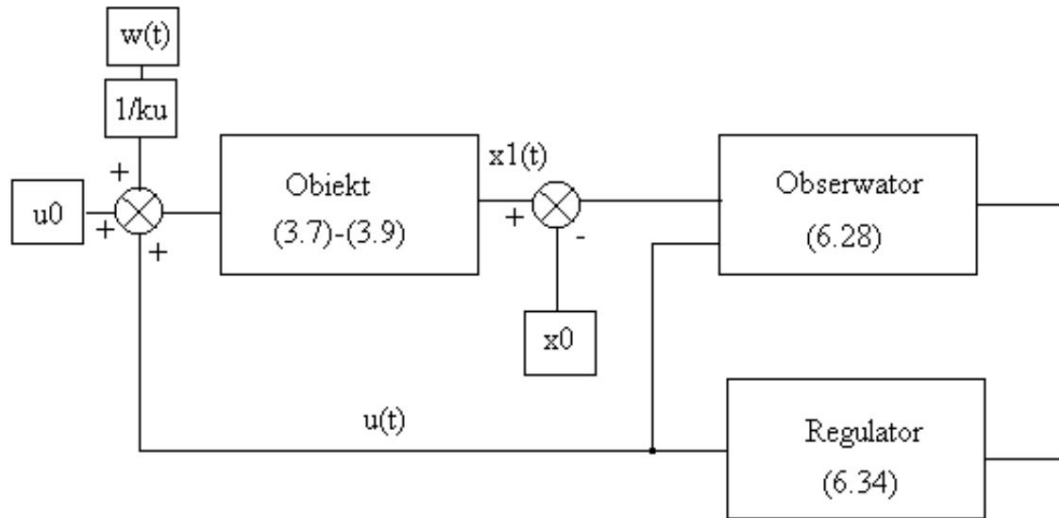


Fig. 6.7. Stabilization scheme using dynamic feedback.

The values  $x_0$ ,  $u_0$  denote the position of the sphere in the steady state and the corresponding control,  $ku$  is the gain factor of the closed system in the steady state,  $x_1(t)$  denotes the position of the sphere, and  $w(t)$  is the set value.

In section 3.3 it was stated that the nonlinear system (3.7)-(3.9) cannot be arbitrarily accelerated. Reducing the duration of transients always entails increase in control amplitude. In a linear system, the maximum control value depends on the location of the eigenvalues of the matrix  $(A-BK)$ . The further to the left of the line  $\text{Re}(s) = 0$ , the faster the system, but this is at the expense of an increase in the control amplitude. This increase causes the linear approximation to stop working and consequently becomes unstable, even though the linear system is stable. Estimates (3.20) and (3.21) give certain a tip on how to avoid this phenomenon. If the controller gain matrix is determined by solving the appropriate Riccati equation, then the weight matrices  $W$  and  $R$  must be selected to approximately satisfy the inequalities (3.20), (3.21). In particular, increasing the control weight  $R$  shifts the eigenvalues of the closed system to the right and leads to a decrease in the control amplitude. Weight matrices can be selected using simulation.

For certain initially assumed values of  $W$  and  $R$ , by solving equation (6.37), we determine the gain matrix  $K$  of the continuous controller. Then, by performing a simulation with such a selected controller, it is possible to determine whether the system is entering saturation. If so, the control weight  $R$  should be increased, a new gain matrix  $K$  should be determined and performed again simulation. In this way it was selected

$$W = \begin{bmatrix} 2 & 0 & 0 \\ 0 & 1 & 0 \\ 0 & 0 & 1 \end{bmatrix}, R = 80, K = \begin{bmatrix} -0.3670 & -10.6590 & 2.0696 \end{bmatrix},$$

the linearization of the state equations was performed at the point  $x_0 = [17 \ 0 \ 0.5549]$ ,  $u_0 = 2.23$ .

The analysis of the frequency response of a continuous closed system allows us to conclude that the bandwidth (see section 6.1) of this system is  $= 40 \text{ rad/s}$ . Period

sampling  $T_s = 2 \text{ ms}$  was selected to meet the  $T$  condition

$$\frac{\pi}{\omega_p} < \frac{10\pi}{10\pi_b} = 7.85 \text{ ms} [2]. \text{ Model}$$

linear was discretized and used to determine the digital version of the controller.

Similarly to the continuous case, the  $W$  and  $R$  weight matrices were selected based on simulations and the  $K$  matrix was determined by solving equation (6.38) and the following values were obtained

$$W = \begin{bmatrix} \ddot{y}_2 & 0 & 0 \\ 0 & 1 & 0 \\ 0 & 0 & 1 \end{bmatrix}, R = 80, K = \begin{bmatrix} 0.3514 & -10.2723 & 1.9974 \end{bmatrix}.$$

The discrete state matrix of the closed system had the following eigenvalues

$$\begin{aligned} z_1 &= 0.9303 + 0.0352i, z_2 \\ &= 0.9303 - 0.0352i, z_3 = \\ &0.7459, \end{aligned}$$

and the steady-state gain was

$$BD = 5.4 \text{ mm}^T, M = k C A D B D K I.$$

Figure 6.8 shows the experimental results when the set value  $w(t)$  was a square signal with an amplitude of 2 mm and a frequency of 1 Hz.

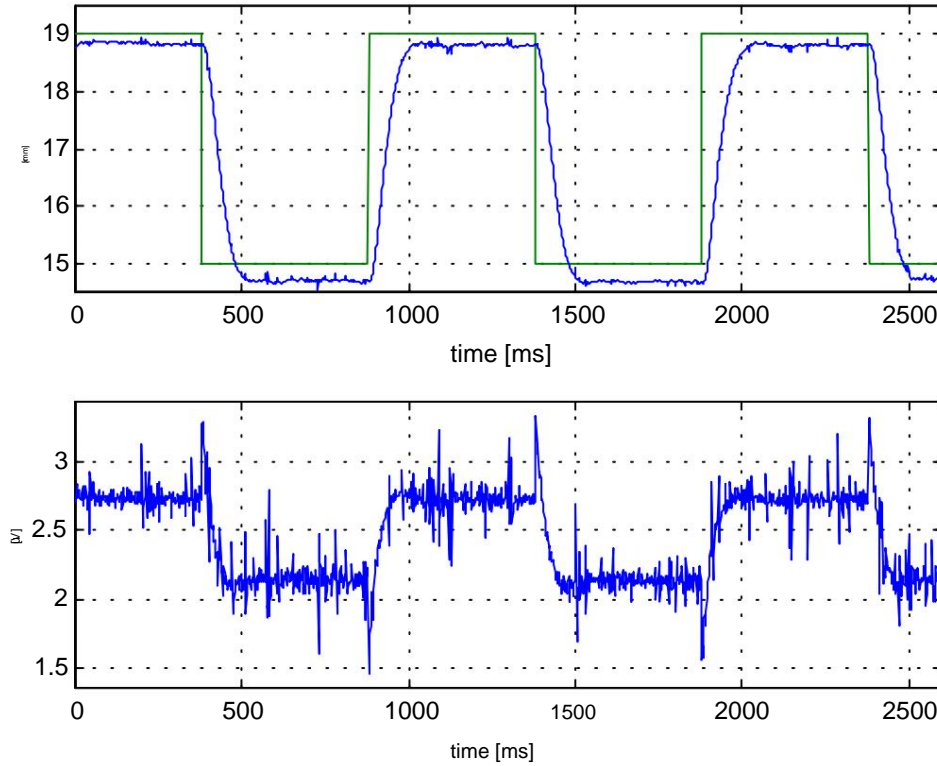


Fig. 6.8. Experimental result in the case of following a square wave signal with an amplitude of 2 mm and a frequency of 1 Hz. The set value is marked in green.

It is clearly visible that the controller does not eliminate the error in the steady state, which is a consequence of the system's nonlinearity and model errors. Figure 6.9 shows the result

experiment in the case of following a sinusoidal signal with an amplitude of 2 mm and a frequency of 1 Hz. The linearization of the equations of state was performed at the point  $x_0 = [15 \ 0 \ 0.503]$ ,  $u_0 = 2.106$ , the weight matrices did not change. The controller had the following parameters

$$K = [-0.3535 \ -9.8316 \ 2.0987].$$

The closed system state matrix had the following eigenvalues

$$z_1 = 0.9268 + 0.0371i,$$

$$z_2 = 0.9268 - 0.0371i,$$

$$z_3 = 0.7457,$$

and the steady-state gain was  $ku = -5.517 \text{ mm/V}$ .

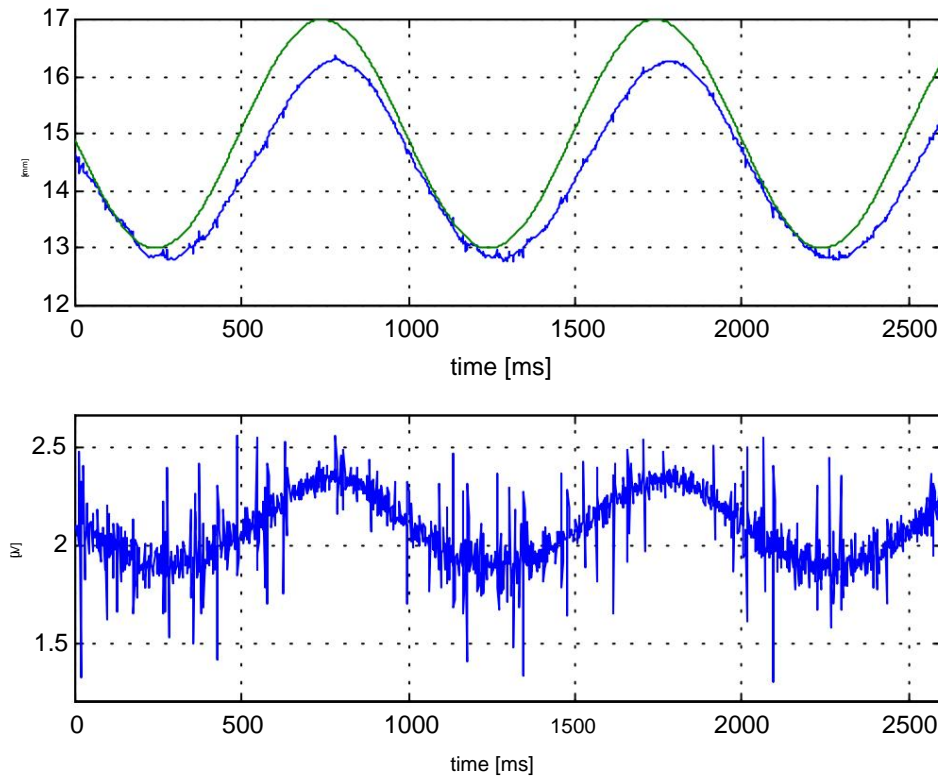


Fig. 6.9 Experimental result in the case of following a sinusoidal signal with an amplitude of 2 mm and a frequency of 1 Hz. The set value is marked in green.

The regulator described above stabilizes the object and allows adjustment within a range of approximately  $\pm 2.5 \text{ mm}$  from the equilibrium position. However, it does not have integrating properties and it cannot be used to set the sphere in a given position. Theoretically, this is possible with stabilization to zero, but model inaccuracies make it practically impossible eliminating the fixed error. To eliminate this shortcoming, we will use an integral controller. For this purpose, let us introduce an additional state  $dx$

$$\frac{d}{dt} \left( \frac{4}{dt} \right) = -g C x v \quad (6.39)$$

where  $v$  is the set value. We will use an observer to recreate the state (6.21)

$$\frac{dw}{dt} = \ddot{y} \quad (\text{And } GC \text{ in } Gy \dot{B} dt$$

(6.40)

where the matrix  $(A - GCT)$  is exponentially stable and the estimation error satisfies Eqs.

$$\frac{de}{dt} = \bar{y} \quad (\text{And GC } \vec{e}) \quad . \quad (6.41)$$

If we introduce control in the system (6.30) cooperating with the observer (6.40).

$$= \ddot{y} (\ ^\wedge \ddot{y}_1) \ddot{y} (\ ^\wedge \ddot{y}) = \ddot{y} \ddot{y} u_2 K x v K x_3 K x K x v \overset{0}{\cancel{u}} K x K x K N e K v \quad 44 \quad + \quad 1, \quad (6.42)$$

then we will get the following system of equations

$$\begin{aligned} \frac{dx}{dt} &= BK x BK x BK Ne_{44} BK v + 1 \\ \frac{dx}{dt} &= C \bar{x} v, \\ \frac{de}{dt} &= (And GC \bar{e}) \end{aligned} \quad (6.43)$$

which can be written in compact form

$$\begin{aligned} \frac{d}{dt} \tilde{x} &= D \tilde{x} + B v, \\ D &= \begin{bmatrix} A & BKQ \\ 0 & I \end{bmatrix} \quad \text{And the GC}^T = \begin{bmatrix} C^T \\ 0 \end{bmatrix}, \quad \tilde{x} = \begin{bmatrix} x \\ u \end{bmatrix}, \quad \tilde{x} = \begin{bmatrix} x \\ u \end{bmatrix} \\ \tilde{K} &= \begin{bmatrix} K_1 & K_2 & K_3 & K_4 \end{bmatrix} \end{aligned} \quad (6.44)$$

You can easily show that a couple  $(AB)$  is controllable, so there is a matrix  $K$  about dimensions  $1 \times 4$  such that the matrix  $(A \tilde{y} BK)$  has eigenvalues with negative real parts. In particular, the matrix  $K$  can be determined using the solution of the algebraic Riccati equation analogous to (6.37). The matrix form  $D$  allows regardless of  $(A \tilde{y} BK)$  and  $(A-GCT)$ , and its spectrum satisfies the equality set the eigenvalues of the matrix yourself (see e.g. [21])

$$\tilde{y}(D = \tilde{y}(A \tilde{y} BK \tilde{y} - \tilde{y}(A \tilde{y} GC)^T)$$

In the discrete case described by equations (5.12), the reasoning is analogous and, after what has been said so far, we will not quote it here.

Let us only note that the equivalent of equation (6.39) is the formula

$$(1) \quad \tilde{y}(x_i C x_i v_i D x_i + \dots) = \dots \quad (6.45)$$

and matrix  $A$  takes form

$$\tilde{y}^{\text{AND}}_D = \begin{pmatrix} \tilde{y} & 0 \\ \tilde{y} C_D^T & 1 \end{pmatrix}$$

The controller gain matrix can be determined using the discrete Riccati equation (6.38). By equating the right side of (6.44) to zero, it is easy to show that the controller has integrating properties and eliminates the error in the steady state. As before, good control effects can be obtained by designing the controller so that the conditions (3.20) or (3.21) are met. The appropriate selection of the  $W$  and  $R$  weight matrices in the Riccati equation allows these requirements to be met. You can also restore the state

use a second-order reduced observer, but its synthesis is not as simple as in the identity case. If we assume  $M=0$   $N=I$  in (6.40), the form will be obtained  
equations analogous to (6.44).

To set the eigenvalues of the matrix  $(A \tilde{y} BK)$ , can also be used

characteristic polynomial  $M(s)=\det(sI - (A \tilde{y} BK))$ , which has the following form

$$M(s) = s + \tilde{y}(s + b_3)(s + bK_2 \tilde{y} K_2^T \tilde{y})(s + b \tilde{y} K_1 \tilde{y} \tilde{y} + bK_3 \tilde{y})b \tilde{y} K_4^T \tilde{y}.$$

The controller parameters are found from the equation  $M(s) = D(s)$ , where  $D(s)$  is a given stable polynomial with a coefficient at the highest power equal to one. You can see that the character  $M(s)$  ensures obtaining any symmetric distribution of the eigenvalues of the matrix

$(A \tilde{y} BK)$ . This method can also be used in other cases, both continuous and discrete.

As before, the controller was first selected based on a continuous model.

The linearization of the state equations was performed around the point  $x_0 = [17 \ 0 \ 0.5549]$ ,  $u_0 = 2.23$ . For certain initially assumed values of  $W$  and  $R$ , the gain matrix  $K$  of the controller was determined by solving equation (6.37). Performing a simulation with such a selected controller allowed to determine whether the system was reaching saturation. If so, the weight was increased control  $R$ , a new gain matrix  $K$  was determined and the simulation was performed again. In this way it was selected

$$W = \begin{bmatrix} 2 & 0 & 0 & 0 \\ 0 & 1 & 0 & 0 \\ 0 & 0 & 1 & 0 \\ 0 & 0 & 0 & 1 \end{bmatrix}, R \approx 80, \tilde{K} = \begin{bmatrix} -3.2188 & -39.4914 & 5.6959 & -0.1118 \end{bmatrix}$$

The analysis of the frequency response of a continuous closed system allows us to conclude that the bandwidth (see section 6.1) of this system is  $= 150 \text{ rad/s}$ . Period

sampling  $T_s = 2\text{ms}$  was selected to meet the  $T$  condition  $\frac{\tilde{y}_b}{10\tilde{y}_b} < \frac{\tilde{y}_b}{10\tilde{y}_b} = 2/09 \text{ ms}$  [2]. Model

continuous was discretized and the controller was selected on its basis. The  $W$  and  $R$  weight matrices were the same as in the continuous case and the controller parameters were

$$\tilde{K} = \begin{bmatrix} -1.8735 & -27.2786 & 4.3021 & -0.0951 \end{bmatrix}.$$

The closed system state matrix had the following eigenvalues

$$z_1 = 0.9187 + 0.1170i,$$

$$z_2 = 0.9187 - 0.1170i,$$

$$z_3 = 0.7487,$$

$$z_4 = 0.8411.$$

Note that this time the gain matrix of the discrete controller is different much more than the gain matrix determined for the continuous model than in the case of the controller without integration. The introduction of integration resulted in the expansion of the bandwidth of the closed system. A wider bandwidth means that more information about the signal waveform is lost due to sampling, which is reflected in the different parameters of the continuous and discrete controller.

Figure 6.10 shows the experimental results in the case of following a square wave signal with an amplitude of  $1.5 \text{ mm}$ , an average value of  $17 \text{ mm}$  and a frequency of  $1 \text{ Hz}$ .

Comparison with Figure 6.8 allows us to determine the integrating properties of the controller. Figure 6.11 shows the experimental result for following a sinusoidal signal with an amplitude of  $1 \text{ mm}$ , an average value of  $17 \text{ mm}$ , and a frequency of  $1 \text{ Hz}$ .

The floppy disk attached at the end of the work contains the files rt\_lq\_01.mdl and rt\_lq\_02.mdl implementing the discussed algorithms. The files make\_lq\_01.m and make\_lq\_02.m can be used to synthesize regulators.

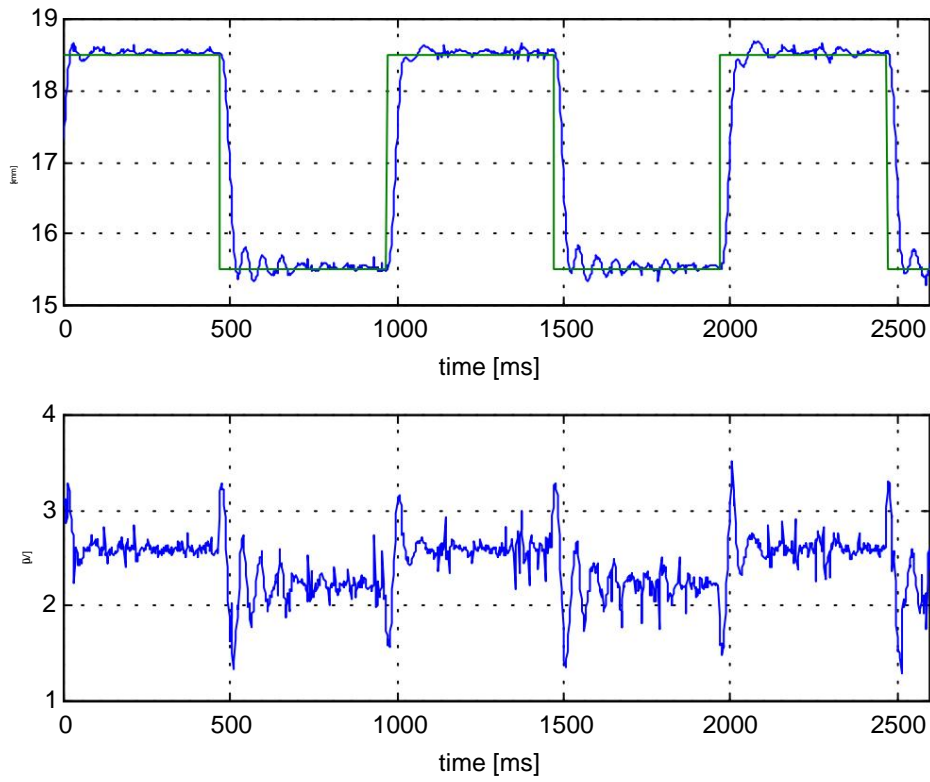


Fig. 6.10. Experiment result. Following a square wave signal with an amplitude of 1.5mm average value 17mm and frequency 1Hz. The set value is marked in green.

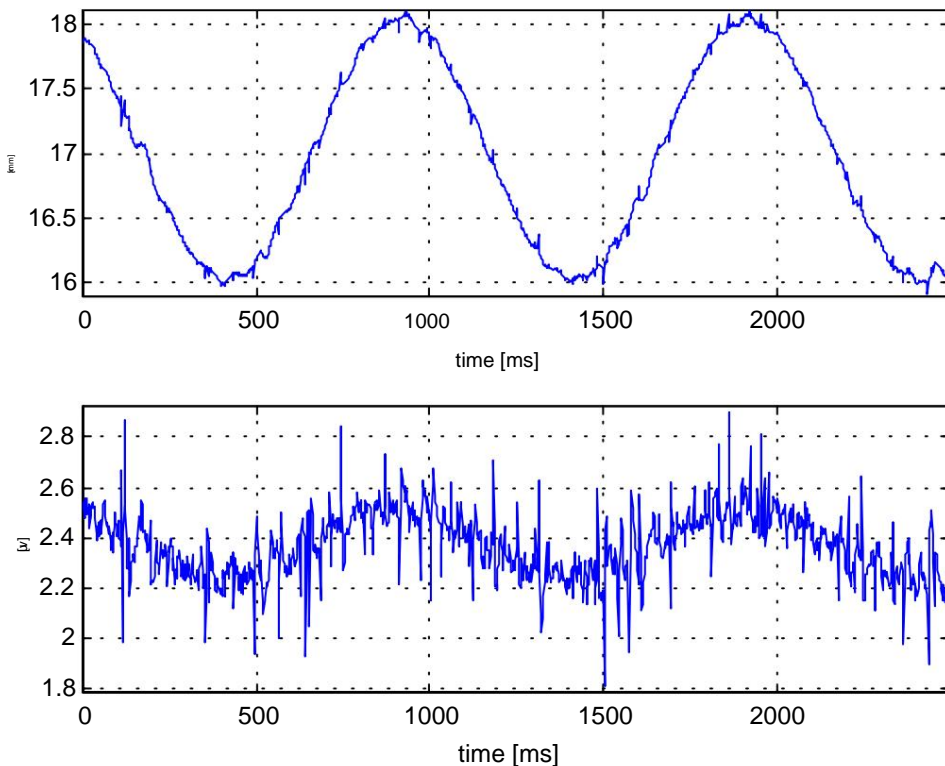


Fig. 6.11. Experiment result. Following a sinusoidal signal with an amplitude of 1 mm average value 17mm and frequency 1Hz.

## 6.4. Regulation with pole placement (Pole Placement)

The pole-locating regulator is, in fact, a method for synthesizing dynamic feedback. The controller parameters are determined by solving certain polynomial equations (*diophantine equation*), which can be

reduce to a system of linear equations. We will continue to use the abbreviation *PP* (*Pole Placement*) instead of the name *pole placement regulation*. Majority

derivations and proofs of the theorems contained in this point can be found in the works [1],[2],[23]. The subject of consideration will be the discrete-time transfer function model, derived in section 5.4. This model is described by the equation

$$y_i(z) = \frac{Bz^{-1}}{U(z)} u_i(z) = \frac{b_0 z + b_1 z^{-1} + b_2 z^{-2}}{1 + a_1 z^{-1} + a_2 z^{-2} + a_3 z^{-3}} u_i(z) \quad (6.46)$$

and is equivalent to the difference equation

$$+ b_1 y_{i-1} + b_2 y_{i-2} + a_2 y_{i-2} + a_3 y_{i-3} = b_0 u_i \quad (1) \quad (2) \quad (3)$$

To simplify the notation, we omit the  $z$  factor denoting polynomials with capital letters of the Latin alphabet, e.g.  $A(z-1)=A$ , while the expression  $nA$  will mean the degree polynomial  $A$ . We will also add a constant disturbance to equation (6.46), which will provide the integrating properties of the controller (see, e.g., [23]).

$$\begin{aligned} y_i(z) &= \frac{B}{\text{AND}} u_i(z) + \frac{d}{\text{AND}} \ddot{y}(z) \\ \ddot{y}(z) &= \begin{cases} \ddot{y}_1, & \text{for } 0_m = \\ \ddot{y}_0, & \text{for } 0_m \neq \ddot{y} \end{cases} \end{aligned} \quad (6.47)$$

The aim of the regulation is to obtain at  $i$  stable closed system with given values denominator and transfer function poles

$$y_i(z) = \frac{KB}{\text{AND}} \frac{w_i(z)}{m} \quad (6.48)$$

and compensation for constant output disturbance. The factor  $Km = Am(1)/B(1)$  provides unitary gain,  $w_i(z)$  is the set value, and  $Am$  is a known stable polynomial. As in the continuous case, the impact of a permanent disturbance may remain

removed after a sufficiently long time. Introducing this disturbance into the object model is equivalent to using an integral controller. The controller synthesis is performed based on the model equation and thus the disturbing factor will be included in the controller. Such behavior is a special case of a general rule called the internal model principle , according to which

the controller should contain a model of the deterministic disturbance that it is supposed to compensate. The disturbance generating polynomial  $Ag$  may have a different form, for example

polynomial  $A = \frac{S}{R} z^m + \frac{T}{R} z^{m-1} + \dots + \frac{B}{R}$  generates a waveform  $d(i) d \sin(\omega i)$  and its inclusion in the model will make the control system resistant to this type of disturbance.

Unlike the P/D controller, the control is not calculated based on the control error but is a linear function of the previous controls, outputs and set values. The regulation algorithm has the form

$$u_i = \frac{S}{R} y_i + \frac{T}{R} w_i + \dots \quad (6.49)$$

and is equivalent to the difference equation

$$y_i = A y_{i-1} + B u_i + C w_i + D \sin(\omega i) \quad (6.50)$$

The method of synthesizing the PP regulator and its basic properties is presented as follows

*Theorem 6.1[23].*

1. The polynomials of the PP control algorithm are given as expressions

$$R = AgF \quad (6.51)$$

$$S = G \quad (6.52)$$

$$T = A0Km \quad (6.53)$$

where  $F$  and  $G$  with degrees

$$nF = nB \quad (6.54)$$

$$nG = \max(nA + nAg - 1, nA0 + nAm - 1 - nB) \quad (6.55)$$

are the solution of a polynomial (Diophantine) equation

$$AmA0 = AgAF + z^{-1}BG \quad (6.56)$$

where  $A0$  is any stable polynomial.

2. The equation of the control system is:

$$y_i = \frac{1}{m} \sum_{k=0}^{m-1} \frac{KB}{A} v_i + \frac{FA}{A} d \sin(\omega i) \quad (6.57)$$

3. The characteristic equation is given by the expression

$$AmA0 = 0 \quad (6.58)$$

4. Perturbations  $H$  of the structure of an object that do not violate stability are defined by inequality

$$|H| < \left| \frac{A_0 A_m}{B G} \right| \quad (6.59)$$

The proof of this theorem and an extensive discussion can be found in [23], on which much of this chapter is based. Here we will prove points 1, 2 and 3 of the theorem. From the equation of the object (6.47) and the controller (6.49) one obtains:

$$y_i(z) = \frac{BT}{AR \text{ with } BS} v_i(z) + \frac{R.A}{AR \text{ with } BS} \frac{d}{\text{AND}_g} \dot{y}(z) \quad (6.60)$$

If the  $A_g$  polynomial is a factor of  $R$ , then for  $i$  the effect of constant disturbance will be removed, hence  $R = A_g F$  and after substituting into (6.60) we have

$$y_i(z) = \frac{BT}{AA_F \text{ with } BS} v_i(z) + \frac{AF}{AA_F \text{ with } BS} d\dot{y}(z) \quad (6.61)$$

Comparing the first factor on the right side of this expression with the regulation goal (6.48) we obtain

$$\frac{T}{AA_F \text{ with } BS} = \frac{KA_m}{A_A} \quad (6.62)$$

from where (6.52), (6.53), (6.56), (6.57), (6.58) result.

Since the polynomials  $A_m$  and  $A_0$  are stable, the second factor in (6.57) decays asymptotically to zero. From (6.59) it follows that the introduction of a stable polynomial  $A_0$  increases the resistance of the control system to changes in the structure and parameters of the facility. The structure perturbations are defined as follows. Let  $K(z-1) = R(z-1) G(z-1)$  be the product of the transmittance of the model and the controller. After closing the feedback loop, we will obtain a control system described by the equation

$$y_i(z) = \frac{K}{1+K} v_i(z) \quad (6.63)$$

$H(z-1)$  is such a transfer function that the perturbed control system described by equation

$$y_i(z) = \frac{K.H(z)}{1+K.H(z)} v_i(z) \quad (6.64)$$

is a better approximation of reality than the model system (6.63). Therefore, if we want to obtain resistance in a certain frequency range, we can choose  $A_0$  so that the right side (6.59) takes large values in this frequency range. The conditions (6.54), (6.55) define the degrees of polynomials  $F$  and  $G$  so that they are the smallest, but polynomials of higher degrees can be used. In the considered case  $nF=2$

$$, nG=3.$$

The Diophantine equation (6.56) allows you to determine the polynomials  $F$  and  $G$  by comparing the coefficients at appropriate powers. It can be shown [1],[2],[23] that the polynomial equation in the form

$$AX+BY=C \quad (6.65)$$

where  $X, Y$  are the sought polynomials of the variable  $z$

$-1$  with degrees  $nX$  and  $nY$  is

equivalent to a system of linear equations

$$\begin{array}{ccccccccc}
 & c_0 & & 0 & 0 \dots & b_0 & 0 & 0 & \dots & x_0 \\
 & c_1 & & aa10 & 0 \dots & bb_1 & 0 & 0 & \dots & x_1 \\
 & \dots & & aa10 & \dots & b_1 & b_0 & \dots & \dots \\
 & = & & and nA & \dots & b_{nB} & b_1 & \dots & x_n \\
 & 0 & & and nA & \dots & 0 & b_{nB} & \dots & y_0 \\
 & 0 & 0 & and nA & \dots & 0 & 0 & b_{nB} & \dots & y_1 \\
 & c_{nC} & & 0 & 0 \dots & 0 & 0 & 0 & \dots & y_n
 \end{array} \quad (6.66)$$

If  $NC + 1 = nX + nY + 2$  and polynomials  $A$  and  $B$  have no common roots, this system has a unique solution. In the case of our system, we have to determine  $nG+nF+2 = 3+2+2 = 7$  coefficients, so the system matrix (6.66) will have dimensions of  $7 \times 7$ . The following polynomials were adopted for the controller synthesis

$$\begin{aligned}
 AND_m &= (1 - qz_1^{-1})(1 - qz_2^{-1})(1 - qz_3^{-1})(1 - qz_4^{-1}), \\
 AND_0 &= (1 - pz_1^{-1})(1 - pz_2^{-1}), \quad (01)
 \end{aligned} \quad (6.67)$$

$$p1=0.8, p2=0.8.$$

The poles of the closed system  $q_1, q_2, q_3, q_4$  are complex numbers lying in the unit circle and must be arranged symmetrically relative to the real axis, because only then will the polynomial  $Am$  be a stable polynomial with real coefficients.

During the experiments, it was found that the controller stabilizes the object when the parameters  $q_1, q_2, q_3, q_4$  belong to the following set

$$Q_{\bar{\tau}} \{q : 0.65 < |q| < 0.98, \operatorname{Re}(q) > 0\} \quad (6.68)$$

the sampling period was 2ms.

The explanation for this effect is as follows. The closer to the point  $(0,0)$  the roots of the denominator of a closed system are, the faster the system is, but this results in an increase in the control amplitude. A large control amplitude causes the system to enter saturation and deviates from the linear model on the basis of which the control algorithm was derived. Hence the lower bound  $|q| > 0.65$ . The upper limit results from approaching the stability limit  $|q| = 1$ . If we set the poles in the left half-plane, the controller will have a ringing effect, see e.g. [2], [24]) and, consequently,

stability is lost. Hence the restriction  $\operatorname{Re}(q) > 0$ . The estimate (6.68) is the result of experiments and should be treated approximately, but it allows for obtaining a stably operating control system. Let us also note that this result is consistent with the inequality (3.21), which imposes a limit on the minimum duration of the transient state. Figures 6.12 and 6.13 show the result of the experiment when  $q_1 = q_2 = q_3 = q_4$

$= q = 0.8$ , and Figure 6.14 shows what happens for  $q = 0.65$ . The widest stabilization zone, approximately 5 mm from the balance point, was obtained for the real eigenvalues located around the point  $(0.9,0)$ . Figure 6.15 shows the experimental result in this case.

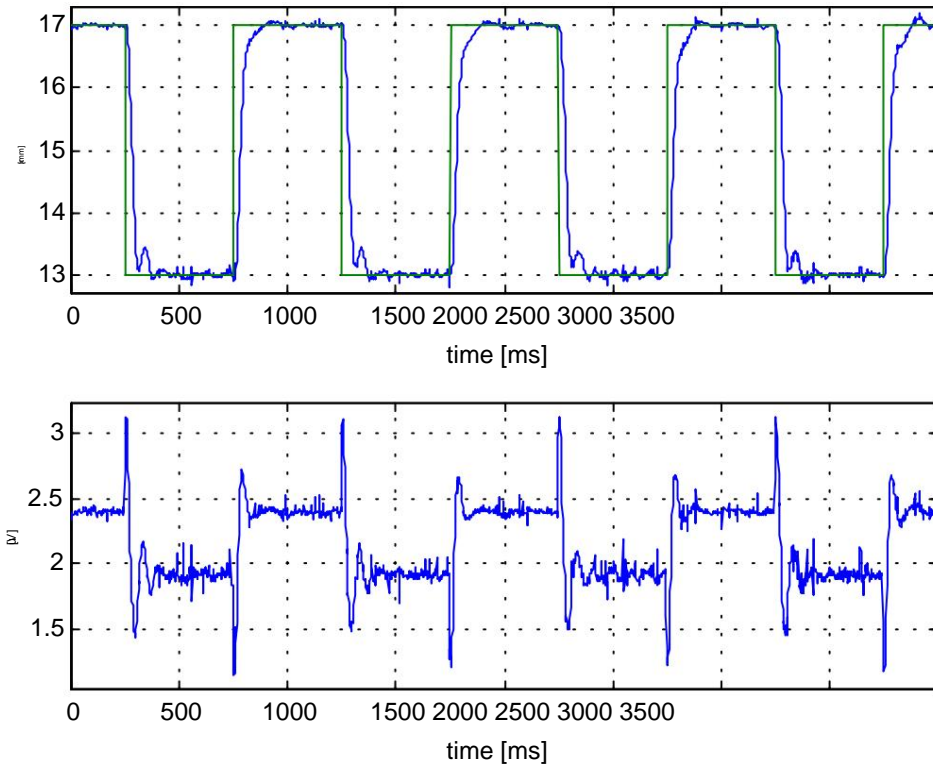


Fig. 6.12. Experimental result for  $q = 0.8$ . Following a square wave signal with an average value of 15 mm, an amplitude of 2 mm and a frequency of 1 Hz.

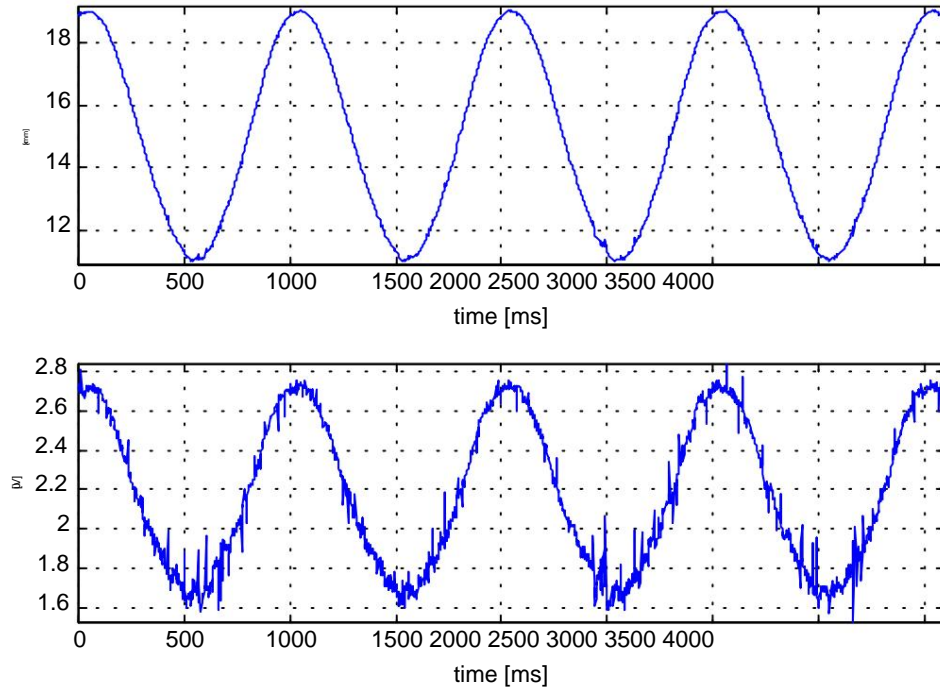


Fig. 6.13. Experimental result for  $q = 0.8$ . Following a sine wave with an average value of 15 mm, an amplitude of 4 mm and a frequency of 1 Hz.

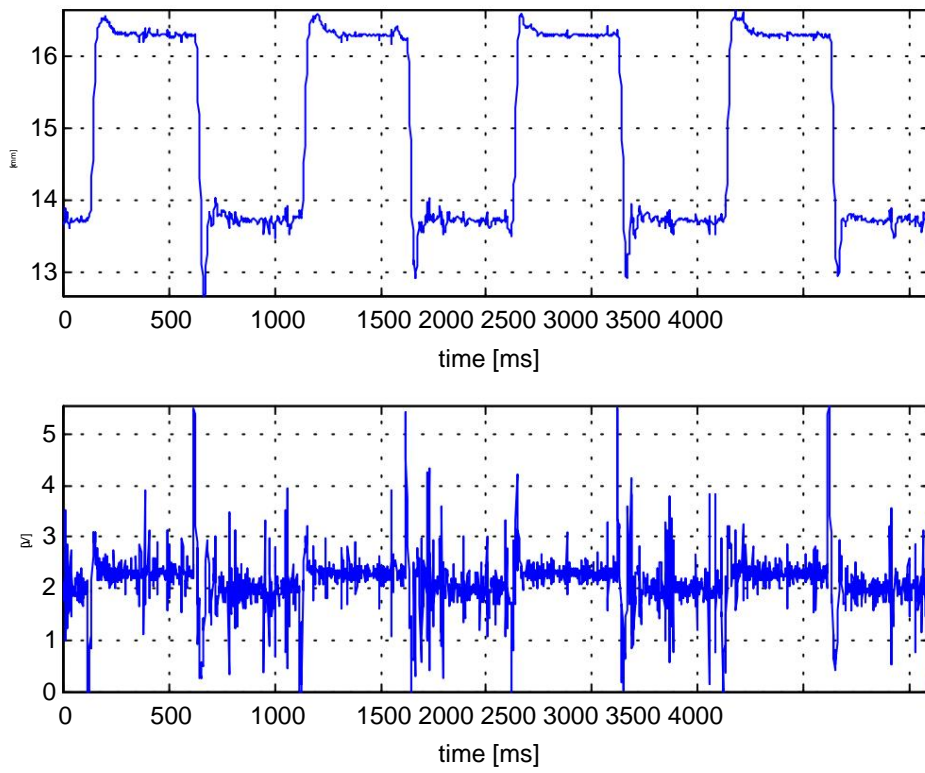


Fig. 6.14. Experimental result for  $q = 0.65$ . Following a square wave signal with an average value of 15mm, an amplitude of 1.3mm and a frequency of 1Hz.

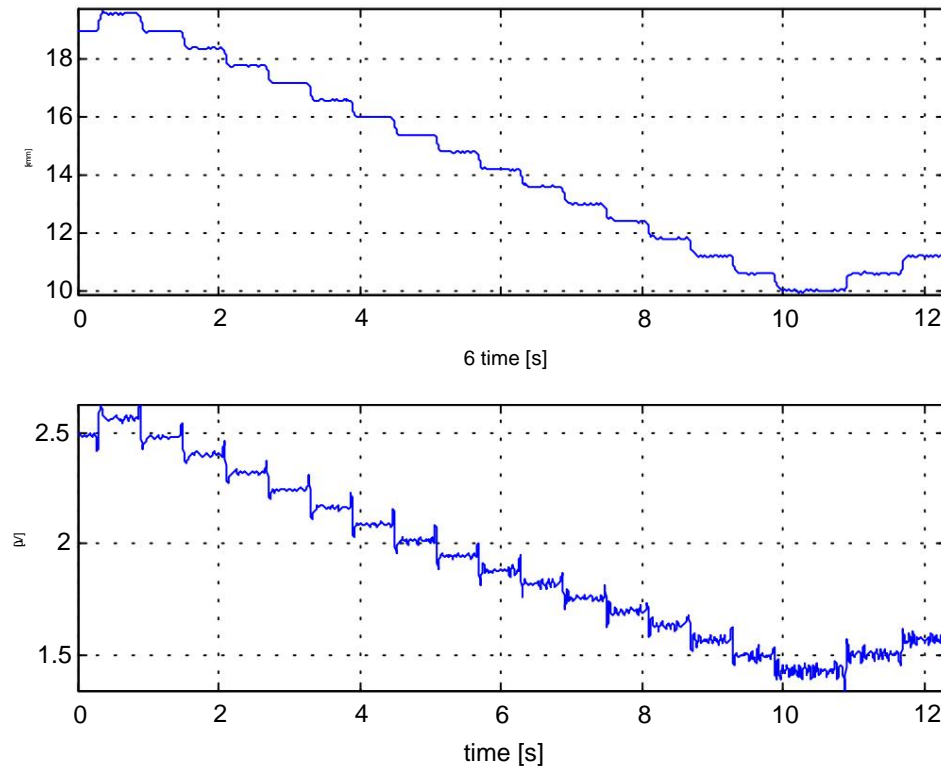


Fig. 6.15. Experimental result for  $q = 0.9$ , showing the widest zone obtained stabilization.

Figure 6.12 confirms the integral properties of the controller. There are slight oscillations the result of model disturbances and nonlinearities. Figure 6.13 shows the tracking properties of the controller, and a comparison with the waveform in Figure 6.12 allows us to conclude that the controller is good at keeping up with the set value as long as it does not change too quickly.

Comparing Figures 6.12 and 6.14 shows the increasing influence of nonlinearity. In the first case, the regulator works calmly and the control is in the range of 1.2–

3.1 V. The behavior of the system shows only minor deviations from the linear model which predicts the aperiodic nature of transients. Acceleration of the system (Fig. 6.14) causes very unstable operation of the controller. The control amplitude increases and now varies in the range 0 – 5.3 V. The control variance is also much larger.

Deviations from the linear model are large, oscillations appear, and further acceleration of the system leads to loss of stability. This behavior is another confirmation of the hypothesis formulated in section 3.3. Let us note that inequality 3.21 requires that (see Fig. 6.14)

$$\frac{3T}{\sqrt{\frac{2\ddot{y}x}{g}}} \exp \left( \frac{3\ddot{y}x}{\sqrt{\frac{2\ddot{y}x}{g}}} \right)^3 = 0.77,$$

meanwhile in the case under consideration it was  $q = 0.65$ . For the waveform in Figure 6.12, we have:

$$\frac{3T}{\sqrt{\frac{2\ddot{y}x}{g}}} \exp \left( \frac{3\ddot{y}x}{\sqrt{\frac{2\ddot{y}x}{g}}} \right)^3 = 0.8,$$

and the  $q$  parameter had a limit value of 0.8. It is now easy to explain the fact that the best properties of the control system were obtained for  $q = 0.9$ .

The above analysis does not apply only to this regulator, but it is a general property nonlinear system (3.7)–(3.9). It follows that when designing the controller, the nonlinearities of the system must be taken into account and the linear theory cannot be used "with impunity".

The make\_pp.m file allows for the synthesis of the *PP regulator*, and the rt\_pp\_01.mdl file is its implementation.

## 6.5. Comparison of algorithms

The previous sections presented four algorithms for controlling the magnetic levitation system. Each of these algorithms has its advantages and disadvantages.

The comparative criteria will be the width of the stabilization zone defined as the maximum deviation from the steady state that does not cause loss of stability, the possibility of shaping dynamic properties (e.g. obtaining a transient waveform without oscillations) and static properties, computational complexity during algorithm synthesis and complexity computational capacity of the algorithm itself. The results of the analysis are presented in the table below

Table 6.1. Comparison of algorithms.

Algorithm	Stabilization zone	Dynamic and static properties	Complexity computational during the synthesis of	Complexity computational capacity of the algorithm
PID	$\pm 1.5\text{mm}$	Unable to obtain any distribution of eigenvalues of a closed system. There is always overshoot.  Zero steady state error $3.5\text{mm}$	the Mayá algorithm, but it is difficult to capture the relationship between the location of the eigenvalues and the controller settings.	Little . 6 additions i 4 multiplication
Dynamic compensator	$\pm$ Arbitrary distribution	Arbitrary distribution of eigenvalues of a closed system.  Steady state error	Large. Solving two matrix Riccati equations, or setting the eigenvalues of the matrix ( $A-BK$ ) and ( $A-GCT$ )	Mean.  Online solving of a 3rd order linear difference equation
Dynamic compensator with integration	$\pm 3.5\text{mm}$	Arbitrary distribution of eigenvalues of a closed system.  Zero error at steady state	Large. Solving two matrix Riccati equations, or setting the eigenvalues of the matrix ( $A-BK$ ) and ( $A-GCT$ ).  Medium.	Mean.  Online solving of a 3rd order linear difference equation and integration.
PP	$\pm 5\text{mm}$	Arbitrary distribution of eigenvalues of a closed system. Zero error at steady state. Possibility shaping immune properties	Solving a system of linear equations with seven unknowns	Mean.  Online solution of a linear difference equation.

As you can see, the PP algorithm gives the best results . The dynamic compensator with integration has a slightly smaller stabilization zone, but its other properties are the same comparable to PP. Despite its simplicity and many applications, the PID algorithm does not work in this case because it does not enable shaping the dynamic properties of the control system.

## 7. Summary

Modern computer techniques make it possible to control fast, unstable objects. The second chapter shows one of the implementations of controlling the magnetic levitation system. The great advantage of the *MATLAB/SIMULINK* package and the *RTW* software cooperating with it is the possibility of quick and simple implementation and testing of virtually any control algorithm. The only limitation here is frequency

sampling, which should not exceed 1000 Hz, because it may cause problems with other tasks, such as data acquisition and communication with the user.

An alternative is to use a faster computer, software or a system of two computers, one of which acts as a controller and the other is the superior layer and performs all tasks that do not require real-time operation. Another one

An option is to use specialized *DSP* processors whose speed action is so large that it would be possible to solve the model equations on-line and, based on the predictions made in this way, select the appropriate control. The mathematical model of the phenomenon and its basic properties are discussed in chapter three. Also given there probable reasons for the observed differences between theory and experience.

Model equations (3.7)-(3.9) can be modified to include the curve magnetization of the electromagnet core and nonlinearities introduced by electronics controlling the current in the coil. Such modifications should be made carefully and so that the model can be identified. Another possibility is to use a neural network as an object model. While training the network is not a major problem, analyzing the properties of such a model is only possible based on numerical methods and there is never a guarantee that the results obtained in this way will be confirmed in reality. Therefore, the author proposes to use the model in the form of differential equations (3.7)-(3.9) or their modifications, especially since the maximum model error was less than 0.15 mm.

The identification procedure proposed in chapter four is one of the possibilities. The author stated that with a regulator that stabilizes the system, identification can be made in less than an hour. This is not an impressive result, but it guarantees the correctness of the obtained results, while the use of numerical procedures for minimizing the quality indicator (4.2) may lead to false results, because the problem is non-linear and may have many local minima.

The control algorithms discussed in chapter six do not exhaust the possibilities of controlling the system. However, they show the nature of the phenomenon and the problems resulting from the instability and nonlinearity of the system. The constraints (3.20), (3.21) imposed on the duration of transient states are confirmed by the control results and constitute a fundamental problem in the synthesis of controllers. It was not possible to design a controller that would stabilize the system in the entire range of sphere positions. This results in the need to use other control techniques, such as adaptive control or the switched gain *scheduling method*, or non-linear controllers. They also belong to this last group neural networks. The author attempted to synthesize a neural regulator that is a generalization of the pole placement (*PP*) algorithm. The network stabilized the object, but learning errors and system instability caused strong oscillations at one operating point, at another the network worked well, and at another nearby point there was a loss of stability.

The analysis of the control results leads to the conclusion that in the case of magnetic levitation, linear theory cannot be uncritically used, and compensation of nonlinearity using adaptive methods or the use of nonlinear controllers may allow to achieve system stabilization in a much wider range of sphere positions.

## Literature

1. Astrom KJ , Wittenmark B. *Adaptive Control*. Addison-Wesley Publishing Company, 1991.
2. Astrom KJ , Wittenmark B. *Computer Controlled Systems*. Prentice Hall, Englewood Cliffs 3. Banach S. *Mechanics*, 1990.
- PWN 4. Box GEP , Warsaw 1956.
- , Jenkins GM *Time Series Analysis. Forecasting and control*. PWN , Warsaw 1983.
5. Chwaleba A. , Poniński M. Siedlecki A. *Electrical metrology*. WNT , Warsaw 1994.
6. Feynman RP , Leighton R.B , Sands M , Feynman lectures on physics , vol. I part 2 , PWN , Warsaw 1969.
7. Findeisen W. , Szymański J. , Wierzbicki A. , *Theory and computational methods of optimization* . PWN , Warsaw 1980.
8. Fortuna Z., Macukow B., Wysowski J. *Numerical Methods* . WNT 9. Górecki H., Fuksa , Warsaw 1993.
- S., Kortowski A., Mitkowski W., *Optimal control in linear systems from* Warsaw 1983.
- square quality indicator*. PWN ,
10. Górecki H., *Optimization of dynamic systems*. PWN Laub AJ , Warsaw 1993.
11. Grace A , Little J.N , Thompson C. , *Control System Toolbox for use with MATLAB*. The MathWorks, Inc., Natic MA , 1992.
12. Grace A. *Optimization Toolbox for use with MATLAB*. The MathWorks, Inc., Natic MA 13. *Magnetic Suspension* , 1992.
- Instruction Manual*. (transl. from French) DIDASTEL PROVENCE 14. Kaczorek Vol. 2 *Control theory* 15. La Salle J., , Marseille 1998.
- Lefschetz S. *Outline of Discrete-time Stability Theory and his* , PWN , Warsaw 1981.
- , Warsaw 1966.
16. Little JN Shure L. *Signal Processing Toolbox for use with MATLAB*. The MathWorks, Inc., Natic MA , 1992.
17. Ljung L. *System Identification Toolbox for use with MATLAB*. The MathWorks, Inc., South Natic MA , 1988.
18. Luenberger DG *An Introduction to observers* . IEEE Trans. Automatic . Control . Vol. AC-16. Yeah. 6 . p.596-602.
19. *MATLAB for Microsoft Windows*. The MathWorks, Inc., Natic MA 20. , 1991.
- Maurin K., *Analysis part. I. Elements* . PWN 21. , Warsaw 1991.
- Mitkowski W., *Stabilization of dynamic systems* . WNT 22. Morrise , Warsaw 1991.
- AH *Physical basis of magnetism*. PWN 23. Niederliński A., , Warsaw 1970.
- Moyciński J., Ogonowski Z., *Adaptive regulation* . PWN 24. Niederliński A., , Warsaw 1995.
- Multidimensional automation systems* . WNT 25. Purcell EM, *Electricity*, Warsaw 1974.
- and Magnetism* . PWN 26. *Real Time Workshop for use* , Warsaw 1975.
- with SIMULINK* 27. Rogg D. *General survey of the* , *User's Guide* . The MathWorks, Inc., Natic , USA , 1994.
- feasible applications and development tendencies of magnetic levitation technology*.
- IEEE Trans. Magn., vol. MAG – 20 no. 5 pp. 1696-1701 1984.
28. *SIMULINK for Microsoft Windows User's Guide* . The MathWorks, Inc., Natic MA 29. Sinha PK *Electromagnetic*, 1992.
- Suspension: dynamics and control*. Stevenage, UK: Peregrinus, 1987.
30. Szymkat M. *Computer-aided design of control systems* . WNT Warszawa 1993.
31. Turowicz A. *Matrix theory* . Script. Ed. 4. Kraków AGH 32. Grega , 1985.
- W., Kołek K., Turnau A.: *Real-time kernel dedicated to fast mechatronic systems* in: Proceedings of the Mediterranean Conference on Electronics and Automatic Control, Marakesch, 480 – 483, 1998.
33. *RT-CON package* – Description on the server: [www.inteco.cc.pl](http://www.inteco.cc.pl)
34. *RT-DAC Multi I/O Board. User's Manual*. INTECO Ltd., Kraków 1998.